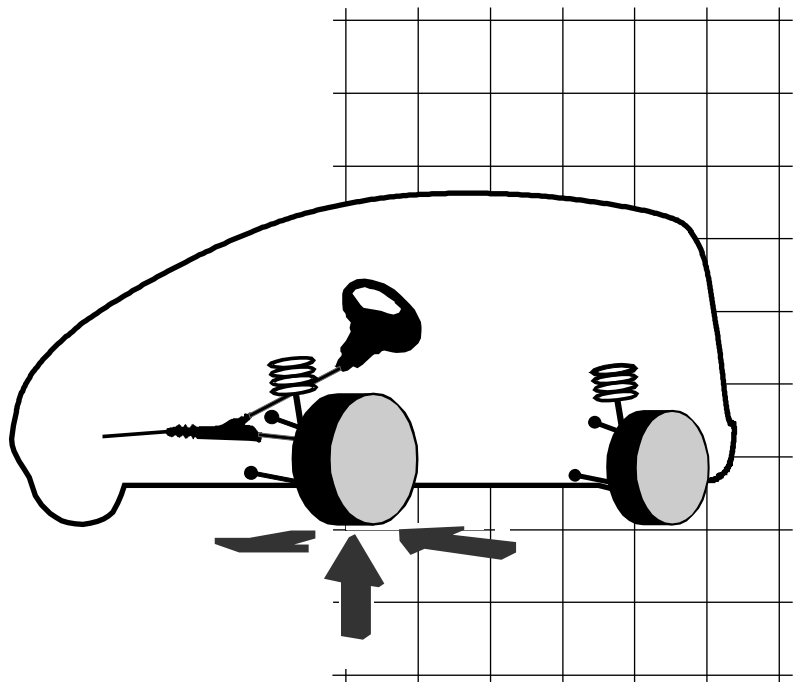


**Henning Wallentowitz**

# **Automotive Engineering II**

## ***Vertical Vehicle Dynamics***

***Suspension Systems*** ●  
***Driving Behaviour*** ●



**Editor**

Prof. Dr.-Ing. Henning Wallentowitz  
Institut Für Kraftfahrwesen Aachen (ika) RWTH Aachen  
Steinbachstraße 7, D-52074 Aachen - Germany  
**Telephone** (0241) 80-25 600 **Fax** (0241) 80 22-147  
**e-mail** office@ika.rwth-aachen.de  
**internet** <http://www.ika.rwth-aachen.de>

**Editorial Staff**

Dipl.-Ing. Florian Fuhr                      Dipl.-Ing. Ingo Albers  
Telephone (0241) 80-25 646,              80-25 612

4th Edition, Aachen, February 2004

Printed by  
Vervielfältigungsstelle der Hochschule

© ika

Reproduction, photocopying and  
electronic processing or translation is prohibited

**Contents**

|         |   |     |
|---------|---|-----|
| 1       | Vertical Dynamics (Suspension) .....                          | 3   |
| 1.1     | Suspension - Demands and Possibilities of Implementation..... | 3   |
| 1.2     | The Road as the Source of Excitation.....                     | 5   |
| 1.2.1   | Spectral Density of the Road Unevenness .....                 | 8   |
| 1.2.2   | Data Acquisition for Road Unevenness .....                    | 11  |
| 1.3     | Components of the total Suspension System .....               | 15  |
| 1.3.1   | Tires.....  | 15  |
| 1.3.2   | Body Springs .....  | 21  |
| 1.3.2.1 | Leaf Springs .....  | 21  |
| 1.3.2.2 | Torsion-bar Springs .....                                     | 27  |
| 1.3.2.3 | Coil Springs .....  | 29  |
| 1.3.2.4 | Gas Springs.....  | 33  |
| 1.3.3   | Vibration Dampers .....                                       | 44  |
| 1.3.4   | Seats.....  | 56  |
| 1.3.5   | Evaluation of Oscillations by Humans .....                    | 57  |
| 1.4     | Single Wheel Suspension Model.....                            | 63  |
| 1.4.1   | Single Mass Model .....                                       | 65  |
| 1.4.2   | Dual-Mass Equivalent System.....                              | 67  |
| 1.4.2.1 | Parametric Study - Automobile Suspension .....                | 72  |
| 1.4.2.2 | Parametric Study of a Truck Suspension .....                  | 85  |
| 1.4.3   | Enhancement of the Model by Seat Suspension.....              | 87  |
| 1.5     | Single-Track Suspension Model.....                            | 89  |
| 1.5.1   | Double-axle Vehicle with bending resistant Structure .....    | 89  |
| 1.5.1.1 | Excitation by real unevenness Routing .....                   | 91  |
| 1.5.1.2 | Mass and Spring Coupling .....                                | 93  |
| 1.5.2   | Two axle Vehicle with additional Degrees of Freedom.....      | 97  |
| 1.6     | Two-Track Suspension Model.....                               | 101 |
| 1.6.1   | Roll Springing .....  | 101 |

|         |   |     |
|---------|---|-----|
| 1.6.1.1 | Stabilizer and Compensating Spring .....                | 103 |
| 1.6.1.2 | Vehicle Conception and Suspension Characteristics ..... | 104 |
| 1.6.2   | Distortion of the structure (twisting) .....            | 106 |
| 1.6.3   | Rigid axle Tramp.....                                   | 108 |
| 1.7     | Suspension Investigation Methods.....                   | 110 |

## **1 Vertical Dynamics (Suspension)**

### **1.1 Suspension - Demands and Possibilities of Implementation**

The roads commonly used by motor vehicles are uneven. This unevenness causes vertical movements of the vehicle and the passengers during the driving process.

The vehicle is connected to the road by the tire. Small unevenness in comparison to the tire contact patch size can be compensated by the tire elasticity, whereas larger unevenness entails a vertical acceleration or deflection of the wheels. In order not to transfer these accelerations into the vehicle structure, a length compensating element has to be placed between the wheel and the vehicle structure.

Steel springs are the technologically most simple elements with variable length. Due to this fact it is also the most common length compensating element, whose force is a function of the length variation. It is usually used in the suspensions of motor vehicles. Different parts connected with springs generate oscillating systems. So there has to be added an energy absorbing element, the damper.

The suspension's job in the motor vehicle is to reduce these vertical movements. The essential criteria specifying the quality of a suspension can be listed as follows:

- suspension comfort for the passengers (Effective acceleration affecting the passengers)
- forces affecting the load (Effective value of structure acceleration)
- wheel load variation (Effective value of the dynamic wheel load), which influences the grip between tires and road (driving safety) and the load application upon the road surface.

The further demands on the suspension in a motor vehicle are various and partially contradicting (Fig. 1.1-1)

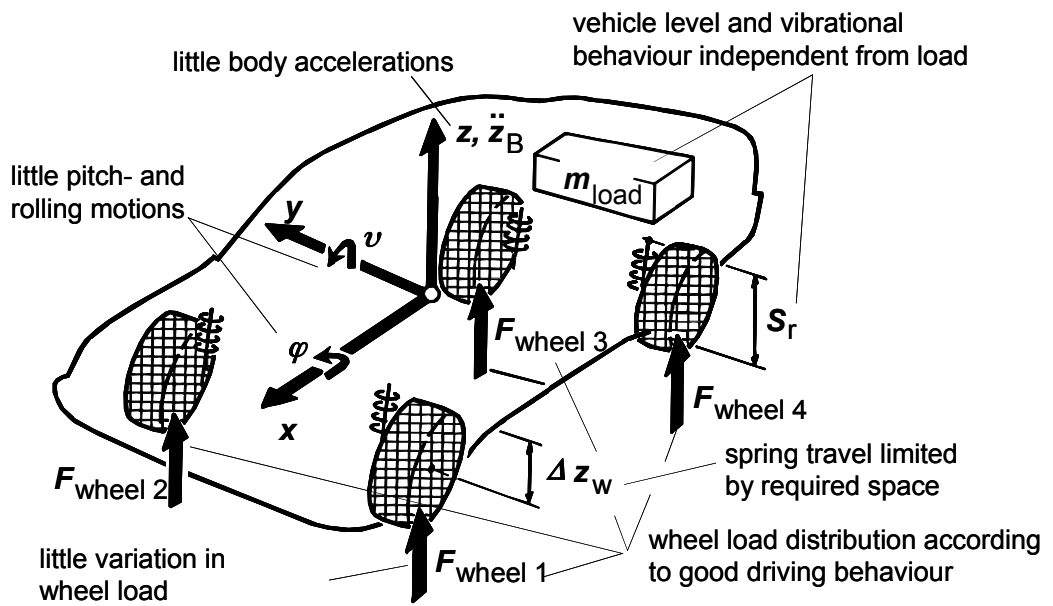


Fig 1.1-1: Demands on a vehicle suspension

Before dealing with the technical details of the spring and absorber elements, first the road and the mathematical description of its unevenness are presented.

## 1.2 The Road as the Source of Excitation

The unevenness of the road represents the most intensive source of excitation for the vibratory system of the motor vehicle in the frequency range up to approximately 30 Hz. The road's unevenness causes vertical movements of the vehicle structure, and as a consequence, the road is affected by tire load variation itself.

Generally road unevenness appears as an excitation with different amplitudes and wavelengths at irregular periods of time. This is called a stochastic excitation of the vehicle. In order to be able to examine the effect of the road unevenness on the vibratory motor vehicle system (see chapter 1.4), this unevenness first has to be described mathematically.

Considering the most simple case of a harmonic (sinusoidal) radiation, where the road unevenness excites an amplitude 'h' at equal distances L, you will get a characteristic unevenness as a result (Fig. 1.2-1).

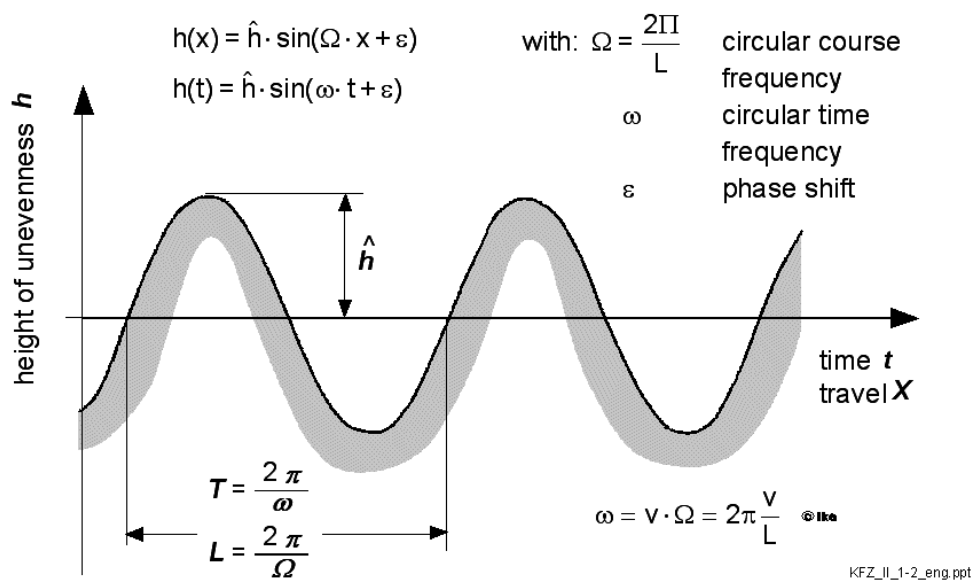


Fig. 1.2-1: Sinusoidal pattern of unevenness

The unevenness height can be described as follows:

$$h(x) = \hat{h} \cdot \sin(\Omega \cdot x + \varepsilon) \quad (1.2-1)$$

including:  $\Omega = \frac{2\Pi}{L}$  as track-dependent circular frequency and  $\varepsilon$  as phase shift.

When driving on this roadway with constant velocity  $v$  this distance-dependent unevenness can be changed into a time-dependent relation:

$$h(t) = \hat{h} \cdot \sin(\omega \cdot t + \varepsilon) \quad (1.2-2)$$

with:  $\omega$  as time-dependent circular frequency.

The equality of  $h(x)$  and  $h(t)$  entails  $\omega \cdot t = \Omega \cdot x$ , and with the relationship  $x = v \cdot t$  the time-dependent circular frequency follows:

$$\omega = v \cdot \Omega = 2\pi \cdot \frac{v}{L} \quad (1.2-3)$$

The next step in the description of the road unevenness is the transition to a non-sinusoidal, but still periodic, unevenness (Fig. 1.2-2).

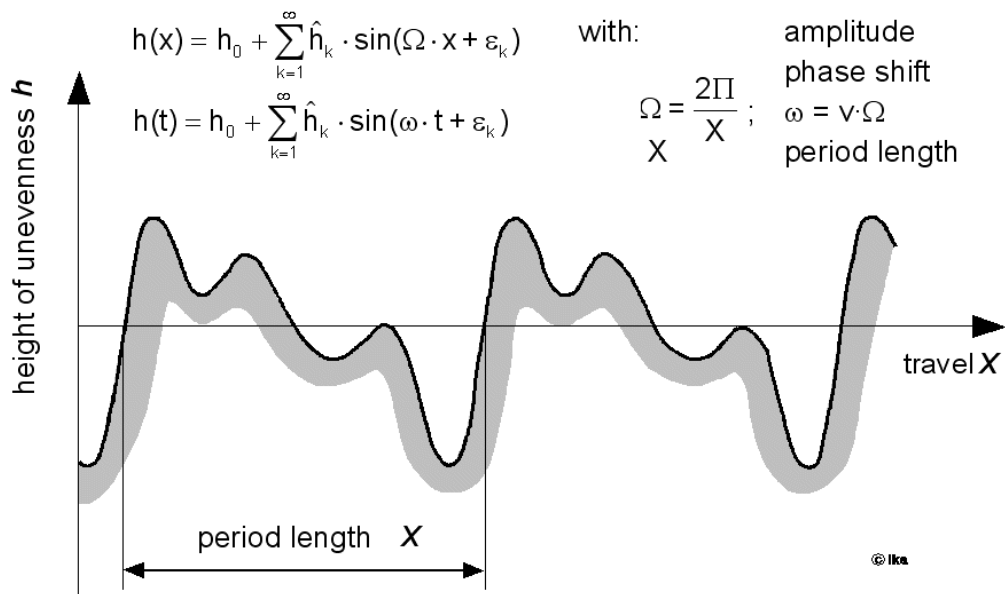


Fig. 1.2-2: Periodic pattern of unevenness

This unevenness can be represented as Fourier series as follows:

$$h(x) = h_0 + \sum_{k=1}^{\infty} \hat{h}_k \cdot \sin(\Omega \cdot x + \varepsilon_k) \quad (1.2-4)$$

or:

$$h(t) = h_0 + \sum_{k=1}^{\infty} \hat{h}_k \cdot \sin(\omega \cdot t + \varepsilon_k) \quad (1.2-5)$$



with:  $\hat{h}_k$  Amplitude

$\varepsilon_k$  phase shift;

$$\Omega = \frac{2\Pi}{X}, \quad \omega = v \cdot \Omega$$

X period length

When the individual amplitudes  $\hat{h}_k$  of the Fourier series are plotted versus the frequency, a discrete amplitude spectrum (line spectrum), belonging to the periodic unevenness, results (Fig. 1.2-3).

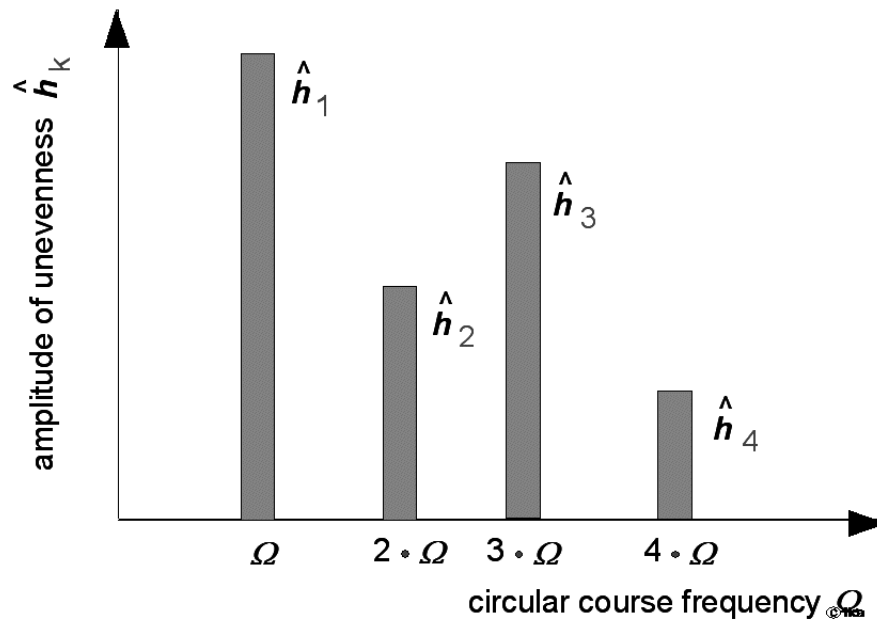


Fig. 1.2-3: Line spectrum of a periodic pattern of unevenness

For the description of real roads there has to be made another step, because they do not show a periodic type of unevenness, but a varying (stochastic) type of unevenness. The representation of the Fourier series in a complex equation, results as following:

$$h(x) = \sum_{k=1}^{\infty} \hat{h}_k \cdot e^{jk\Omega x} \quad (1.2-6)$$

$$h(t) = \sum_{k=1}^{\infty} \hat{h}_k \cdot e^{jk\omega t} \quad (1.2-7)$$

$$\text{with: } \underline{\hat{h}}_k = \frac{\Omega}{2\pi} \cdot \int_{-\frac{x}{2}}^{\frac{x}{2}} h(x) \cdot e^{-ik\Omega x} dx \quad (1.2-8)$$

On the assumption that the regarded period length is very large, the distance between the frequencies in the amplitude spectrum  $\Delta\omega$  becomes very small as a consequence.

In the boundary condition ' $X \rightarrow \infty$ ' implies that  $\Delta\Omega \rightarrow 0$  and the Fourier transformation changes into a Fourier integral as:

$$h(x) = \frac{1}{2\pi} \int_{-\infty}^{\infty} \underline{\hat{h}}(\Omega) \cdot e^{j\Omega x} d\Omega \quad (1.2-9)$$

with the continuous amplitude spectrum

$$\underline{\hat{h}}(\Omega) = \int_{-\infty}^{\infty} h(x) \cdot e^{-j\Omega x} dx \quad (1.2-10)$$

$$h(t) = \frac{1}{2\pi} \int_{-\infty}^{\infty} \underline{\hat{h}}(\omega) \cdot e^{j\omega t} d\omega \quad (1.2-11)$$

$$\underline{\hat{h}}(\omega) = \int_{-\infty}^{\infty} h(t) \cdot e^{-j\omega t} dt = \frac{1}{v} \cdot \underline{\hat{h}}(\Omega) \quad (1.2-12)$$

### 1.2.1 Spectral Density of the Road Unevenness

For theoretical investigations of the vehicle oscillations caused by road unevenness, the knowledge of the unevenness as a function of time or the distance travelled is usually not very important. It is much more interesting to find out which kinds of excitation appear statistically during the process of travel on a roadway with a characteristic unevenness. That means which kinds of amplitudes and which kinds of frequencies are excited by road unevenness at certain fixed distances.

The resulting square average value is defined as follows:

$$\overline{x^2}(t) = \frac{1}{T} \int_0^T x^2(t) dt \quad (1.2-13)$$

The characteristic line of unevenness results as follows:

$$\bar{h}^2(x) = \frac{1}{x} \int_0^x h^2(x) dx = \int_0^\infty \lim_{x \rightarrow \infty} \frac{|\hat{h}(\Omega)|^2}{x} d\Omega \quad (1.2-14)$$

or:

$$\bar{h}^2(t) = \frac{1}{T} \int_0^T h^2(t) dt = \int_0^\infty \lim_{T \rightarrow \infty} \frac{|\hat{h}(\omega)|^2}{T} d\omega \quad (1.2-15)$$

The limit values occurring here indicate that these simple expressions give a result only for very large time intervals T or distances X. The expressions

$$\Phi_h(\Omega) := \lim_{X \rightarrow \infty} \frac{|\hat{h}(\Omega)|^2}{X} \quad \text{and} \quad (1.2-16)$$

$$\Phi_h(\omega) := \lim_{T \rightarrow \infty} \frac{|\hat{h}(\omega)|^2}{T} \quad (1.2-17)$$

are called circular path frequency or periodical spectral power density (power density spectrum).

With  $X = v \cdot T$  (see above) similarly the following connection results for the unevenness spectra:

$$\Phi_h(\omega) = \frac{1}{v} \cdot \Phi_h(\Omega) \quad (1.2-18)$$

If one measures the power density spectra  $\Phi_h(\Omega)$  of different roads and applies this on a double-logarithmic scale, then similar characteristic curves result for all types of roads (Fig. 1.2-4).

In this presentation the power density spectra can be approximated by straight lines, which then can be described by the following equation:

$$\Phi_h(\Omega) = \Phi_h(\Omega_0) \cdot \left( \frac{\Omega}{\Omega_0} \right)^{-w} \quad (1.2-19)$$

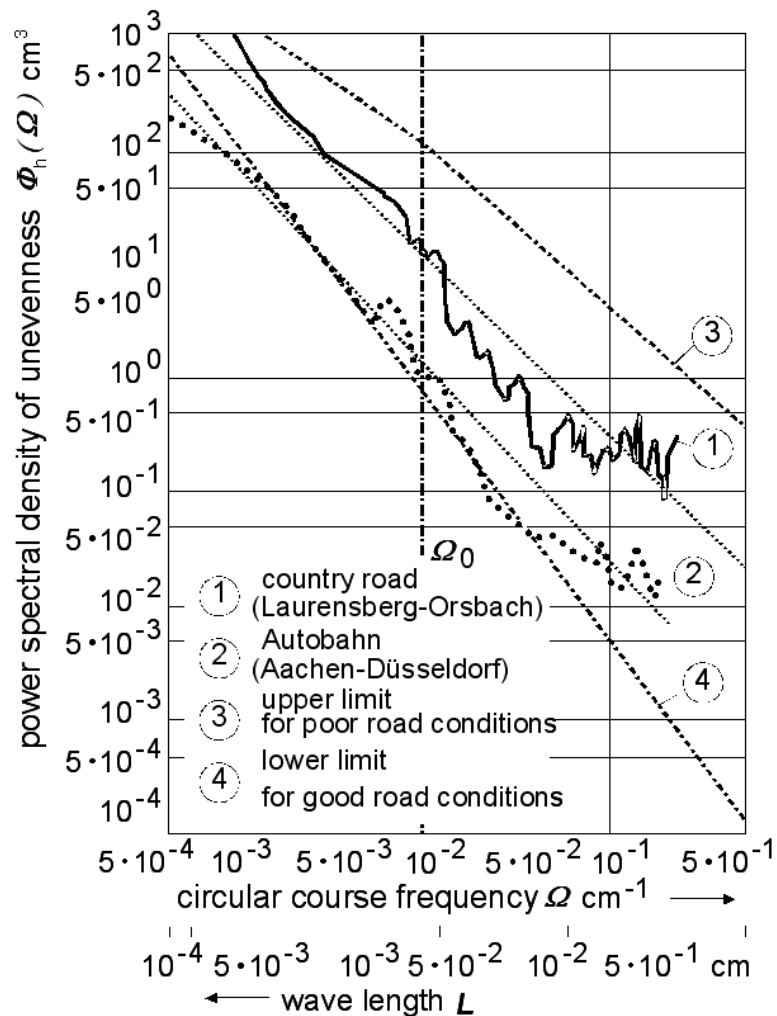


Fig. 1.2-4: Power spectral density of unevenness dependent on circular course frequency.

Here  $\Phi_h(\Omega_0)$  represents the power spectral density dependent on  $\Omega_0$  (reference circular path frequency), which is usually selected as  $\Omega_0 = 10^{-2} \text{cm}^{-1} = 1 \text{m}^{-1}$ . This corresponds to a reference wavelength of  $L_0 = 2\pi/\Omega_0 = 6.28 \text{m}$ .  $\Phi_h(\Omega_0)$  is also called the degree of unevenness of the road.

$W$  defines the gradient of the straight line and is also called undulation (in German: "Welligkeit"). The undulation of the roadway varies depending on the road design between 1.7 and 3.3 (standardized road:  $w = 2$ ) /7/.

The degree of unevenness (and undulation) are considered as assessment criteria for the condition of a road. An increase of  $\Phi_h(\Omega_0)$  corresponds to a larger unevenness of the roadway, while an increasing value of ' $W$ ' means a higher proportion of long waves in the

spectrum. The relationship between the curve of the spectral density and an increase of the degree of unevenness  $\Phi_h(\Omega_0)$  or undulations  $w$  is shown in Fig 1.2-5.

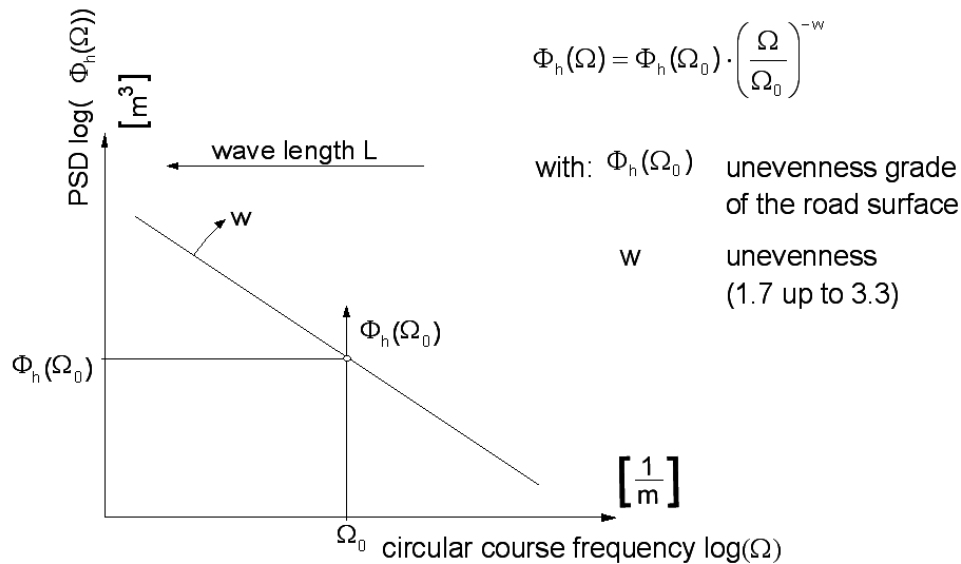


Fig. 1.2-5: Power spectral density dependent on the circular path frequency

For road unevenness of wavelengths  $L$  between 0.15 m to 80 m there result excitation frequencies  $\Omega$  from 0.06 Hz up to 267 Hz (see eq. 1.2-3) in the case of driving speeds  $v$  between 5 m/s ( $\approx 20$  km/h) and 40 m/s ( $\approx 160$  km/h).

### 1.2.2 Data Acquisition for Road Unevenness

For the determination of the spectral power density of the road unevenness, one proceeds from the longitudinal section of the road. For the measurement of road unevenness different measuring procedures were developed, which are adapted partially to both road construction as well as for the application in the Automotive technique. About 70 different unevenness measuring procedures are available.

An exact measurement of the road surface is possible only with subgrade level and levelling instrument. Because of the high demand on time in the measurement of longer distances and the disturbance by the flow of traffic etc. these procedures are less important in technical application. Those so-called geometrical unevenness measuring instruments were developed mainly for application in road construction.

The measuring procedures used in automotive technology operate according to the principle of the dynamic unevenness measurement. During these measuring procedures the reference level is not fixed, but derived continuously from an average value of the road unevenness, formed over a sufficiently long period of time. Fig 1.2-6 shows a test vehicle equipped with devices for the measurement of road unevenness.



Fig. 1.2-6: Instrumentation for unevenness measurements (ika)

The measuring job is divided into two sub-problems:

- 1) Measurement of the change in distance  $\Delta z$  between roadway surface and points of reference at the vehicle bodywork
- 2) Measurement of the vertical structure movement  $z_A$  at the points of reference

The change in distance  $\Delta z$  is entered continuously for each track with the help of a contactless laser measuring system. The measuring system is based on the triangulation principle, Fig. 1.2-7.

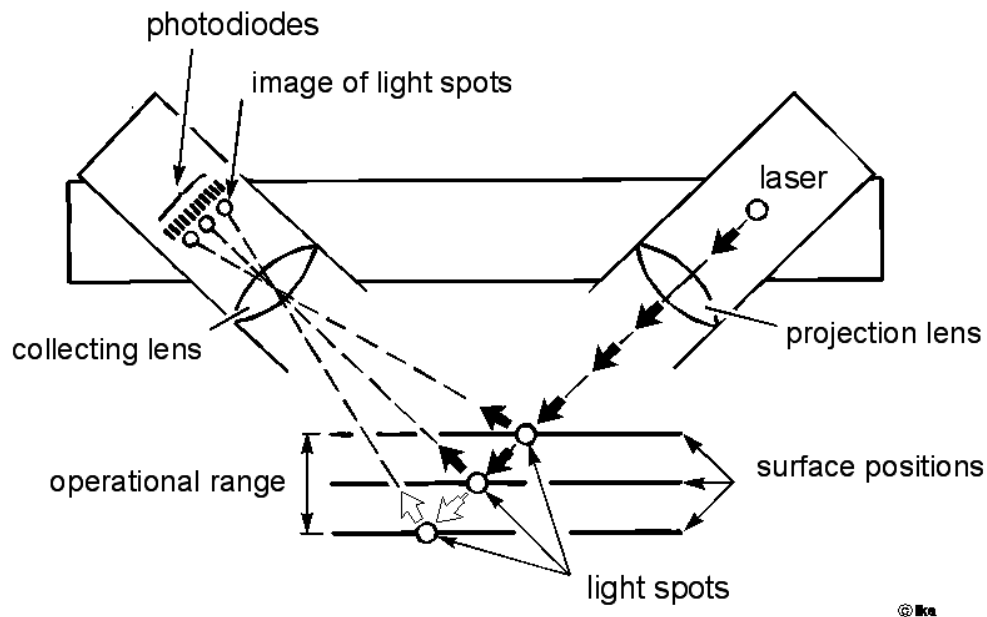


Fig. 1.2-7: Operational principle of the contactless distance measurement

With the help of a laser beam, incident at a certain angle on the road surface, a light spot is produced, which is received through a lens on the surface of a light-sensitive photodiode. According to the angle of incidence of the laser beam, the spot of light on the surface of the photodiode shifts as illustrated, and its movement is proportional to the vertical distance between the point of reference and the road surface. Thereby it can be converted into a measuring signal.

The measurement of the displacement of the vehicle body  $z_B$  is managed by acceleration adaptors fastened to the vehicle bodywork perpendicularly over the points of reference for the distance measurement.

The low-pass effect of the vehicle suspension system results in accelerations  $\ddot{z}_B$  of max. 1 to 2 g, and so sensitive acceleration sensors can be selected accordingly, which record low-frequency structure accelerations with sufficient accuracy.

The displacement of the vehicle body  $z_B$  is determined continuously by the double integration of the vehicle body acceleration  $\ddot{z}_B$ . The characteristic of unevenness  $h(t)$  or  $h(x)$  results from the addition of the displacement of the vehicle body  $z_A$  and the change in distance  $\Delta z$ .

The procedure to define the determination of the unevenness spectrum  $\Phi_h(\Omega)$  metrologically from a recorded measuring signal  $h(t)$  is schematically represented Fig 1.2-8 /38/.

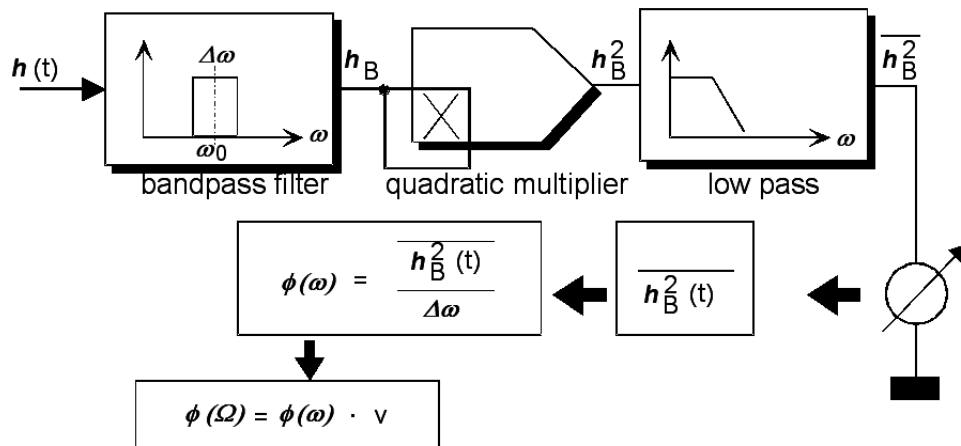


Fig. 1.2-8: Metrological determination of an unevenness spectrum

From the measured signal which can be analyzed with a bandpass filter with mean frequency  $\omega_0$  a frequency range  $\Delta\omega$  is filtered. Then the band-pass filter signal generated is squared and the average value is calculated over a certain period of time. From this average value, defined in Fig 1.2-8 as  $\overline{h_B^2}$ , the value of the power density spectrum for  $\omega_0$  is determined by division with the filter bandwidth  $\Delta\omega$ .

By shifting the bandpass filter center frequency the power density spectrum for the entire frequency range of interest can be determined.

From the time-frequency-dependent power density spectrum the spectral unevenness density can be calculated as a function of the circular path frequency  $\Omega$  by simple multiplication with the driving speed  $v$  (see Eq. 1.2-18). In this case it is assumed that the measurement of the characteristic of unevenness  $h(t)$  was determined at constant driving speed  $v$ .



### 1.3 Components of the total Suspension System

#### 1.3.1 Tires

In the following section, the vehicle tire is considered only from the technical point of view of the suspension and damping. Further representation of the characteristics of vehicle tires can be found in chapter 2.2. The transverse characteristics of the tire are described there, e.g. generation and transfer of side forces.

- Tire as a spring

The wheel load is transferred to the tire by the rim and pressure is applied to this contact area. The reaction force, which opposes the load on the tire, consists of different components. Fig. 1.3-1 shows the proportions of the load carrying components of a tire as a function of compression.

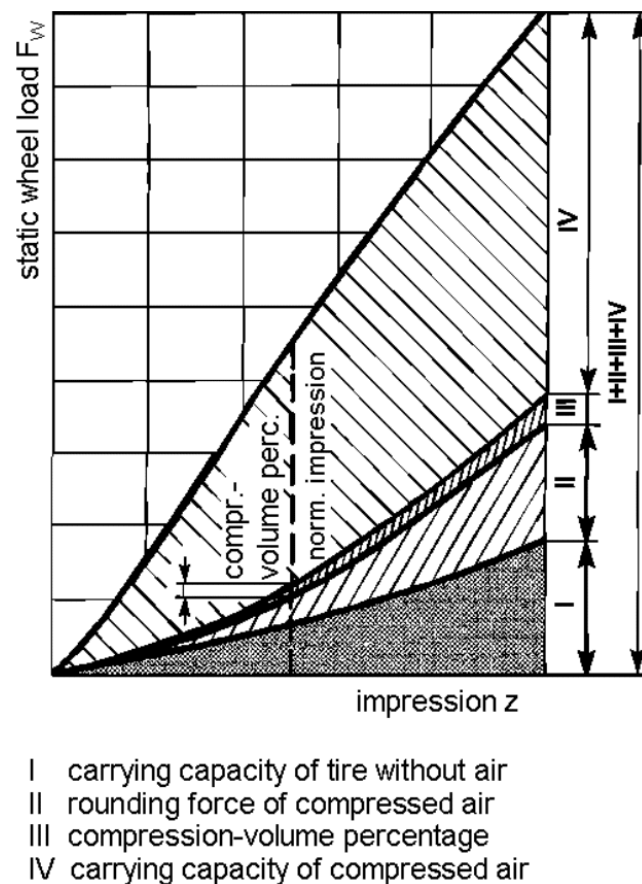


Fig. 1.3-1: Structure of the spring characteristic of a pneumatic tire/41/

The component I corresponds to the proportion of the load carrying capacity of the solid rubber fabric body, due to elastic deformation. The component II represents the so-called

circular retaining force of the compressed air, which reinforces the tire in its walls (balloon effect). The component III represents the very small proportion of the air compression.

The component IV represents the principal part, which is based on the adaption of the road contact area  $A$  to the vertical load  $G_w$ :

$$G_w \approx p_i \cdot A$$

(with  $p_i$  inflation pressure, that means the pressure in the wheel road contact area  $A$  corresponds to the inflation pressure.)

Due to the tire compression an oscillatory subsystem develops in the wheel or in the unsprung masses. In this way, the spring characteristic of a tire influences natural frequency of the wheel or axle. Also the inflation pressure has decisive influence on the suspension system beside the structure of the tire.

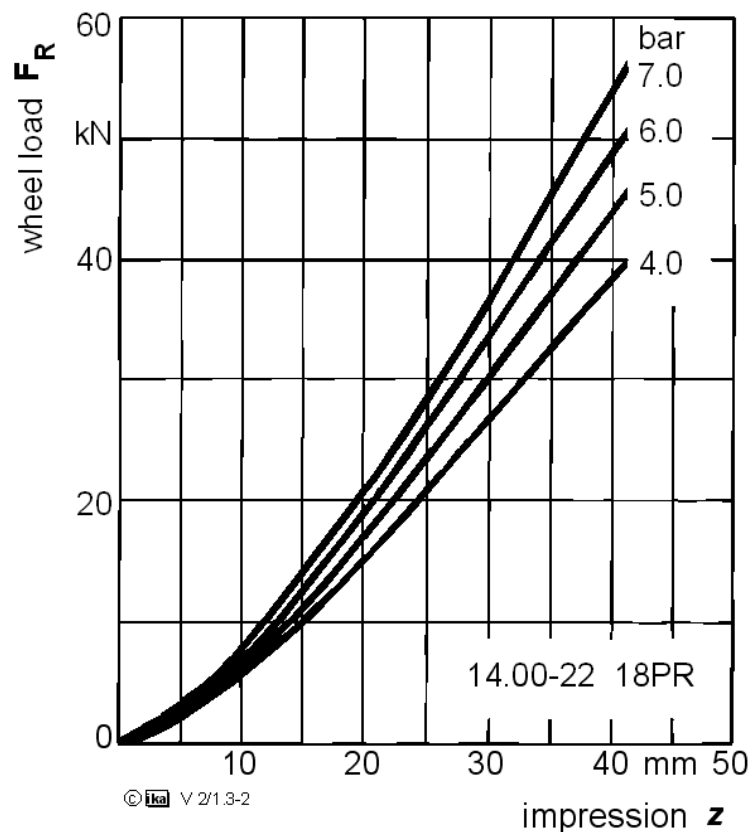


Fig. 1.3-2: Spring characteristic of a Truck tire with four different air pressures

The spring characteristics indicate a linear characteristic in the operating range. By the modification of the vertical load  $F_w$  as function of the compression  $z_w$  (lowering of the wheel axle) the spring rate  $c_R$  can be determined.

$$c_W = \frac{dF_W}{dz_W} \quad (1.3-1)$$

Since the force characteristic is not a constant function of compression, the spring rate is variable. Therefore a constant spring rate can be considered only as an approximation for a certain area of the curve, where the static wheel load and the compression is appropriate to Fig. 1.3-3.

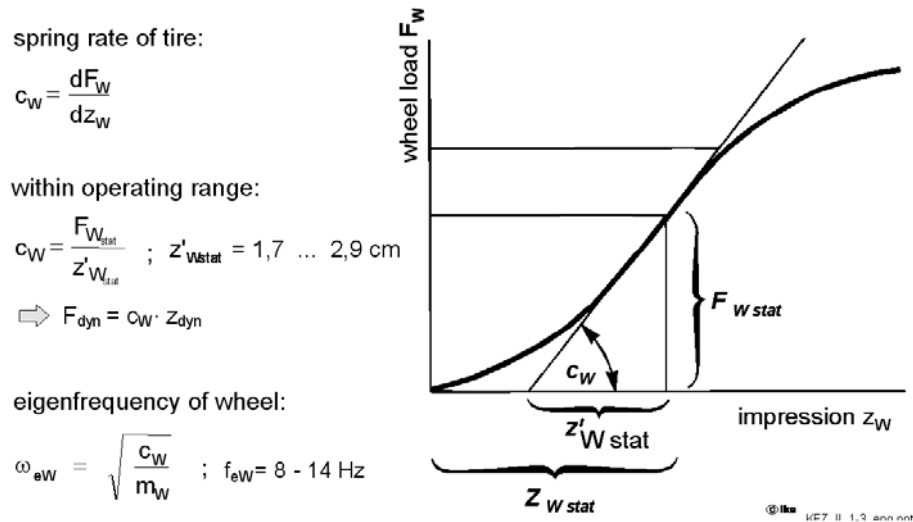


Fig. 1.3-3: Linearisation of the tire spring rates.

In the operation range, the spring rate is given by

$$c_W = \frac{F_{W_{stat}}}{z'_{W_{stat}}} \quad (1.3-2)$$

If the tire compression is increased or reduced over  $z_{dyn}$ , the force approximation changes around

$$F_{dyn} = c_W \cdot z_{dyn} \quad (1.3-3)$$

As measure for driving safety and protection of the road, the ratio of total load to the static load is indicated as:

$$\frac{F}{F_{W_{stat}}} = \frac{F_{W_{stat}} + F_{dyn}}{F_{W_{stat}}} \quad (1.3-4)$$

With the equation (1.3-2)

$$\frac{F}{F_{Wstat}} = 1 + \frac{c_W}{F_{Wstat}} \cdot z_{dyn} \quad (1.3-5)$$

The quotient  $\frac{F_{Wstat}}{c_W}$  is according to Fig. 1.3-3 equal to the sub-tangent with the length  $z'_{Wstat}$

$$z'_{Rstat} = F_{Wstat} / c_W \quad (1.3-6)$$

This parameter is a measure for the additional load relative to the static load with a compression  $z_{dyn}$ , e.g. as a result of unevenness. To all tires (passenger cars and trucks) applies approximated:

$$z'_{Wstat} = 1.7 \dots 2.9 \text{ cm}$$

The lower value refers to diagonal tires and the upper value to radial tires, that means the latter are softer and with a certain tire compression  $z_{dyn}$ , induce smaller additional loads  $F_{dyn}$ . With this reference value, the approximate wheel natural frequency can be determined:

$$\omega_{eW} = \sqrt{\frac{c_W}{m_W}} \approx \sqrt{\frac{F_{Wstat}}{z'_{Wstat} \cdot m_W}} \quad (1.3-7)$$

The wheel natural frequency is usually approximately  $f_{eW} = 8 - 14$  Hz. This estimation proceeds from a static spring characteristic of the tire. In driving condition, the radial spring rigidity of the tire is further influenced by a multiplicity of parameters. Due to the viscoelastic behavior of the rubber, the spring rigidity increases e.g. with increasing excitation frequency when excited by road unevenness (chapter 1.4).

Besides, the respective operating point of the tire also influences the spring rate. While e.g. with increasing driving speed the influence of the centrifugal force at the tire circumference causes an increase of the spring rigidity, the side forces generated at the tire due to the side slip angles (Chapter 2.2.4) lead to a lateral displacement of the tire road contact area. This causes a more uneven load of the tire shoulders and thus a reduction of the spring rate.

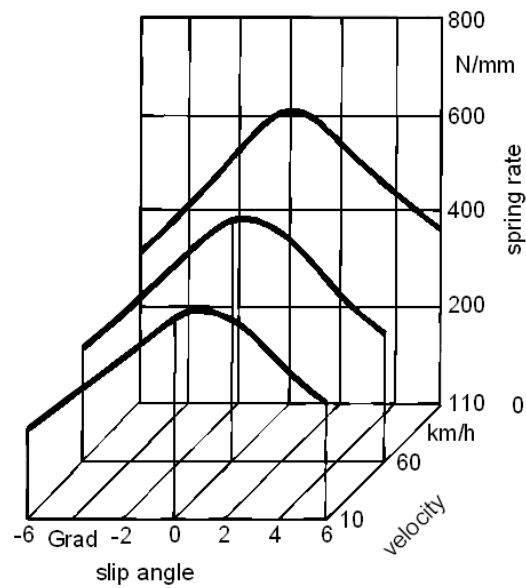


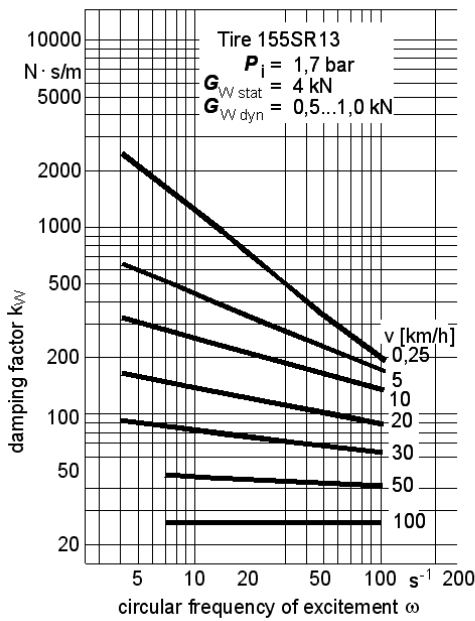
Fig. 1.3-4: Radial spring stiffness of a truck tire as a function of vehicle velocity and side slip angles/17/

- Absorption capacity of the tire

Besides the suspension the absorption capacity of the tire becomes a special meaning, since it is in direct relation to the tire comfort. The term absorption capacity characterizes thereby the characteristic of the tire to absorb unevenness, which are short in relation to the tire contact length, without vertical movement of the axle/9/. The tire behaves in relation to such obstacle more softly than in relation to an equivalent high compression of the entire tire contact patch. The absorption capacity is influenced mainly by the rigidity of the sidewall.

- Tire damping

The tire damping is a material damping. It is a cause for the temperature rise of the tire and increases with the number of plies and the material mass in the tire. The damping factor  $k_w$  is thereby no constant, it depends on several influence parameters like the radial spring rigidity of the tire, Fig. 1.3-5.



experimentally determined damping rule:

$$k_w = \frac{\lambda}{\omega^e}$$

with:  $\lambda$  constant } tire specific and  
 $e$  exponent } dependent on velocity  
 $\omega$  circular frequency of excitement

approximation formula for damping factor:

$$k_w \approx \frac{0,1 \cdot c_w}{\omega}$$

tire damping within resonance range:

$$D_{Wres} = \frac{k_w}{2 \cdot m_W \cdot \omega_{eW}} = \frac{0,1 \cdot c_w}{2 \cdot m_W \cdot \omega_{eW} \cdot \omega_{eW}}$$

$$= \frac{0,1 \cdot \omega_{eW}^2}{2 \cdot \omega_{eW}^2} = 0,05$$

© Ika

KFZ\_II\_1-3\_eng.ppt

Fig. 1.3-5: Damping factor  $k_w$  of a tire as a function of rolling speed and excitation frequency

The influence of the excitation frequency by unevenness can be described after experimental testing by the following absorption rule/20.

$$k_w = \frac{\lambda}{\omega^e} \tag{1.3-8}$$

$\omega$  circular frequency of the excitation

The constant  $\lambda$  and the exponent  $e$  do not depend on the tire design only, but particularly from the rolling speed  $v$ .

With high rolling speeds  $e$  is  $\approx 0$ , i.e:  $k_w$  depends only on  $\lambda$  or  $v$  and is independent thereby of  $\omega$  (see Fig. 1.3-5).

For estimation of the order of the tire damping rate  $D_w$  the following approximation formula for the damping factor factor is suitable.

$$k_w \approx \frac{0,1 \cdot c_R}{\omega} \tag{1.3-9}$$

The tire absorption is important particularly in the resonance area ( $\omega = \omega_{eW}$ ). With the approximation formula (Gl.1.3-8):

$$D_{R.res} = \frac{k_W}{2 \cdot m_W \cdot \omega_{eW}} = \frac{0,1 \cdot c_W}{2 \cdot m_W \cdot \omega_{eW} \cdot \omega_{eW}} = \frac{0,1 \cdot \omega_{eW}^2}{2 \cdot \omega_{eW}^2} = 0,05 \quad (1.3-10)$$

A damping rate of  $D_{Wres}$  of 0,05 is not sufficient for the damping of the wheel masses. For a satisfying absorption of the wheel oscillations a damping rate of  $D_W$  of approximately 0.4 is required, that means that the hydraulic vibration damper-for the body (see chapter 1.3.3) must take over the main part of the wheel damping at the same time.

### 1.3.2 Body Springs

Those sections of wheel suspension systems, which give restoring force under elastic deformation, are described as body springs in this chapter. Besides conventional coil, leaf and torsion bar springs gas springs can also be mentioned.

#### 1.3.2.1 Leaf Springs

Leaf springs represent the classic leaf spring form, which were already used with carriages.

The substantial advantage of leaf springs in relation to other spring design concepts consists of the fact that they cannot be used as spring elements only, but as design elements for the coupling of body and axle (in particular for the guidance of the axle) as well. Multilayer leaf springs possess damping characteristics due to frictional forces between the leaves.

In connection with rigid axles, conventional leaf springs nowadays are used for a few car types (Station wagon and offroad vehicles) only. Front and rear suspension systems of trucks are usually designed like this. Fig. 1.3-6.

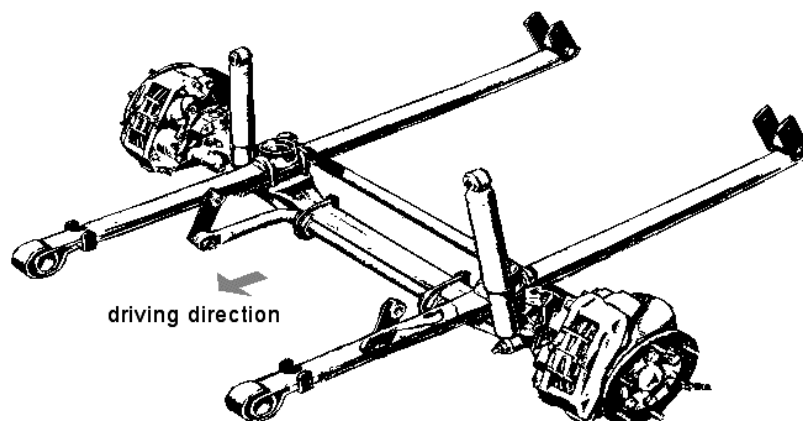


Fig. 1.3-6: Leaf spring guided front axle of a truck (Daimler-Benz)

Without any special measures the spring characteristic of the leaf spring is linear. The relationship between the deflection and the load at the end of a clamped bending beam is known from the strength theory.

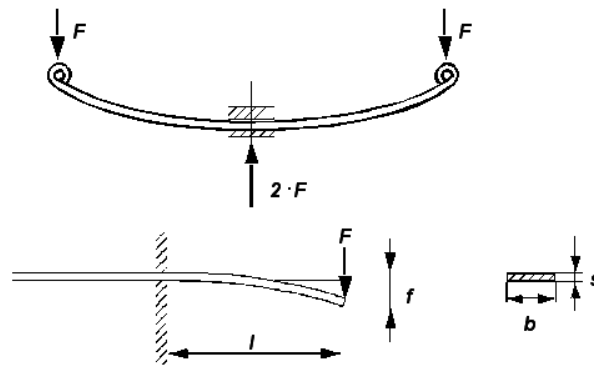
$$f = \frac{F \cdot l^3}{3 \cdot E \cdot J} \quad (1.3-11)$$

With  $l$ : length of the bending beam,

$E$  : elastic modulus

$J$  : moment of inertia

$$J = \frac{b \cdot s^3}{12} \quad (1.3-12)$$



$$f = \frac{F \cdot l^3}{3 \cdot E \cdot J} \quad E = E \text{ modulus}$$

$$J = \frac{b \cdot s^3}{12} \quad J = \text{planar moment of inertia}$$

$$\frac{F}{f} = c = \frac{1}{4} \cdot \frac{b \cdot s^3}{l^3} \cdot E = \text{const}$$

**leaf spring has a linear characteristic curve**

Fig. 1.3-7: Deflection of a leaf spring

Thus, one receives following spring rate for one half of a leaf spring system corresponding to Fig 1.3-7:

$$c = \frac{F}{f} = \frac{1}{4} \cdot \frac{b \cdot s^3}{l^3} \cdot E \approx \text{const} \quad (1.3-13)$$



In order to ensure the guidance characteristics of the axle leaf spring, the width  $b$  and the thickness  $s$  can be varied for the definition of the leaf spring rigidity  $c$  only within certain limits. Usually relatively large spring lengths are necessary in practice. Truck leaf springs are up to 1800 mm long.

Since the bending force decreases accordingly from the spring center to the ends, one arranges springs from different length in layers in such a way that a high and even degree of utilization of material is achieved. The bending stress corresponds to the trapezoidal one leaf spring Fig. 1.3-8. So this kind of leaf spring is called the trapezoid spring.

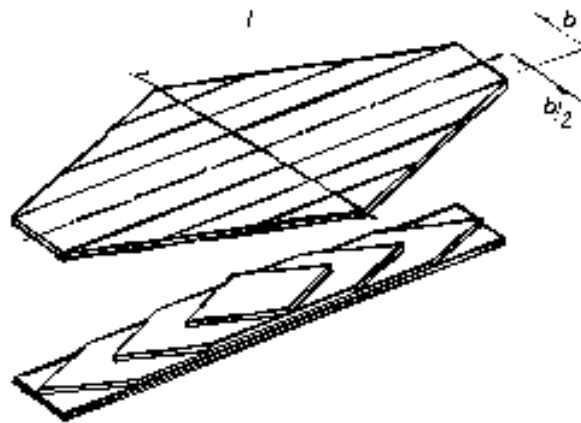


Fig. 1.3-8 trapezoidal spring

Due to the linear spring characteristic two main disadvantages of the leaf spring result:

- Spring travel

In the application of high loads the available spring travel can often reduce  $\Delta Z_{\text{Reserve}}$  to no longer sufficient values (recommended values for passenger car:  $\Delta Z_{\text{Reserve}}$  50mm, truck:  $\Delta Z_{\text{Reserve}}$  70mm)

- Natural frequency  $\neq$  const.

Since the spring rigidity does not change with loading, the body natural frequency in the unloaded condition is larger than the natural frequency in the loaded condition because of  $m_{\text{B,loaded}} > m_{\text{B,unloaded}}$ . The acceleration of the body mass is described in chapter 1.4.

These disadvantages of multi layer leaf springs can be reduced by a progressive behavior of the leaf spring characteristic. This can be achieved by the different pre-load of the individual leaves and/or by the parallel addition of auxiliary springs, which come into use only when the load exceeds a certain limit, Fig. 1.3-9.

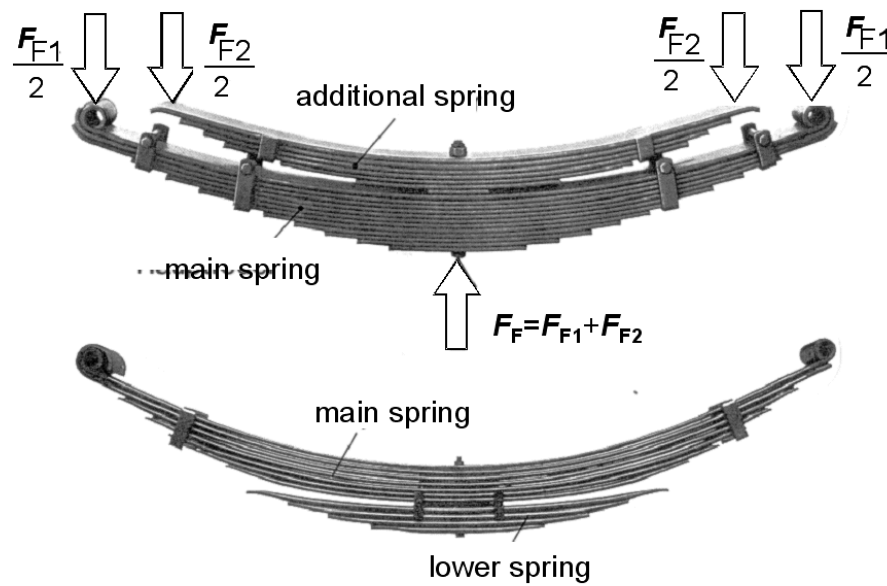


Fig. 1.3-9 Leaf springs with auxiliary springs

The natural frequency remains constant, if the upward gradient of the spring characteristic changes proportionally to the load:

$$\frac{c_{\text{loaded}}}{c_{\text{empty}}} = \frac{m_{B_{\text{loaded}}}}{m_{B_{\text{empty}}}} \quad (1.3-14)$$

The difference in spring travel between unloaded and loaded condition decreases in case of such a progressive spring characteristic. So the entire spring travel can be reduced, which is important for the space requirement in the wheel housings, the entrance height of buses etc., Fig. 1.3-10.

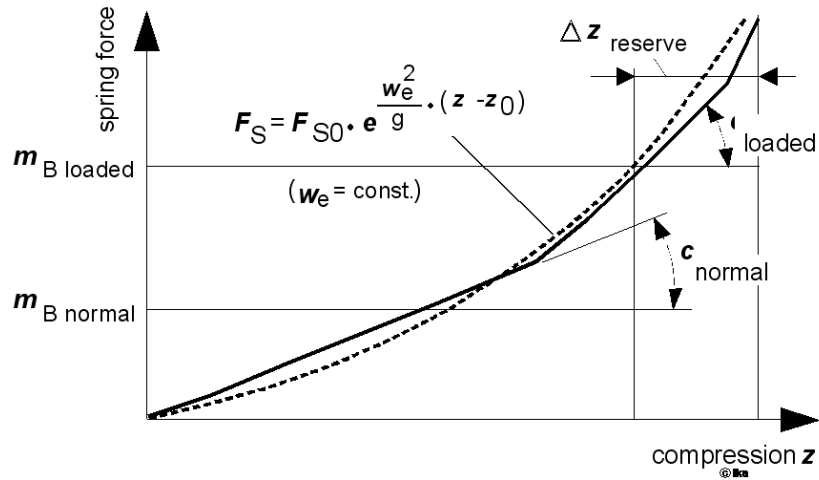


Fig. 1.3-10: Spring rate of a leaf spring with additional springs

Another disadvantage of the leaf spring consists of the fact, that both in the suspension and between the leaves of the multi layer leaf spring, dry friction occurs (Fig. 1.3-11). This affects the suspension characteristics unfavourably.

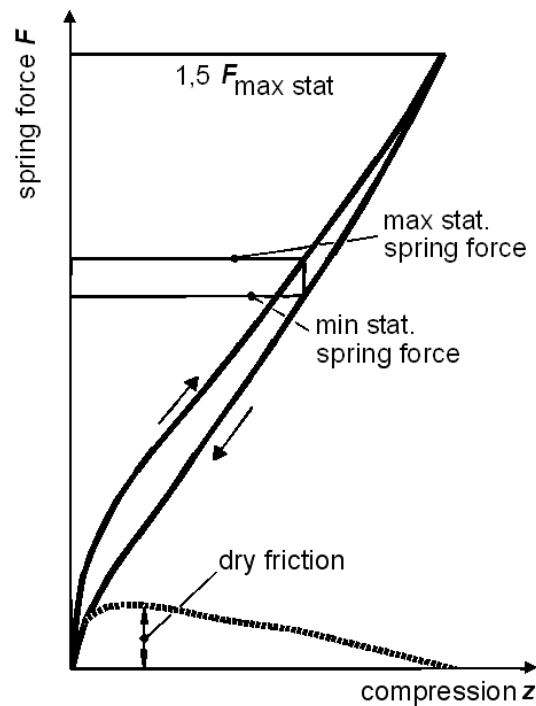


Fig. 1.3-11: Spring characteristics of a leaf spring with dry friction (rear axle of a commercial van)

The disadvantages can be moderated by the use of shackles instead of sliding shoes in the suspension or by the application of plastic layers between the spring leaves.

A small number of leaves in the spring influences the decrease of the frictional forces positively. This is possible, not by the use of additional spring leaves but by the use of stronger leaves which can withstand a higher bending force in the spring centre. This leads to a higher degree of utilisation of material. The bending stress is constant along the length of the leaf, if the spring halves indicate a parabolic profile in the longitudinal section. Leaf springs with such leaves are called parabolic springs. The development of the conventional laminated leaf spring to the parabolic spring is illustrated in Fig. 1.3-12:

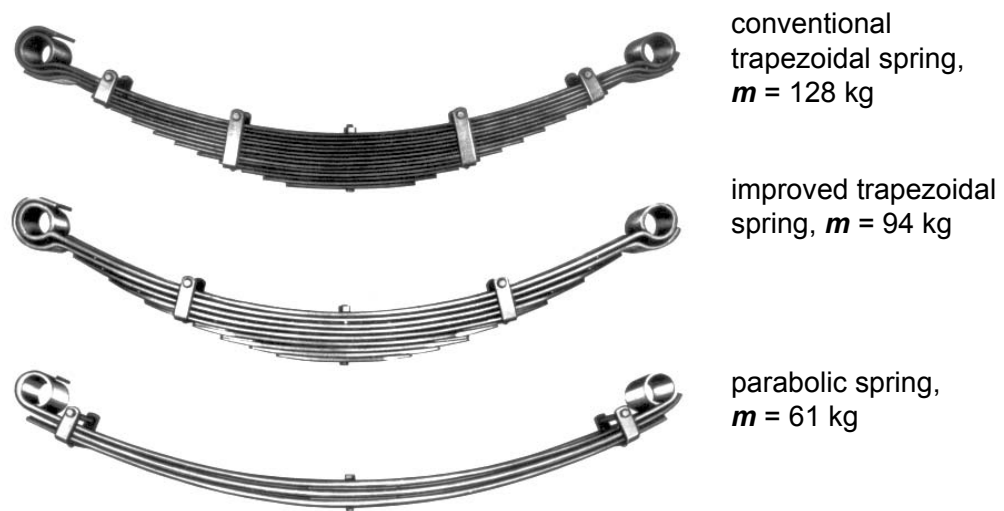


Fig. 1.3-12: Parabolic spring

These three springs have the same length, spring rate and nominal load. The advantage of the parabolic spring, apart from the decrease of friction, is the decrease of the spring weight by around 50% (minimization of the unsprung masses). The main advantage of the leaf spring is the combination of suspension and axle location, which is partially lost with the transition to parabolic springs with few leaves. During braking, the parabolic springs tend to be affected by the S-impact, which must be prevented by an additional torque support. Otherwise, changes in the running speed between the roadway and the tire can result in brake-hopping (Fig. 1.3-13).

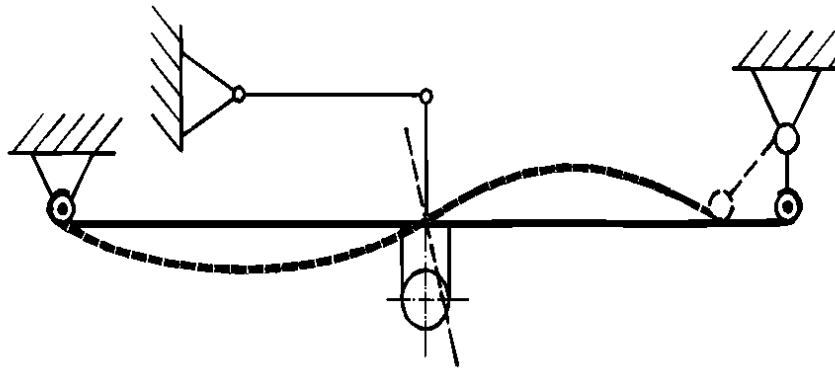


Fig. 1.3-13: Leaf spring with torque support

### 1.3.2.2 Torsion-bar Springs

Torsion-bar springs are mainly used for the suspension of passenger cars and commercial vans. Torsion-bar springs are rods made of spring steel, that are predominantly stressed by torsion. The shafts are clamped at one end and free to twist at the other, so that the shaft can be twisted flexibly by a moment acting in the direction of the axle.

For the use of torsion-bar springs as vehicle suspension elements, the elastic twist of the bar is converted into a reciprocating motion with the help of a crank, which is located to the swivelling free end and which applies the twisting moment, Fig. 1.3-14.

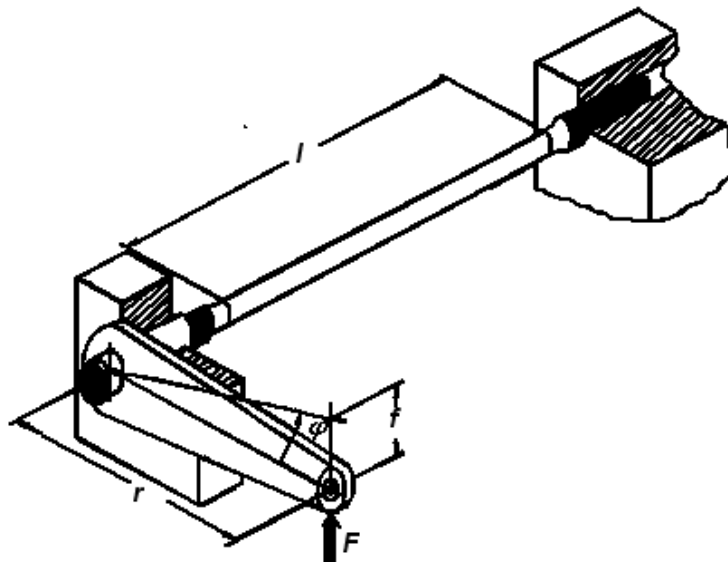


Fig. 1.3-14: Crank mechanism of a torsion bar

The strut of the axle or the suspension builds up the crank arm. The torsion-bar springs are arranged normally along the bearing axle facing the body of the strut, at the opposite end of which the vertical wheel force applies as the outside load.

Between the twisting angle  $\varphi$  and the torsional moment  $M_t$  of a torsion bar with circular cross-section, the following context exists:

$$\varphi = \frac{M_t \cdot l}{G \cdot J_p} \quad (1.3-15)$$

with  $G$ : shear modulus

$J_p$ : polar surface moment of inertia

$l$ : length of torsion bar

The polar moment of inertia of a full bar with a circular cross-section applies:

$$J_p = \frac{\pi \cdot d^4}{32} \quad (d : \text{shaft diameter}) \quad (1.3-16)$$

So the torsional stiffness  $c_{\text{tor}}$  of such a bar follows :

$$c_{\text{tor}} = \frac{G}{l} \cdot \frac{\pi \cdot d^4}{32} \quad (1.3-17)$$

Related to the crank end the spring stiffness follows approximately:

$$\Delta z \approx r \cdot \Delta \varphi$$

$$\Delta F \approx \frac{1}{r} \cdot \Delta M_t$$

$$c = \frac{\Delta F}{\Delta z} = \frac{1}{r^2} \cdot c_{\text{tor}} \quad (1.3-18)$$

While the spring characteristic of a torsion bar is linear, the effective spring stiffness at the crank end depends on the kinematics of the strut arrangement. In the equation 1.3-18 corresponding trigonometric relations have to be used for exact calculations.

At the surface of a torsion bar with circular cross section the shear stress amounts to:

$$\tau_t = \frac{16 \cdot M_t}{\pi \cdot d^3} \quad (1.3-19)$$

The torsion bar diameter  $d$  cannot be selected freely for the achievement of a suitable torsional rigidity  $c_{\text{tor}}$ . A minimum diameter has to be specified as a function of the expected maximum twisting moment and the admissible shear stress.

In practice, to achieve a suitable spring stiffness, relatively large torsion bar lengths are necessary.

Torsion bar springs are combined both with transverse and longitudinal control arms and in some cases even with semi-trailing arms. They are arranged predominantly parallel to the vehicle floor.

For front wheel suspensions torsion-bar springs are used predominantly in combination with wishbones and arranged in the vehicle's longitudinal direction, Fig. 1.3-15. With the axle shown in the picture a vertical adjustment is intended at the end of the bars.

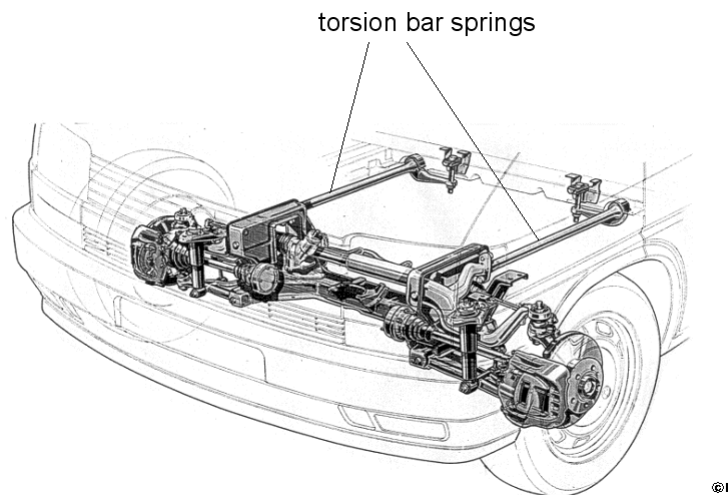


Fig. 1.3-15: Torsion-bar suspension (VW T4)

### 1.3.2.3 Coil Springs

The most common spring used in passenger cars is the coil spring. It can be imagined as a wound torsion bar. The spring material is stressed predominantly by torsion.

If you consider  $D/2$  as the lever arm of the spring force  $F$ , which affects the wound torsion bar, its value follows as half of the diameter of the coil spring ( $D/2$ ). The spring stiffness is shown in equation 1.3-18:

$$c \approx \frac{4}{D^2} \cdot c_{\text{tor}} \quad (1.3-20)$$

$$\text{with } c_{\text{tor}} = \frac{G}{l} \cdot \frac{\pi \cdot d^4}{32}$$

The total length  $l$  of the wound torsion bar follows approximately as:

$$l \approx i \cdot \pi \cdot D \quad (1.3-21)$$

with:  $i$  number of turns

So you receive the spring stiffness of a cylindrical coil spring with circular wire cross section

from Eq.1.3-20 and Eq.1.3-21:  $c \approx \frac{G \cdot d^4}{i \cdot 8 \cdot D^3}$  (1.3-22)

The normally linear characteristic of the coil spring can be changed into a progressive characteristic by the variation of the overall diameter, the wire thickness and the gradient, see Fig. 1.3-16:

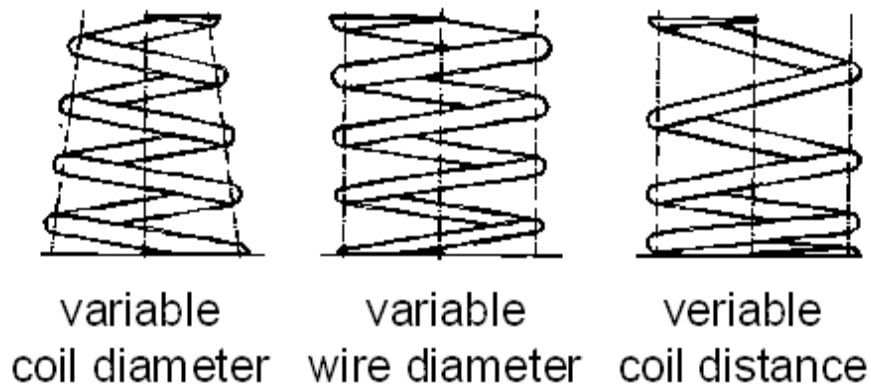


Fig. 1.3-16 Coil springs

The effect is based on the fact that with increasing spring load some of the windings are forced to contact each other, whereby the effective length  $l$  of the wound torsion bar shortens, see equation 1.3-22.

The combination of all three measures results in the so-called mini block spring, shown in Fig. 1.3-17. Apart from its progressive behavior, the mini-block spring also has the advantage of an extremely low overall height, since the coils partially lay one into another when they are stressed by load.



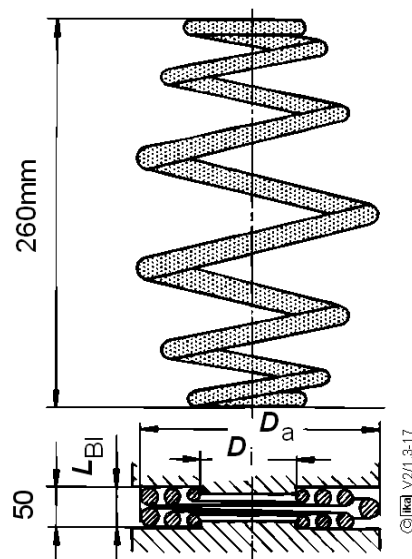


Fig. 1.3-17: Miniblock spring

Coil springs can essentially compensate higher forces towards their longitudinal axis in comparison with their transverse axis. As a consequence they are used similar to torsion bars in combination with the struts of the wheel suspension, which support the force components not portable by springs, Fig. 1.3-18.

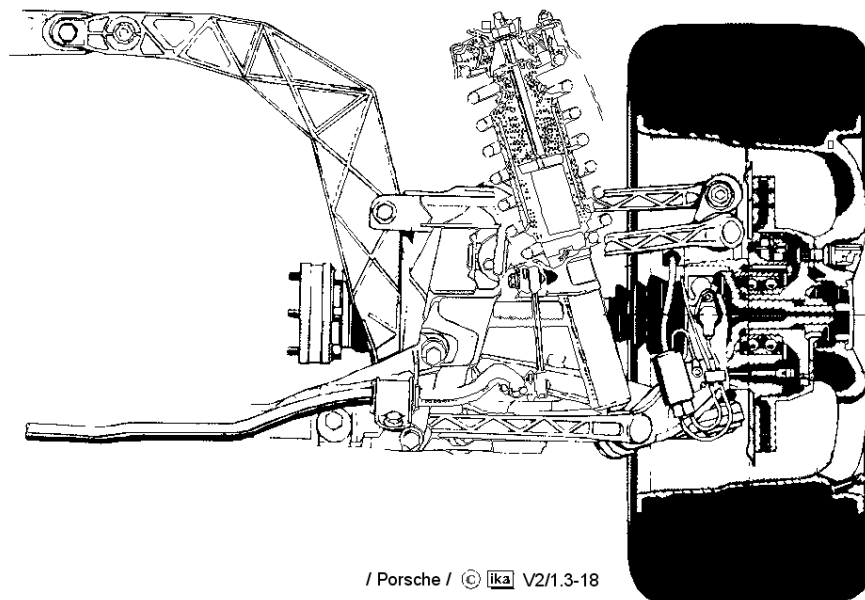


Fig. 1.3-18: LSA rear wheel suspension (Porsche 911 Carrera)

The spring is connected on the one hand with the body and on the other hand with the strut, at whose axle-facing end the wheel load acts as an external force.

Depending on the kinematics of the wheel suspension and the arrangement of the springs, there exists a ratio  $i$  for independent suspension, which is represented by the relation between the variation of the force affecting the body spring  $\Delta f$  and the displacement of the tire contact patch  $\Delta z_W$ :

$$i = \frac{\Delta f}{\Delta z_W} \quad (1.3-23)$$

The spring ratio  $i$  is usually smaller than 1 and not constant, but changes depending on the instantaneous position of the transmission components of the wheel suspension, thus dependent on the instantaneous condition of compression.

Between the wheel load  $F_W$  and the spring load  $F_S$  the following equilibrium exists with the leverage  $l$

$$F_S = \frac{F_W}{i} \quad (1.3-24).$$

By that the so-called wheel specific spring stiffness of an independent suspension for a certain compressed condition can be indicated

$$\begin{aligned} c_{\text{radbezogen}} &= \frac{dF_W}{dz_W} = \frac{d(F_F \cdot i)}{dz_W} \\ &= \frac{dF_F}{dz_W} \cdot i + \frac{di}{dz_W} \cdot F_F \\ &= \frac{dF_F}{df} \cdot \frac{df}{dz_W} \cdot i + \frac{di}{dz_W} \cdot F_F \\ &= c \cdot i^2 + \frac{di}{dz_W} \cdot F_F \end{aligned} \quad (1.3-25)$$

A progressive characteristic of the suspension can also be obtained possibly by appropriate configuration of the wheel suspension kinetics.

### 1.3.2.4 Gas Springs

With the springs regarded so far, the springing medium was solid and the spring absorbed energy by deformation. With the springs considered in this paragraph, the springing medium is gaseous and the spring absorbs energy by a variation of volume. Fig. 1.3-19 shows the structure of an air spring in principle.

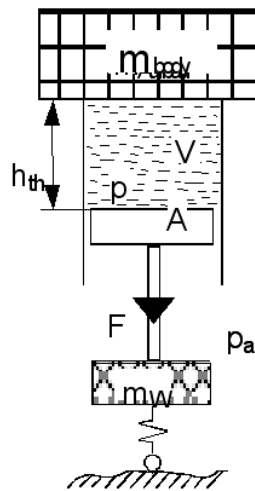


Fig. 1.3-19: Piston cylinder gas spring

The theoretical spring length  $h_{th}$  is a characteristic dimension which is given by the quotient of the active volume  $V$  (inclusive of additional volume) and the effective surface area  $A$  affected by the gas pressure:

$$h_{th} = \frac{V}{A} \quad (1.3-26)$$

The spring force  $F$  is given by

$$F = (p - p_a) \cdot A \quad (1.3-27)$$

With:  $p$ : gas pressure

$p_a$ : external pressure

Considering the gas equation  $p \cdot v^n = \text{const.}$  with  $n$  as the polytropic exponent, the spring rigidity of an air spring can be calculated from the relation:

$$c(f) = \left. \frac{dF_F}{df} \right| \quad (1.3-28)$$

$$c(f) = A \cdot n \cdot p(f) \cdot \frac{1}{h_{th}} \quad ; \quad h_{th} = \frac{V(f)}{A} \quad (1.3-29)$$

The polytropic exponent is situated between  $n=1$  (isothermal, slow spring movement) and  $n=1.4$  (adiabatic, quick spring movement). Fig. 1.3-20 shows, that with finite  $h_{th}$  the spring action changes for both quasi-static ( $F_{stat}$ ) and dynamic ( $F_{dyn}$ ) movements.

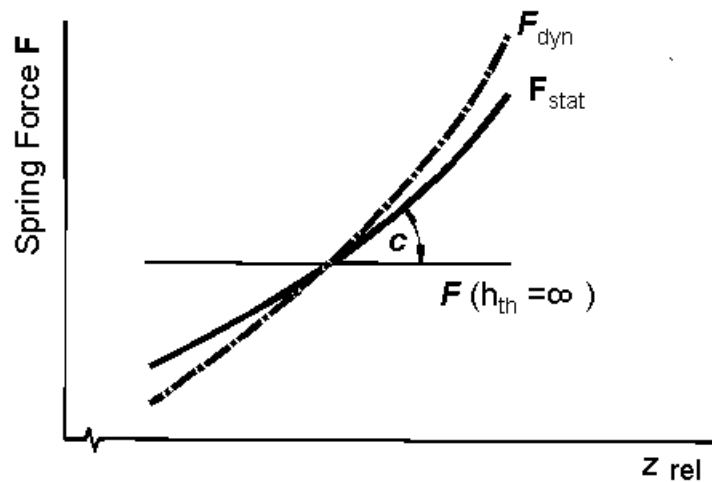


Fig. 1.3-20: Spring force in relation to the compression of a gas spring

The relation between variation of the spring force and the variation of the displacement defines the spring rigidity  $c$ . As a reference value, a line for  $h_{th} = \infty$ ,  $c = 0$  is added. A small spring rigidity (low natural frequency) requires a large  $h_{th}$ , that means a large spring volume.

The oscillation of a mass  $m$  on an air spring features the following natural frequency:

$$\omega_e = \sqrt{\frac{c}{m}} = \sqrt{\frac{c \cdot g}{(p - p_a) \cdot A}}$$

with equation 1.3-29 follows:

$$\omega_e = \sqrt{\frac{g \cdot n \cdot p}{h_{th} \cdot (p - p_a)}} \quad (1.3-30)$$

If one considers a spring ratio  $i$  (here simplifying  $di / dz_w = 0$ ), then you receive in accordance with equation 1.3-24 and equation 1.3-25:

$$\omega_e = \sqrt{\frac{c_{wheel\ rel.}}{G_w / g}} = \sqrt{\frac{g \cdot n \cdot p}{h_{th} \cdot (p - p_a)}} \quad (1.3-31)$$

With relatively small spring diameters follows:  $p \gg p_a$ . The equations for the spring rigidity and the natural frequency are simplified to:

$$c \approx \frac{g \cdot n \cdot m}{h_{th}} \quad ; \quad m \cdot g \approx p \cdot A$$

$$\omega_e = \sqrt{\frac{g \cdot n}{h_{th}}} \quad (1.3-32)$$

The theoretical piston-cylinder gas spring is used in motor vehicles only in a modified specification. In practice, gas springs are differentiated between hydro-pneumatic springs and gas bellows or u-type gas bellows.

- Hydropneumatic spring

Hydropneumatic spring elements are used by Citroen in different car types, Fig. 1.3-21.

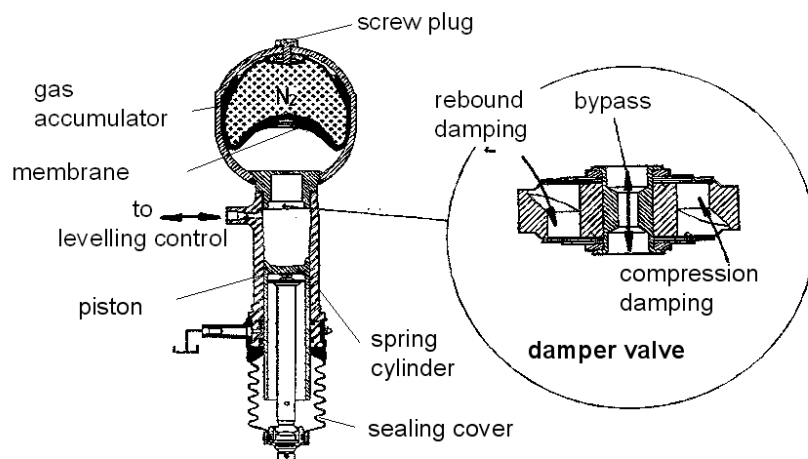


Fig. 1.3-21: Hydropneumatic spring (Citroen)

The spring action is transferred by the piston, first to a fluid and then to a gas. Fluid and gas are separated by an impermeable rubber membrane.

The presence of the fluid permits to a large extent wear-free and low-friction sealing between piston and cylinder. Additionally there is a possibility of providing the spring elements with an integrated hydraulic damper and a hydraulic level regulator. The hydro-pneumatic air spring with level control has the following characteristic:

**Gas weight = const.**

In hydro-pneumatic springs, the compression  $\Delta z$  with the increase of load is balanced only by pumping of fluid. The theoretical spring length is given by ( $A \approx \text{const.}$ ):

$$h_{th} \approx h_{th1} - \Delta f \quad (1.3-33)$$

With the change of the operating point of an air spring  $n=1$  has to be fixed. The Gas equation simplifies to

$$p_1 \cdot V_1 = p \cdot V \quad \text{with} \quad A = \text{const.}$$

$$p_1 \cdot h_{th} = p \cdot (h_{th1} - \Delta f) \quad (1.3-34)$$

The spring stiffness of a hydro-pneumatic suspension follows from equation (1.3-29):

$$c(f) \approx A \cdot n \cdot p^2(f) \cdot \frac{1}{h_{th1} \cdot p_1} \quad (1.3-35)$$

As a result, the spring stiffness increases in this case with the square of the spring load (the body mass which has to be cushioned):

$$\frac{c_{load}}{c_{empty}} > \frac{F_{load}}{F_{empty}} = \frac{m_{load}}{m_{empty}} \quad (1.3-36)$$

By the compression-conditioned decrease of  $h_{th}$  the natural frequency of the structure oscillations rises with the increasing load.

Hydro-pneumatic spring elements are used predominantly at the rear axle of vans, estate cars and heavy limousines, since they enable an effective level control. Also partially carrying installations are used in combination with steel springs (parallel connection), Fig. 1.3-22. The advantage of this combination consists of the fact that setting the natural frequencies of the two spring types against each other leads finally to a suspension with an almost constant natural frequency.

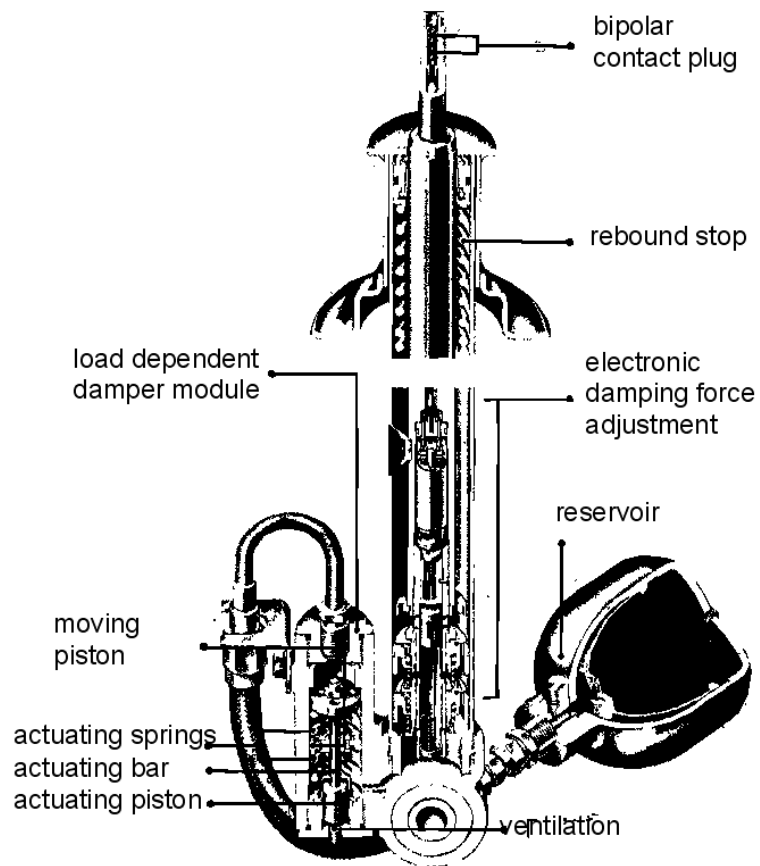


Fig. 1.3-22: Partially carrying spring cylinder with hydraulic level regulation and adjustable damping (Sachs)

- Gas spring bellows

Fig. 1.3-23 shows the two designs of bellows, the gas spring bellow and the U-type bellow. The gas spring bellow is composed, similar to a pneumatic tire, of rubber material reinforced by textile fabric.

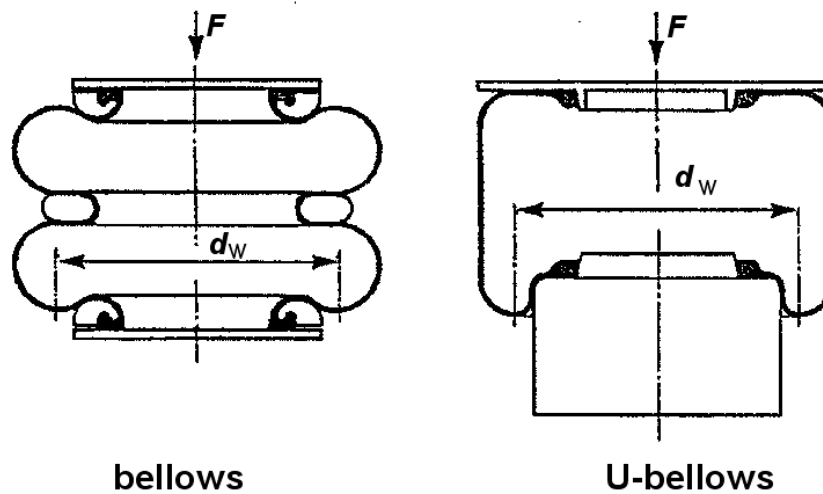


Fig. 1.3-23: Gas spring bellows

The surface area of the pneumatic spring affected by the positive pressure, which entails a force to the vehicle structure, is called effective surface area  $A_w$ . In contrast to the hydro-pneumatic gas spring mentioned above, the effective surface area  $A_w$  of the gas spring bellows changes proportionally to its travel. In Fig.1.3-23, the effective surface area is represented by the effective diameter  $d_w$  for both designs.

The load carrying capacity of the spring is determined from the product of positive pressure and effective surface area. In the particular case of the U-type bellows the possibility of a direct influencing control is given, because the effective surface is defined by the outer contour of the piston, Fig. 1.3-24 and Fig. 1.3-25.



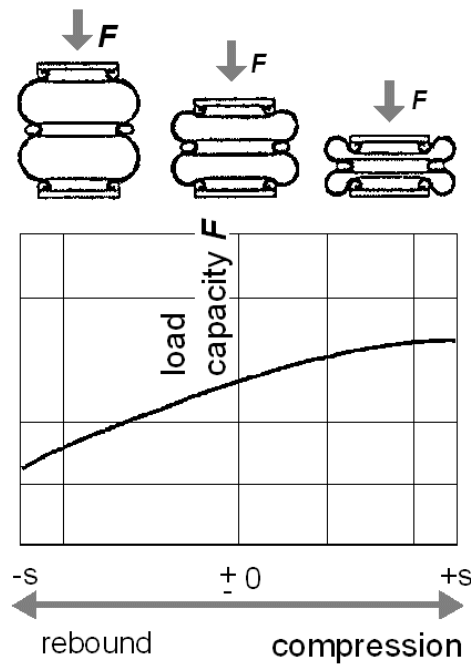


Fig. 1.3-24: Characteristics of the load capacity of an air spring bellow

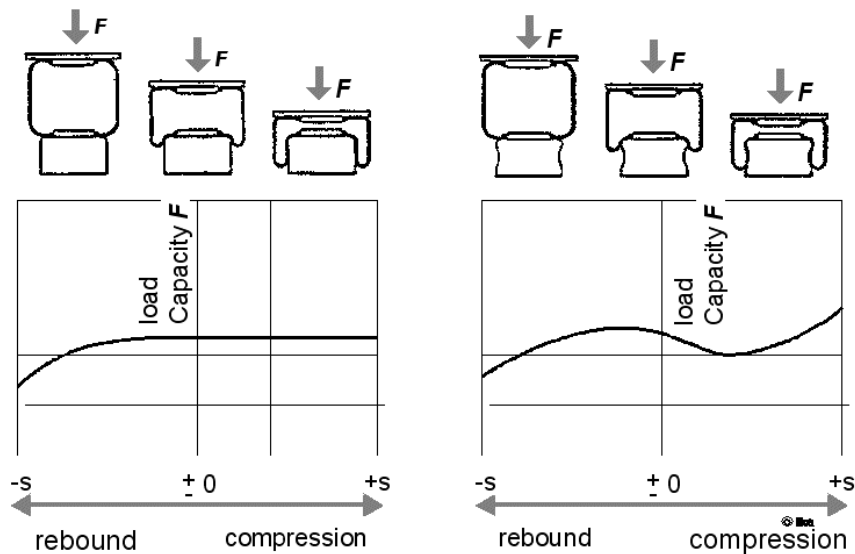


Fig. 1.3-25: Characteristics of air springs with u bellows

Besides, the general possibility exists of implementing an additional volume formed by an air chamber (increase of  $h_{th}$ ) to realise a less progressive spring rate.

Also gas spring bellows enable a level control of the vehicle bodywork with increasing load. The spring compression by a static load is balanced by the additional pumping of gas. So the

theoretical spring length  $h_{th}$  remains constant. The feature of a gas spring bellow with pneumatic regulation is therefore:

**Gas volume = const.**

Thus, for the spring stiffness of a gas spring bellow applies:

$$c(f) = A \cdot n \cdot p(f) \cdot \frac{1}{h_{th}} \quad (1.3-37)$$

In this case, the spring stiffness is directly proportional to the spring load:

$$\frac{c_{bel}}{c_{leer}} = \frac{F_{bel}}{F_{leer}} = \frac{m_{bel}}{m_{leer}} \quad (1.3-38)$$

As a consequence, the natural frequency of the body oscillation does not change here with loading ( $h_{th} = \text{const.} \Rightarrow \omega_e = \text{const.}$ ).

Gas springs (in most cases U-type bellows) are mainly used in buses (constant entrance height) and trucks (high additional load compared to the dead weight). A spring element with fully carrying pneumatic U-type bellow for a passenger car is shown in Fig. 1.3-26.

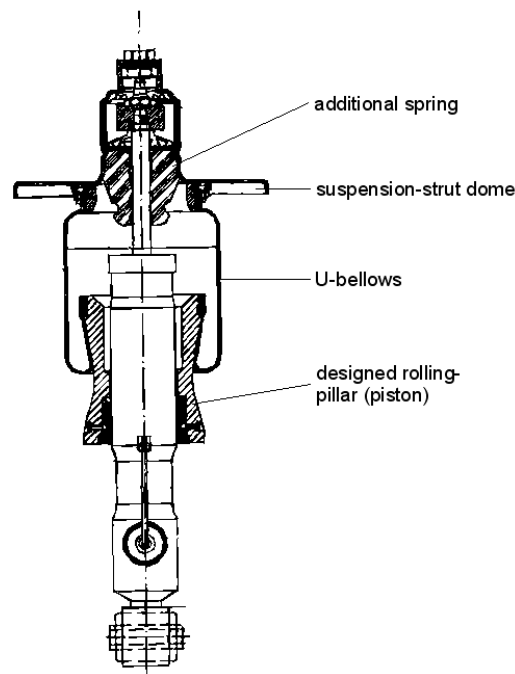


Fig. 1.3-26: Gas spring and damper unit with U-type bellow

Apart from a level control in this case an infinitely variable pneumatic damping control is implemented (soft characteristic favourable for travelling comfort, stiff characteristic favourable for driving stability).

The defined outline of the rolling piston influences the spring characteristic by a variation of the effective surface area  $A_w$ . Additionally, the auxiliary spring (bumper) causes a highly progressive behavior of the spring characteristic in compression.

The responsiveness of the pneumatic spring is influenced particularly by the orientation of the spring bellow cord angle. Drastic improvements result, if the resistance carrier is arranged axially to the spring direction. However this orientation of cords requires an outside guidance of the pneumatic spring bellow implemented by the use of a supporting tube, in order to be able to compensate tangential forces. A final overview about the most important features of steel springs and pneumatic springs is given in the fig.1.3-27 and 28.

### **Steel spring**

#### 1.) Driving comfort (Fig. 1.3-27)

The driving comfort changes in order to the loading condition. The driving comfort is measured as the natural frequency and is proportional to  $c/F$  and changes with const. spring stiffness  $c$  and variable load  $F$ .

#### 2.) Total spring travel (Fig. 1.3-28)

The total spring travel results from the addition of the static and the dynamic compression:

$$S = S_{\text{stat}} + S_{\text{dyn}}$$

A steel spring cannot be dimensioned any soft, since the total spring travel would be too large. For this, the necessary space is not available in the wheel housing. The driving comfort however is directly proportional the spring softness.

#### 3.) Level control

Due to static compression, a steel spring suspended vehicle has different body level positions dependent on the loading status.

#### 4.) Space requirement

Modern design methods of coil springs cause an ever decreasing space requirement. The overall height is minimized to a small number of coil diameters by the use of spiral coil springs.

## **Air spring**

### 1.) Driving comfort

The travelling comfort remains almost constant, independent of the load. With constant effective surface area, the natural frequency is proportional  $p/p_0$

### 2.) Total spring travel

The total spring travel results as:  $s_{\text{tat}} = s_{\text{dyn}}$ .

The static spring travel's value is zero, since, depending upon load the air pressure is varied with constant vehicle height. So the pneumatic suspension can be dimensioned more softly than the steel spring suspension.

### 3.) Level control

An air-suspended vehicle has a constant level position due to the loss of the static compression.

### 4.) Space requirement

U-Type bellows air springs always require additional components (covers and rolling pistons). In this case, the length of the rolling piston is proportional to the half of the pneumatic spring's travel. The block dimension of the pneumatic spring corresponds to the height of its components.

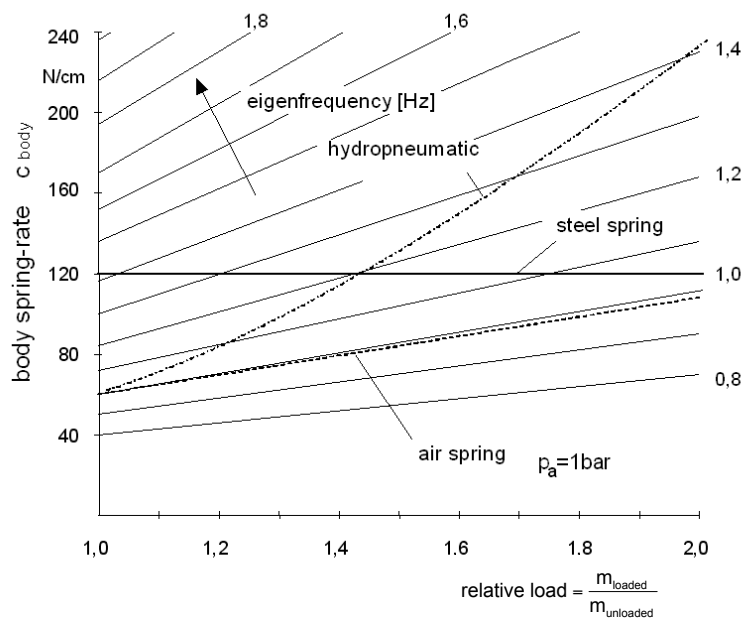


Fig 1.3-27: Natural frequencies of different suspension systems dependent on the additional load

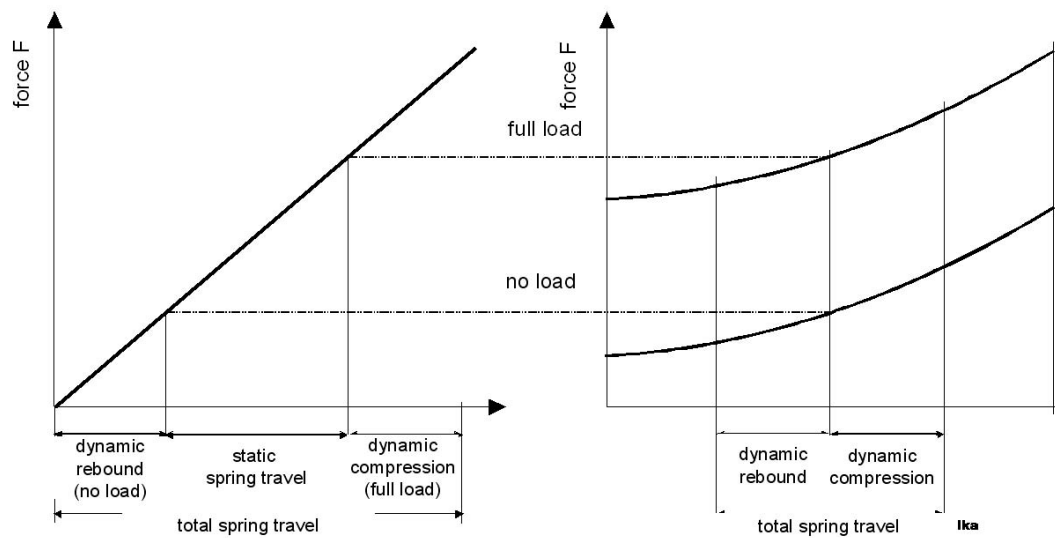


Fig 1.3-28: Differences between steel and air springs

### 1.3.3 Vibration Dampers

Vibration dampers serve both to guarantee driving safety of a vehicle and to optimise the travelling comfort (Fig. 1.3-29).

Driving safety is highly influenced by the road grip of the wheels. Oscillations of the wheel masses, which are also called unsprung masses together with the proportionate masses of the wheel suspension components, have to be minimised by damping, because they are suspended only by the tire spring but not by the vehicle body suspension ( $c_R \gg c_A$ ).

A satisfactory driving comfort requires on the one hand, that the amplitudes of the body oscillations are small, and on the other hand, that the body accelerations which are induced by the damping forces are as small as possible. This implies a rather weak damping.

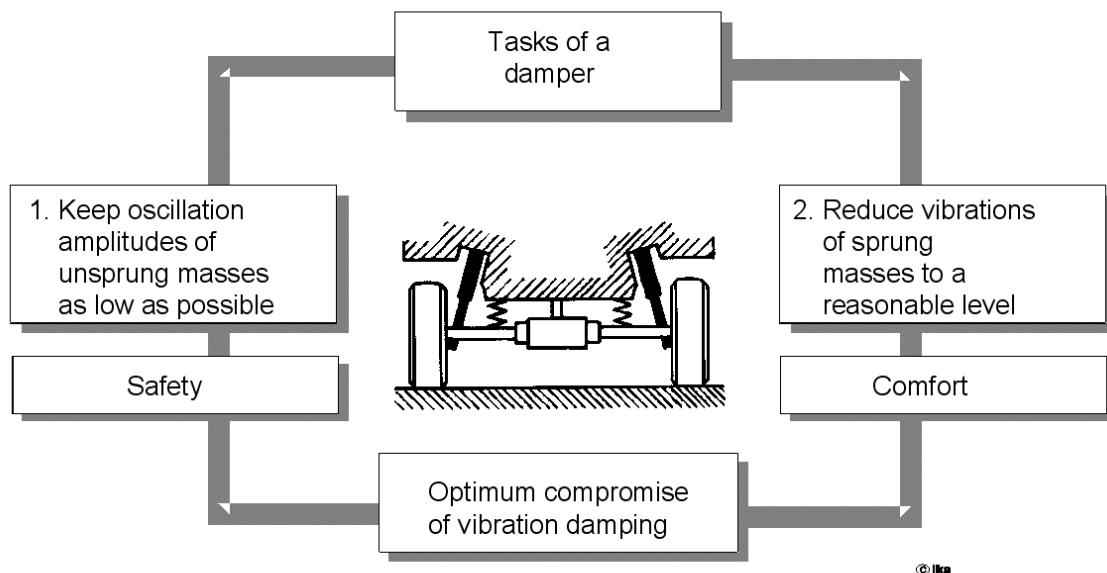


Fig. 1.3-29: Functions of the shock absorber

During the selection of a damper therefore a compromise between hard damping for safety and a soft damping for comfort has to be implemented.

Vibration dampers or shock absorbers differ basically in the type of friction, which causes the transformation of oscillation energy into heat, Fig. 1.3-30.

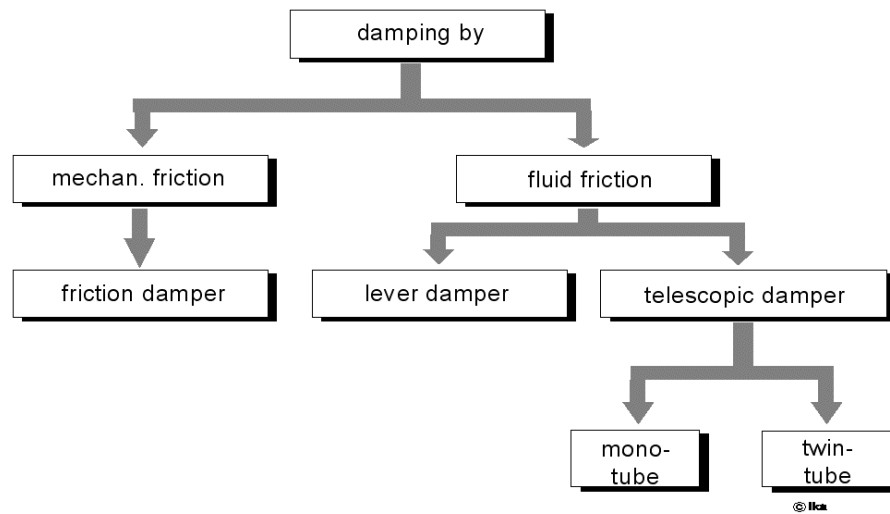


Fig. 1.3-30: Different damper designs

While shock absorbers of vehicles in the 20s and the 30s operated with mechanical friction, liquid dampers became generally accepted in the course of development, since the exponential relationship between damping force and the spring rate given renders a better adaptation of the absorption characteristics to the vibratory vehicle system. It enables an asymmetrical configuration of rebound and compression stage at relatively small effort and predominantly, these dampers show a better responsiveness (damper force application at very low compression speeds).

The first shock absorbers based on liquid friction were the lever absorbers. In these absorbers oil is pressed through a valve by a piston which is moved by a lever, that is often applied as a transverse arm. This type of damper is rarely used nowadays. Today, there are almost exclusively used telescopic shock absorbers.

Apart from the omission of wearing parts such as levers, bearings and operating cams, these dampers indicate the advantage of the possibility of a more precise adjustments in absorption in comparison to lever-type dampers, since spring travel and plunger lift mostly correspond. Due to the large plunger lift the liquid recirculation is bigger. The direct absorber can therefore operate with a much lower pressure (compared with the lever absorber), which facilitates the design of the absorber valves and has a favourable effect on its life span.

The telescopic absorbers can be differentiated into mono tube and twin-tube dampers. Fig. 1.3-31 shows the configuration and principle of the two absorber systems:

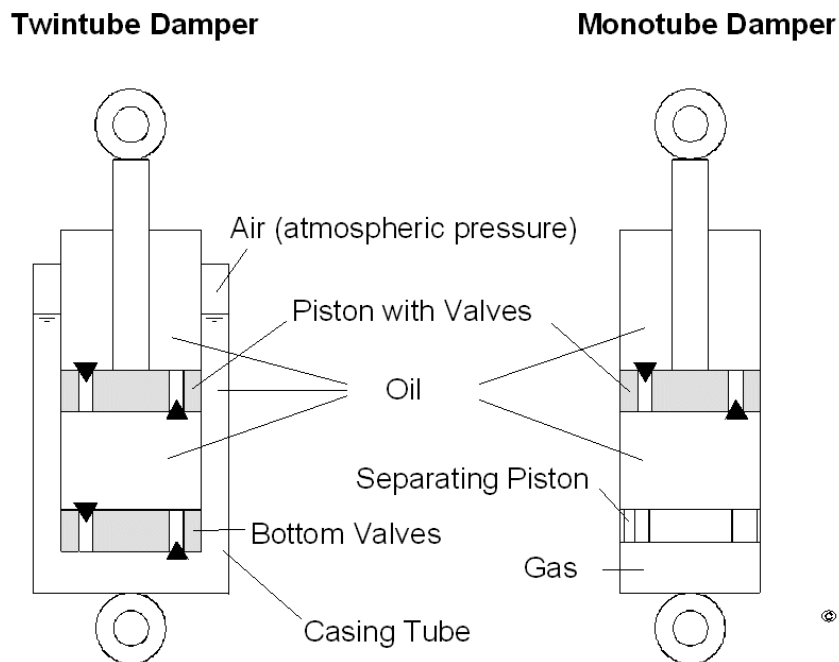


Fig. 1.3-31: General assembly of different damper designs

In types of absorbers there is a piston moving in a cylinder filled with liquid while overcoming the flow resistance, which features throttling elements. The absorbed mechanical labour is converted into heat and transferred to the environment over the absorber's external tube. If the absorber surface is not large enough for the heat dissipation, the surface must be enlarged. Otherwise the absorber would overheat, which could cause damage to the rubber parts.

In the conventional twin tube absorber, the liquid volume displaced by the immersing piston rod is pressed through the bottom valve into the casing tube which serves as the compensational volume and re-aspirated when the piston rod exits again. In the rest condition the liquid pressure is equal to the ambient pressure.

In order to suppress cavitation occurrences at the valves, considerable absorption work can be achieved by those oil flows, which are not aspirated into an enlarging part of the working room.

During the compression of the twin-tube absorber, most of the absorption work is achieved by the oil flow that is pressed through the bottom valve into the casing tube due to the intrusion of the piston rod. The other oil flow is leading into the upper part of the working room without any resistance.

On the other hand, during the dilatation of the conventional twin-tube absorber, the absorption work is compensated by the oil flow, which is leading through the piston valve



from the upper part of the working room to the lower part of the working room. Accordingly, the oil flow that is running back from the compensational volume due to the returning piston rod, is not prevented by any resistance.

In the mono tube absorber, the liquid volume displaced by the piston rod is compensated by compressing a gas volume included in the absorber. This gas volume is either above the surface of the oil and is separated from the hydraulic oil by an impact plate, or is separated from the oil volume by a dividing piston, if the gas is placed in the lower part of the absorber.

The gas force exerted on the absorber piston surface by the gas pressure must be bigger than the maximum damping force, as otherwise the gas volume would be compressed with sudden movement of the piston, while in the part of the absorber work space facing the gas volume, the pressure would drop to 0 bar. With sudden reversal of the direction of the piston rod movement, this would cause a brief breakdown of the absorber and cavitation in the area near to the piston valves. The gas pressure usually amounts to 30-40 bar. The gas pressure acting on the cross section of the piston rod results in a driving out force of the piston rod, which must be considered during the design procedure of the body suspension.

The advantage of the twin tube absorber is its cost and its life span, while the tendency towards cavitation, unfavourable heat dissipation, its relatively large diameter and the fact that it can generally be installed only perpendicularly or pettily inclined, are the disadvantages.

The main disadvantage of the mono tube absorber in comparison to the twin tube absorber is the fact that the precision required in production makes it more expensive and that its life span may be shorter because of the critical piston rod sealing.

- Examples of design

The constructional design of the telescopic absorbers are different from one manufacturer to another, but also in addition to the field of application.

Fig. 1.3-30 shows a telescopic damper designed according to the principle developed by De Carbon in the 40s. A dividing piston separates the gas volume from the in order to prevent the foaming of the oil.

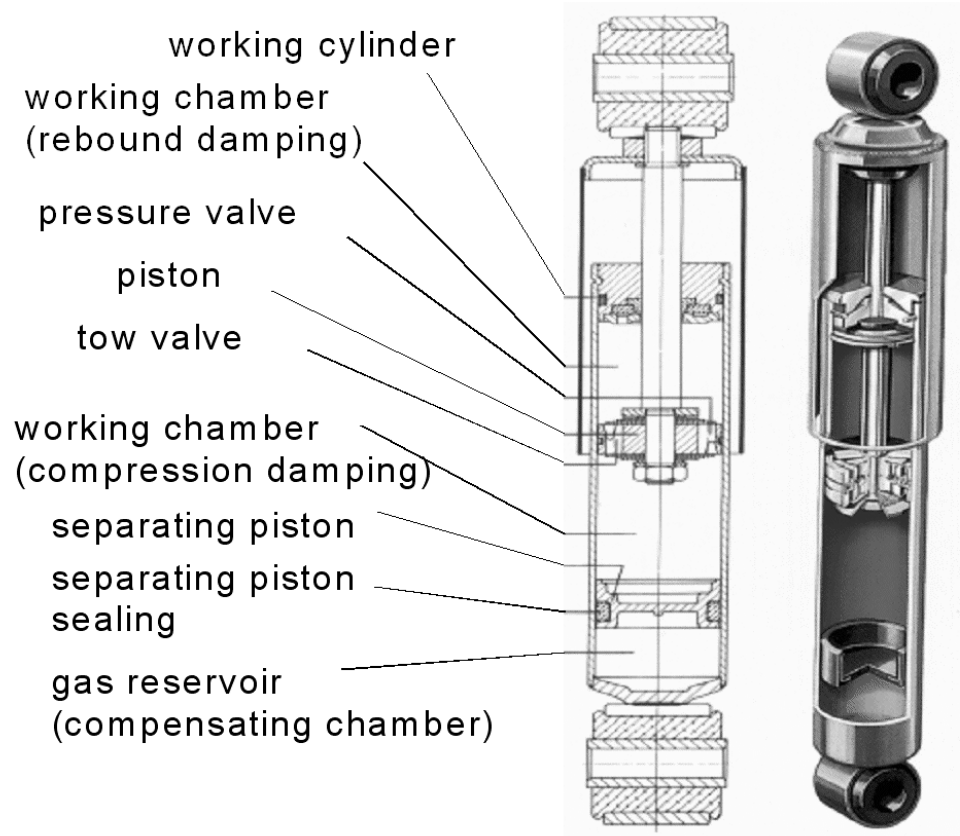


Fig. 1.3-32: Example of a mono tube absorber

This dividing piston enables any arbitrary position of installation, but it does not influence the function of the absorber. The foaming of oil and gas can also be prevented by other measures. For example, an impact disk already reduces the foaming of oil and gas, by deviating and decelerating the high speed oil jets escaping from the piston valves and rushing up the cylinder wall.

A sectional view of the twin tube absorber is shown in Fig. 1.3-31. The working volume, in which the piston moves, is totally filled up with oil, and the storage volume between the working cylinder and the container pipe is filled with oil up to an amount of  $2/3$ . This tube space serves as balancing volume for the oil displaced by the immersing piston rod. The absorption valves - base valves and piston valves - consist of a system of spring washers and valve bodies with throttle bores. The valves are held in position against the valve seat by a weak coil spring and can also execute the function of a non return valve at the same time.

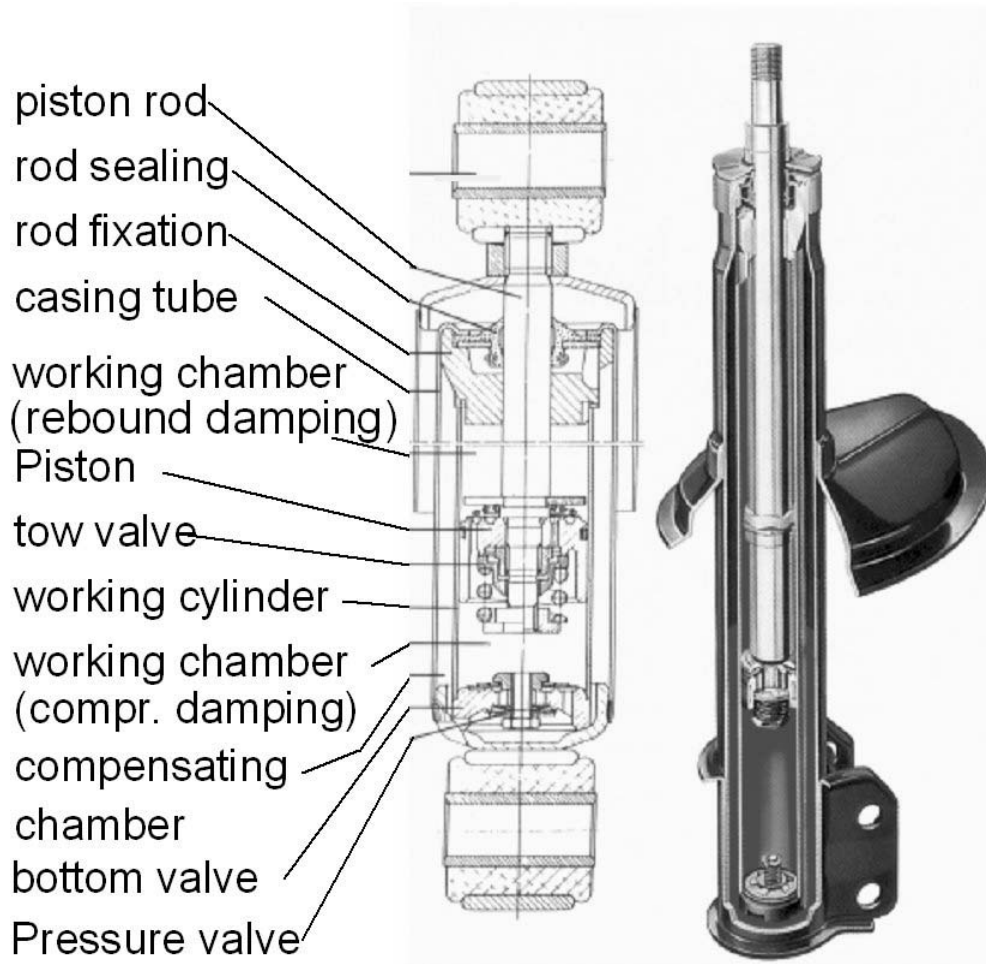


Fig. 1.3-33: Design of a twin tube absorber

The gas pressure twin tube absorber was developed specially for the application in suspension struts. With spring suspension and shock absorber strut wheel suspensions, the piston rod of the absorber is not only used for the transfer of the absorber forces, but also for wheel control at the same time. In order to keep a deflection of the piston rod caused by the transverse forces within limits, larger piston rod diameters ( $\sim 25$  mm) are necessary compared to absorbers or spring carriers exclusively stressed by expansion and compression ( $\sim 12$  mm).

Accordingly, during retracting and emerging the piston rod, the oil volumes flowing from the work space to the balancing volume and the other way round are also bigger. For this fact, the danger of cavitation at the non return valves in the piston and at the base of the absorber becomes bigger too. This leads to a brief breakdown of the absorber. A significant improvement of the operational behavior of these absorbers could be obtained if the oil reservoir is exposed to a relatively small gas pressure (usually 6-8 bar).

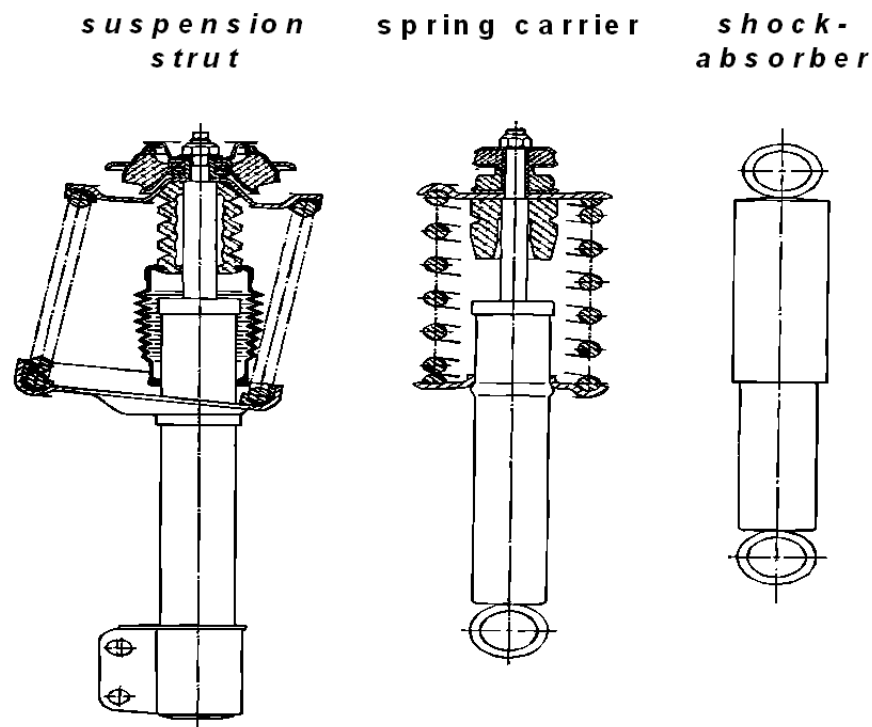


Fig. 1.3-34: Typical designs of absorbers

By that, one receives an exact function of the absorber without having to accept the disadvantage of a mono tube absorber, that the response of the absorber is impaired by the clamping friction due to the piston rod seal which has to be dimensioned with high surface pressing because of the high internal pressure.

- Operational behavior and damper characteristics

As previously mentioned, the absorbers used today operate based on hydraulics without any exception. The damping force  $F_D$  is a function of the compression velocity, and so follows the relation:

$$F_D = -\text{sign}(\dot{z}_{\text{rel}}) \cdot k \cdot |\dot{z}_{\text{rel}}|^n \quad (1.3-39)$$

with :

n absorption exponent

k absorption factor

“sign ( $\dot{z}_{\text{rel}}$ )” indicates the direction of the absorber force. The absorber characteristics describe the functional relation between the absorber force and compression velocity. For the determination of the absorber characteristics of an implemented absorber, the absorber forces can be measured on a testing machine with a pushing crank mechanism at constant

travel and varying test speeds, that cause different max. piston speeds in each case, Fig. 1.3-33.

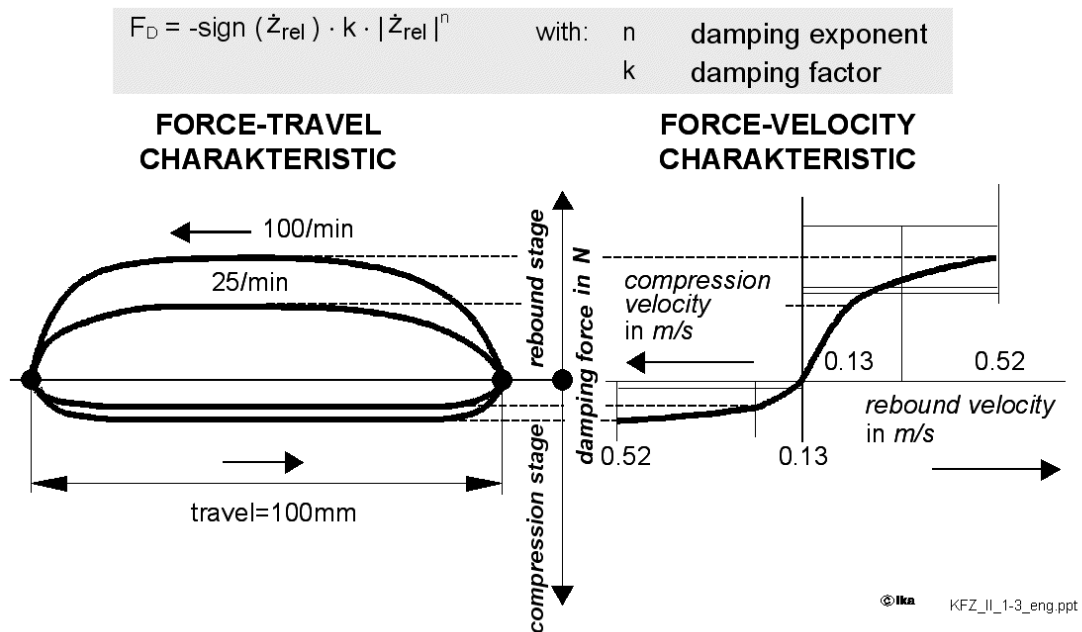


Fig. 1.3-35: Damper work chart of the absorber operation for the determination of the absorber characteristics

For scheduling the absorber characteristics, the max. traction and thrust forces are registered as functions of the max. piston speed.

The sequence chart is closely coupled with the absorber characteristics. Fig. 1.3-36 shows the possible cases of design.

The degressive process characteristics “3” has to be assigned to the sequence chart with the largest surface, and so the dimensioning indicates the highest mean absorption. In comparison of “3” to the designs “1” and “2”, its gradient at the zero point is higher, which indicates a relatively large damping force with small piston speeds. This has an unfavourable effect on the absorption capacity of the suspension on small unevenness, which however brings certain advantages concerning the roll and pitch absorption.

The progressive absorption “1” has the advantage that the forces around the zero point are small and so, favours a smooth rolling comfort, even for hard tires. The piston forces, significantly rising with higher piston speeds, cause an increase of wheel and body absorption, which positively affects the contact to the ground on bad road surfaces.

The mean absorption is smaller than in the case of the degressive dimensioning “3”, as shown in the sequence chart.

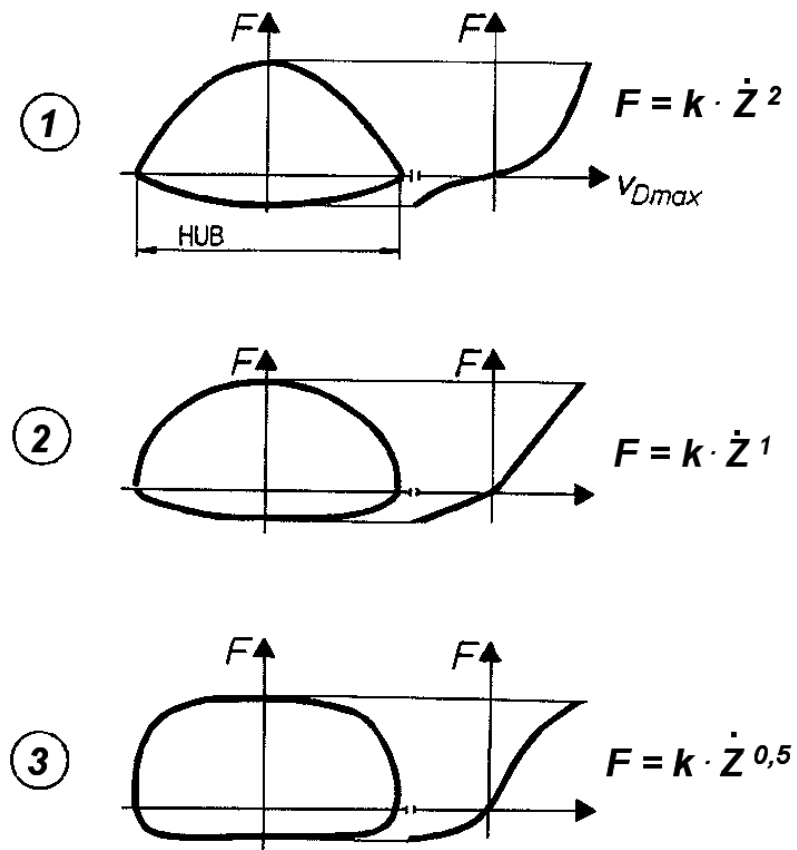


Fig. 1.3-36: Damper force depending on relative velocity at different damping coefficients

The relation between expansion and compression stage is different depending on the manufacturer and the targeted application of the vehicle. Fig. 1.3-37 shows the influence of the damper layout on the wheel load fluctuations.

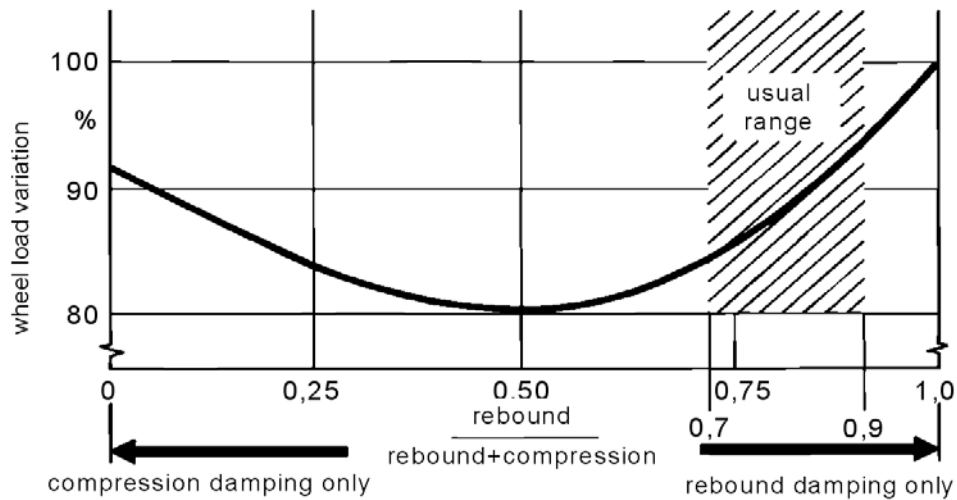


Fig. 1.3-37: Influence of damper layout on wheel load variation

A relation between rebound and compression stage of 1 enforces axle oscillations to fade away very quickly. The wheel load fluctuations achieve a minimum for this tuning, which means a better road grip of the wheels. This layout is however not favourable regarding the suspension comfort.

Both the relation between rebound and compression stage and the absolute magnitude of the absorber constant "k" are usually investigated based on tests. With that, an optimum damper design is determined for the spectrum of the possible loading conditions of a vehicle and for all possible road surfaces .

In order to reduce the conflicting aims between a high driving safety and max. attainable comfort as far as possible, some vehicles are provided with an adjustable chassis absorption.

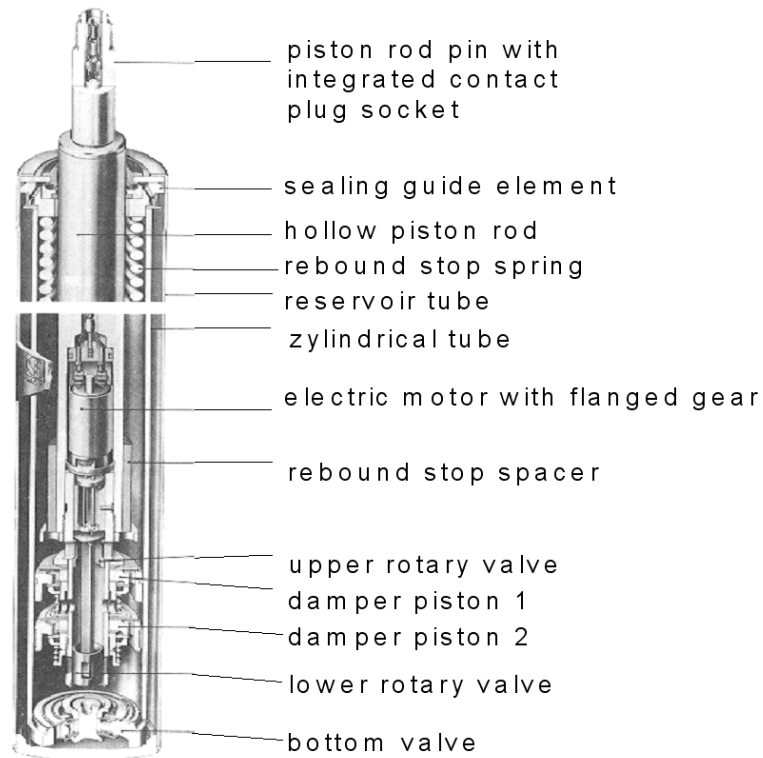


Fig. 1.3-38: Double piston absorber with discontinuously variable absorber characteristics

The main parts are a couple piston and a direct current motor placed in the hollow piston rod. This motor actuates two rotary valves situated in the piston rod, which are both equipped with individual piston valves. By that, two independent characteristics are realizable, Fig. 1.3-39. In order to make the adjustment in rebound and compression direction effective, a spring loaded check valve is assigned to each rotary valve for the rebound stage and a soft one for the compression stage.



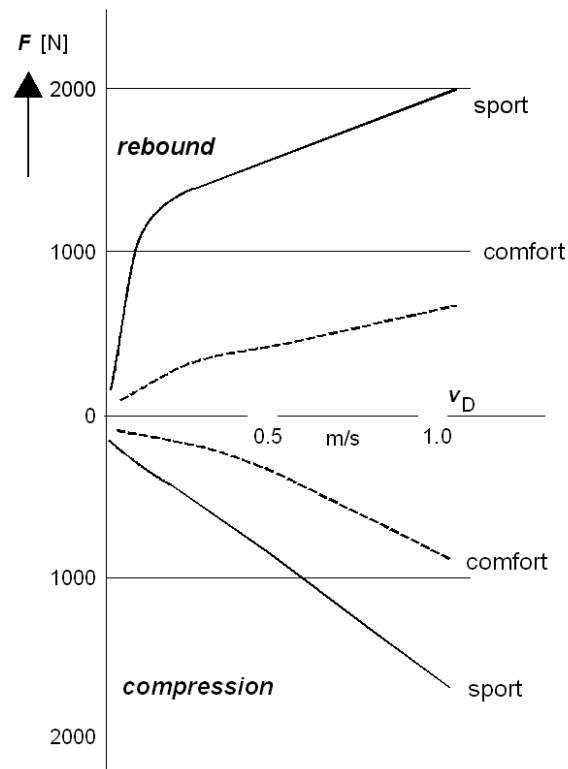


Fig. 1.3-39: Absorber characteristics with the adjustments 'Sport' and 'Comfort'

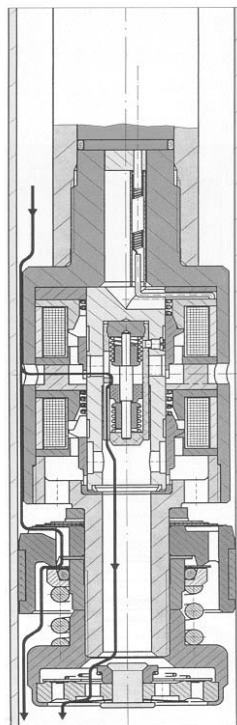


Fig. 1.3-40: Adjustable absorber with switching valves at the inside

The adjustment times for the ADC-1 system are in a time range of 30-200 ms, which does not permit reacting to single obstacles. Adjustable absorbers with switching valves at the inside enable significantly shorter switching times (20-100 ms) and also a reaction on single obstacles in a limited extend. Fig. 1.3-40 shows an adjustment system fully integrated in the absorber. The control of the piston valves is performed by electromagnets (solenoid valves).

Continuously adjustable absorbers without fixed characteristics which could be implemented by proportional valves, for example, are still in the development stage at present.

### 1.3.4 Seats

Spring-cushioned seats originally have only one function, the 'upholstery'. With humans placed on it, the seat forms an oscillatory system, whose natural frequency is in the range of 2,5 – 5 Hz, depending on the spring rigidity of the bolster, Fig. 1.3-41.

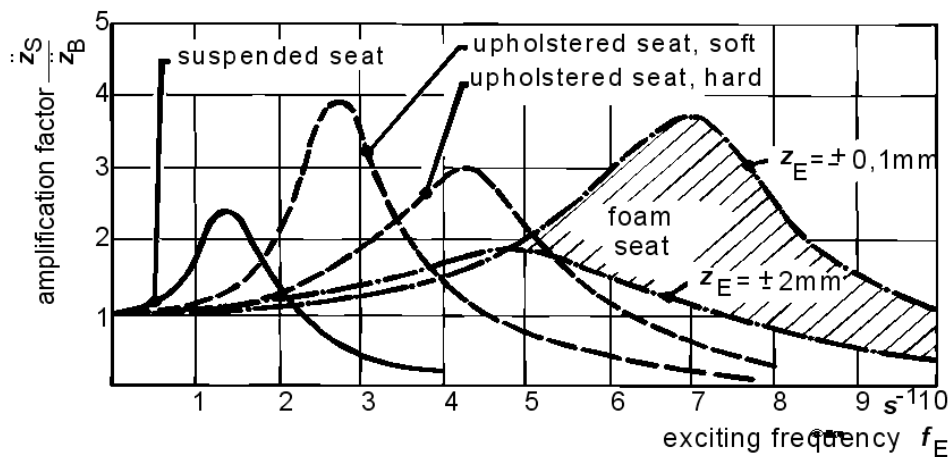


Fig. 1.3-41: Amplification functions of different vehicle seats

The location of increased resonance between seat ( $\ddot{z}_S$ ) and body acceleration ( $\ddot{z}_A$ ) of  $\frac{\ddot{z}_S}{\ddot{z}_A} > 3$  may reduce the suspension comfort significantly, in particular, if the body natural frequency is high, as in case of construction machines, agricultural tractors and partly of trucks, since body and seat resonance frequency are close to each other in this case. A remedy can be obtained here by the application of suspended seats, Fig. 1.3-42.



Fig. 1.3-42: Suspended seat

### 1.3.5 Evaluation of Oscillations by Humans

The quantitative evaluation of the oscillation comfort requires a standard level for oscillation exposure (and a reference road). For this, serial investigations have led to the guidelines VDI 2057 and ISO 2631. In these guidelines, there exists a difference between the perception intensity and the duration of exposure.

- Perception intensity of sitting humans

The human body represents an oscillatory system, which can be approximated by a backup system for humans sitting in the vehicle according to Fig.1.3-43.

Since humans are oscillatory systems themselves, it is impossible for them to evaluate the effects of oscillation only by their intensity, but they tend to perceive oscillations of the same intensity but of different frequencies variably. As a consequence, there exists a frequency-dependent evaluation between the physically measured values and subjective perception, which is different for individual parts of the body and different directions of action.

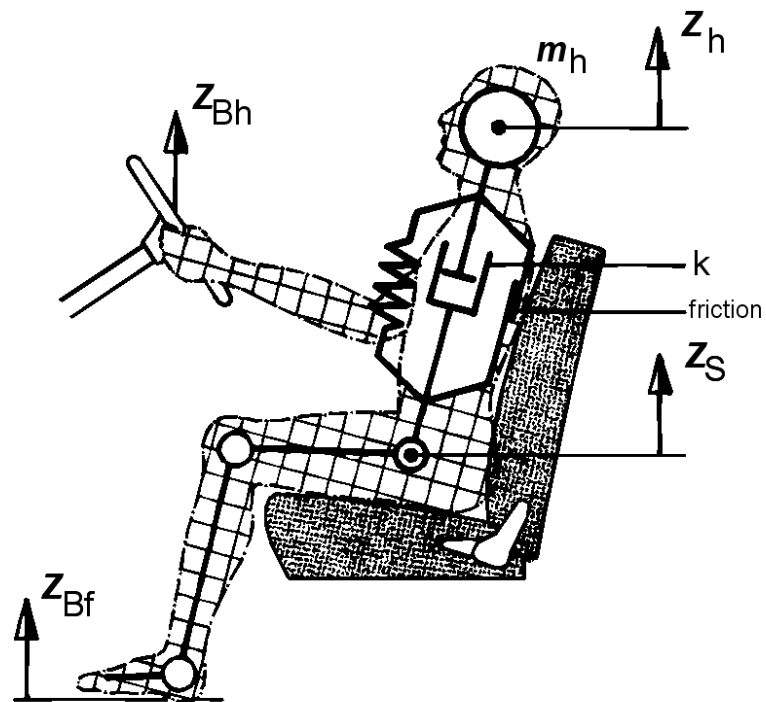


Fig. 1.3-43: Backup system of a seated person

If one considers at first only the excitation of the body by the seat and if the average friction  $R$  occurring in the bolster between back and backrest is added to the velocity-dependent absorption, then the following results are given for this simple damped oscillator due to appropriate tests with different test persons:

$$f_e \approx 5s - 1, D \approx 0,45$$

and the appropriate amplification function, see Fig. 1.3-44.

$$V = z_k(f)/z_s(f) \quad (1.3-40)$$

or, for sinusoidal vibration simulation:

$$V = \ddot{z}_k(f)/\ddot{z}_s(f) \quad (1.3-41)$$

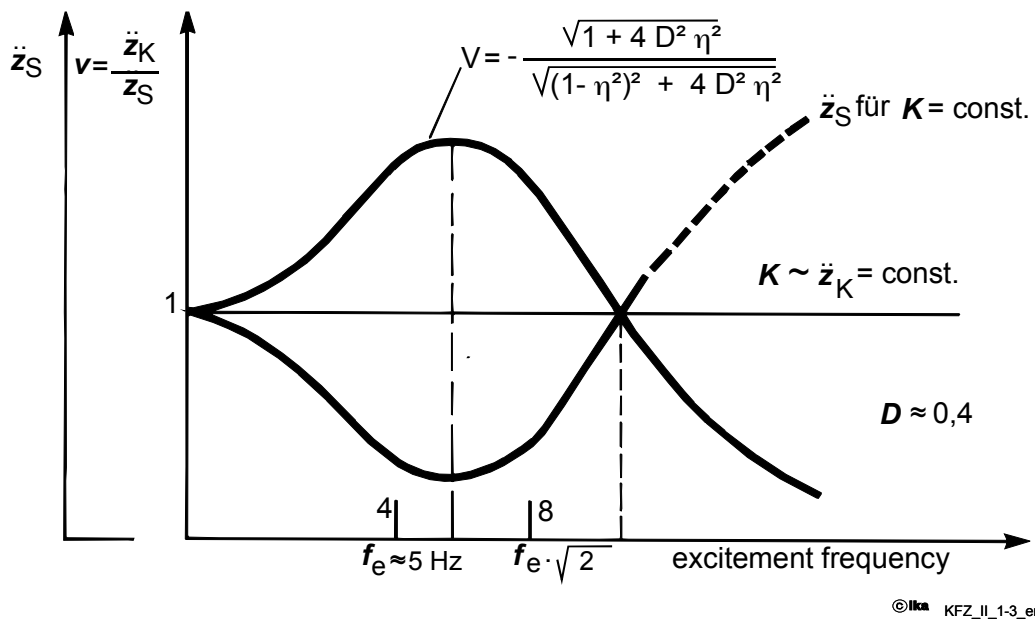


Fig. 1.3-44: Amplification function of head acceleration during vertical excitation of seat

If the vertical acceleration of the head  $\ddot{z}_k$  is considered as a measure for the perception intensity, then you will receive for the perception intensity:

$$K \approx \ddot{z}_k(f) = V(f) \cdot \ddot{z}_s(f) \quad (1.3-42)$$

with the amplification function  $V$  for a simple oscillator follows:

$$K \approx \ddot{z}_s \cdot \frac{\sqrt{1 + 4 D^2 \eta^2}}{\sqrt{(1 - \eta^2)^2 + 4 D^2 \eta^2}} \quad (1.3-43)$$

$$\text{with: } \eta = \frac{f}{f_e}$$

This entails the excitation  $\ddot{z}_s(f)$ , which leads to a constant perception intensity  $K^*$ :

$$\ddot{z}_s(f) \approx \frac{1}{V(f)} \quad (\text{for } K^* = \text{const.}) \quad (1.3-44)$$

Fig. 1.3-45 shows the curves of equal perception intensity determined for sitting and standing humans in the VDI specification 2057. For comparison, the reciprocal amplification function (eq. 1.3-44) is included.

The curves are divided into three areas, which were linearised for the simplification of the analysis.

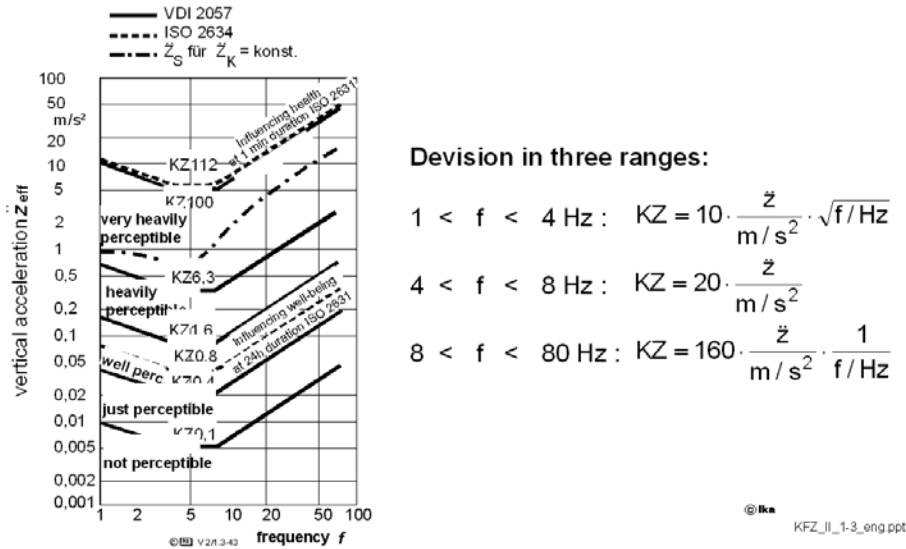


Fig. 1.3-45: Curves of equal perception intensity KZ of sitting and standing humans according to VDI 2057 and ISO 2631.

Since all investigations done up to now show a correspondence in the fact that the perception of humans begins at approx. 0.8 to 1 Hz and ends at approx. 70 to 100 Hz, the curves are applied in a frequency range between 1 and 80 Hz. The first segment of the curve is from 1 to 4 Hz. Within this segment the KZ values are calculated as follows:

$$KZ = 10 \cdot \frac{\ddot{z}}{\text{m/s}^2} \cdot \sqrt{f/\text{Hz}} \tag{1.3-45}$$

With  $\ddot{z}$  as the effective value in a narrow frequency band  $\Delta f$  around the frequency  $f$ .

In the range between 4 and 8 Hz humans have the highest oscillation sensitivity:

$$KZ = 20 \cdot \frac{\ddot{z}}{\text{m/s}^2} \tag{1.3-46}$$

Within the range between 8 and 80 Hz the KZ value is calculated as follows:

$$KZ = 160 \cdot \frac{\ddot{z}}{\text{m/s}^2} \cdot \frac{1}{f/\text{Hz}} \tag{1.3-47}$$

While the perception of an exposing oscillation occurs immediately, the stress depends, apart from the intensity of the oscillation, also on the duration of exposure. Fig. 1.3-46 shows the evaluated vibration intensity (effective value of vertical accelerations evaluated according to the eqations 1.3-45 to 1.3-47) as a function of the duration of exposure with equal intensities for the criteria ‘wellness’, ‘performance’ and ‘health’.

As a consequence, durations of exposure between 1 and 10 minutes lead to the same stress. If the exposure continues for a longer time, the stress remains the same, if the square of the evaluated vibration intensity  $K$  decreases with respect to the exposure time  $t$  (Fig. 1.3-45 with double logarithmic scale)

A  $K$ -value of 20 is considered as limit value, which impairs the wellness of humans also for short durations of exposure. With the same stress after 1.5 hours, impairments of performance increase, and a daily duration of exposure of more than 4 hours may lead to health damage.

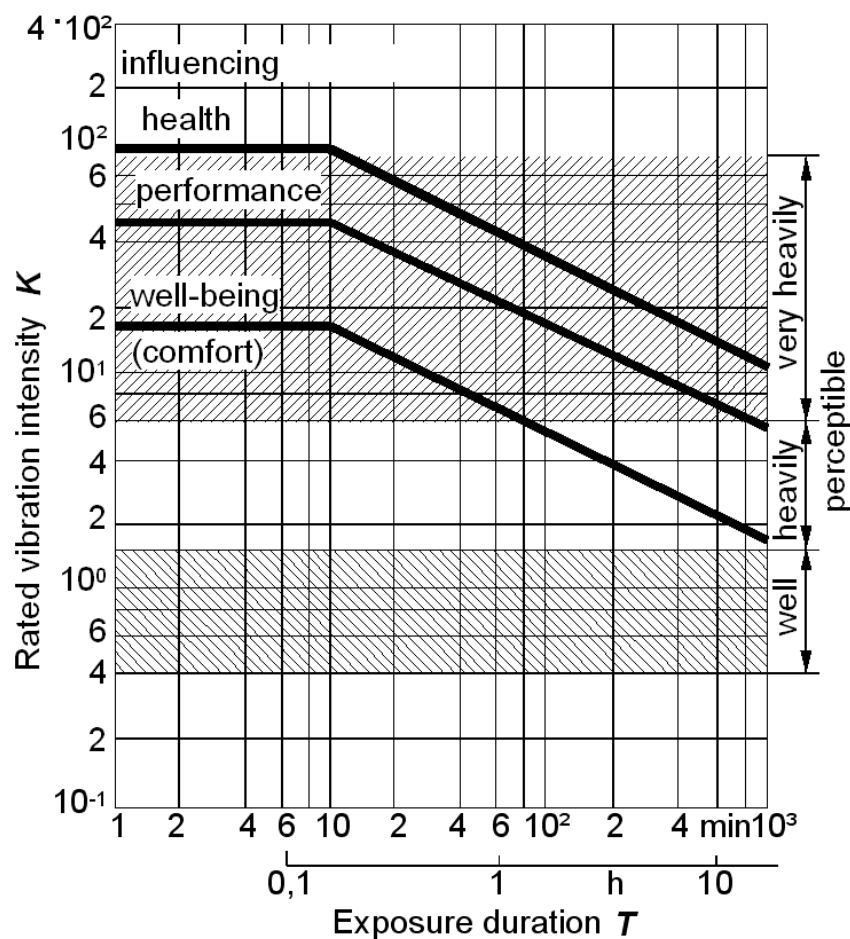


Fig. 1.3-46: Evaluated vibration intensity as a function of the duration of exposure with equal stress for the criteria 'wellness', 'performance' and 'health'.

- Perception intensity of lying humans

The oscillation exposure on lying humans is of interest, for example, in long distance trucks with sleeping cabins or in ambulance and rescue cars. A huge number of tests results already available points to the fact that, because of the direct oscillation effect on the head, the acceleration acting here can be applied as a measure for the oscillation stress of lying

humans without evaluation. The curves of equal perception intensity for lying humans prescribed in the VDI specification 2057 are given in Fig. 1.3-47.

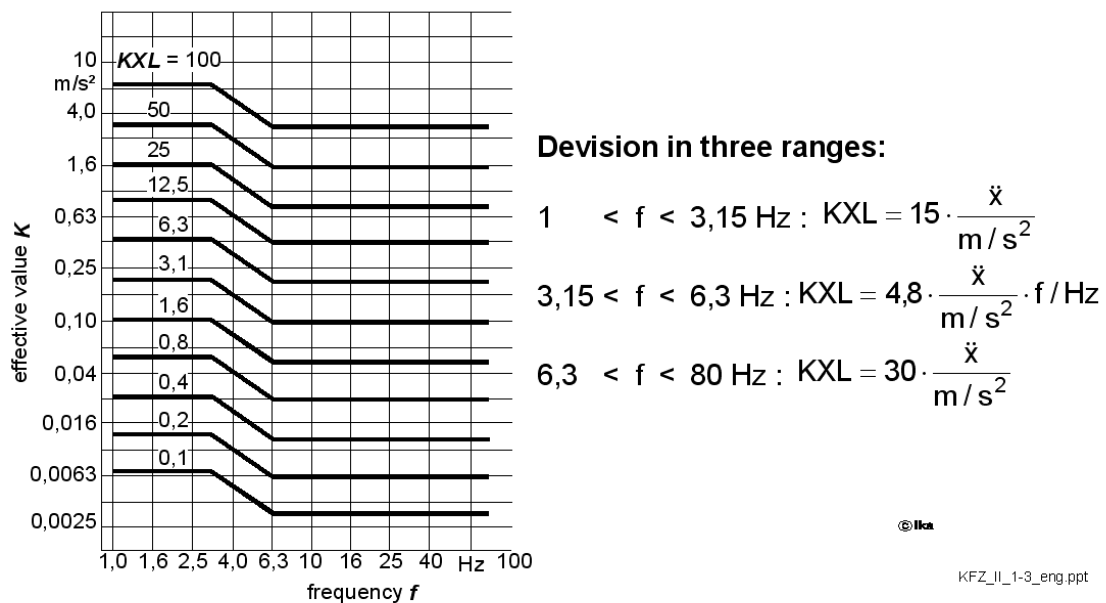


Fig. 1.3-47: Curves of equal perception intensity for lying humans based on VDI 2057

The frequency range is also divided here into three areas for the exposure executed perpendicularly to the direction of the spinal column:

$$1 \leq f \leq 3,15 \text{ Hz} \quad KXL = 15 \cdot \frac{\ddot{x}}{\text{m/s}^2} \quad (1.3-48)$$

$$3,15 \leq f \leq 6,3 \text{ Hz} \quad KXL = 4,8 \cdot \frac{\ddot{x}}{\text{m/s}^2} \cdot f / \text{Hz} \quad (1.3-49)$$

$$6,3 \leq f \leq 80 \text{ Hz} \quad KXL = 30 \cdot \frac{\ddot{x}}{\text{m/s}^2} \quad (1.3-50)$$



## 1.4 Single Wheel Suspension Model

To describe the vertical dynamics of motor vehicles, different mechanical models can be used. They vary from the simple single-mass system up to spatial vehicle oscillation models. In the following section, a few models are presented.

Of central importance to all model approaches is the model of the vertical tire characteristics, Fig.1.4-1.

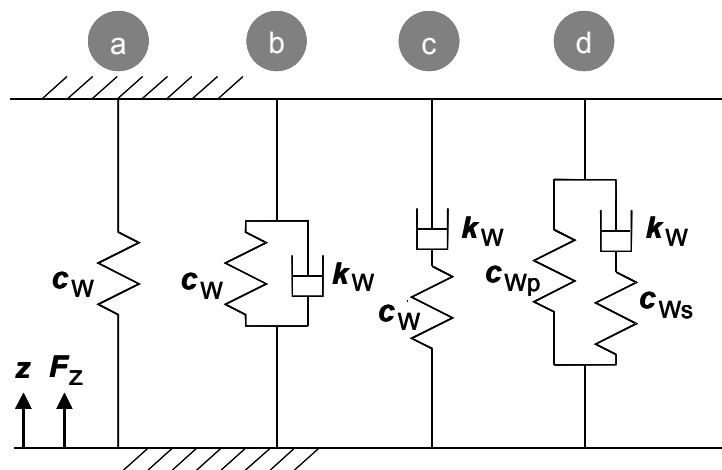


Fig.1.4-1: Tire models (vertical dynamics)

In the simplest case the tire can be modelled as a linear spring (a). The tire absorption mentioned in chapter 1.3.1 is considered in the models after Voigt-Kelvin (b), Maxwell (c) and Gehmann (d).

Below, the four modeling approaches will be compared with regards to their dynamic behavior. For this purpose, the Laplace transformations

$$\text{Model a} \quad \frac{F_z(s)}{z(s)} = c_W \quad (1.4-1a)$$

$$\text{Model b} \quad \frac{F_z(s)}{z(s)} = c_W + k_W \cdot s \quad (1.4-1b)$$

$$\text{Model c} \quad \frac{F_z(s)}{z(s)} = \frac{k_W \cdot s}{1 + \frac{k_W \cdot s}{c_W}} \quad (1.4-1c)$$

Model d

$$\frac{F_z(s)}{z(s)} = \frac{c_{Wp} + k_W \cdot \left(1 + \frac{c_{Wp}}{c_{Ws}}\right) \cdot s}{1 + \frac{k_W}{c_{Ws}} \cdot s} \quad (1.4-1d)$$

of the four models are presented in the frequency domain.

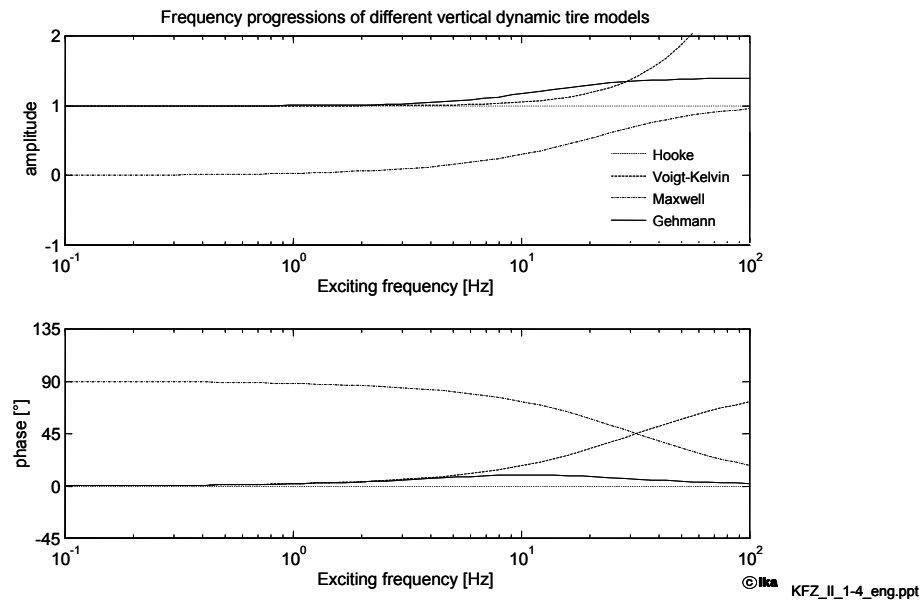


Fig.1.4-2: Frequency responses of the tire models according to Fig.1.4-1 (the amplitude response shows the normalised response  $z$ )

The behavior of Hooke's approach (a) expresses itself in a constant amplitude response without phase. In comparison, the tire models with damping elements (b)-(d), show frequency dependent responses, whereby it becomes evident that the Maxwell model is inapplicable as a tire model. The static spring rate disappears, while over the entire frequency range the standardised absolute value of the amplitude is smaller than unity.

The dynamic spring stiffening, which occurs with rubber tires as the excitation frequency increases, can be simulated with the models of Voigt Kelvin (b) and Gehmann(d), as the respective amplitude responses show. As this stiffening transitions into saturation, the Gehmann model describes the tire behavior in a more realistic manner.

In chapter 1.3.1 (Fig. 1.3-5) it was shown that, with tires at standstill (slow rolling), tire damping decreases with increasing excitation frequency. This effect is also reproduced by model (d), as the phase response of the Gehmann model shows. For high frequencies the phase response of model (d) goes down to zero.

Overall, the Gehmann model shows the best approximation of the vertical-dynamic tire behavior. For fundamental investigations, as carried out in the following, also the Voigt Kelvin model can be used.

#### 1.4.1 Single Mass Model

The simplest vehicle model is the single mass model as shown in Fig.1.4-3. The mass corresponds to the share of the body mass, with which the wheel is loaded. The axle mass is connected as unsprung mass to the body. The task of the suspension - e.g. with construction machines or dump trucks - is taken over by the tire. Only the tire damping acts as a shock absorber.

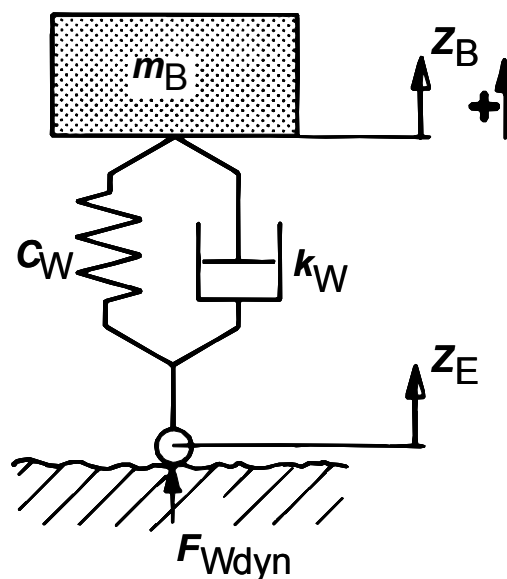


Fig.1.4-3: Single mass suspension model

The system is described by the following equation of motion:

$$m_B \cdot \ddot{z}_B = -k_W \cdot (z_B - z_E) - c_W \cdot (\dot{z}_B - \dot{z}_E) \quad (1.4-2)$$

$$\ddot{z}_B = -\frac{k_W}{m_B} \cdot (z_B - z_E) - \frac{c_W}{m_B} \cdot (\dot{z}_B - \dot{z}_E) \quad (1.4-3)$$

The natural frequency  $\omega_e$  as well as the Lehr absorption  $D$  can, in case the base excitation is disregarded, i.e. by solving the homogeneous portion of this differential equation by means of the approach  $z = z_0 \cdot e^{\omega t}$ , be derived as:

$$\omega_e = \sqrt{\frac{c_W}{m_B}} \quad \text{and} \quad D = \frac{k_W}{k_{\text{krit}}} = \frac{k_W}{2 \cdot m_B \cdot \omega_e} \quad (1.4-4)$$

Thereby the following correlation exists between undamped natural frequency  $\omega_e$ , damped natural frequency  $\omega_{e,m,D}$  and damping  $D$ :

$$\omega_{e,m,D} = \omega_e \sqrt{1 - D^2} \quad (1.4-5)$$

To determine the motion of the body as well as the spring and damper forces during arbitrary excitation (e.g. a measured road surface profile) computers are most suitable, particularly when non-linear characteristics (e.g. tire lift off, kinked shock-mount and feather/spring characteristic curves) are to be considered.

If one uses a swept sine (sine of constant amplitude and varied frequency) as excitation signal, the amplification function can be determined from the peak values of body amplitude and excitation amplitude:

$$V(f) = \frac{z_B}{z_E} \quad (1.4-6)$$

Note: The amplification function  $z_B/z_E$  for the body amplitudes normalised to the excitation amplitudes is identical to the amplification function  $\ddot{z}_B/\ddot{z}_E$  for body acceleration normalised to the excitation accelerations, as follows from the double differentiation of a sine oscillation with the frequency  $f = 2 \cdot \pi \cdot \omega$ :

$$\ddot{z}_E(t) = -\omega^2 \cdot z_E(t)$$

$$\ddot{z}_B(t) = -\omega^2 \cdot z_B(t)$$

and with

$$\frac{z_B(t)}{z_E(t)} = \frac{\ddot{z}_B(t)}{\ddot{z}_E(t)}$$

The amplification function of the single mass suspension model is shown in Fig.1.4-4 for tire data in as per paragraph 1.2.1.

Due to the negligible self damping behavior of the tires, a pronounced resonance peak occurs. The natural frequency – resulting from proportionate body and axle mass and the tire spring rate – which is approximately 3 - 4 Hz, is situated in a frequency range of high human sensitivity to vibration.

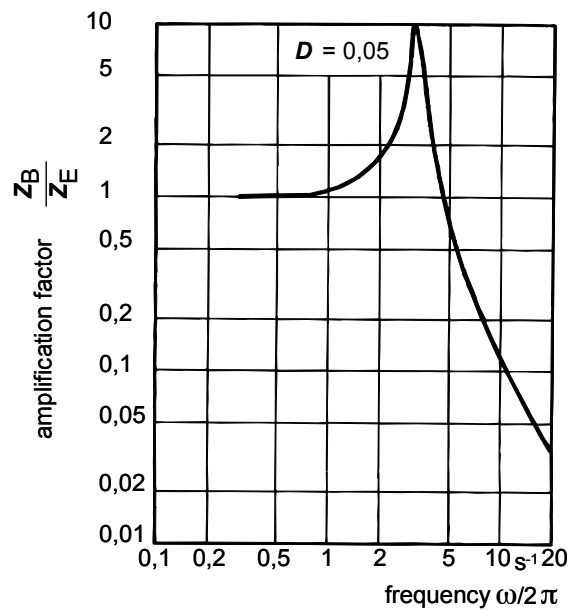


Fig.1.4-4: Amplification function of the single-mass suspension system

#### 1.4.2 Dual-Mass Equivalent System

Common motor vehicles not only feature tire (wheel) but also body suspension. The simplest equivalent system, which nevertheless possesses essential features of a real vehicle suspension, is represented by the dual-mass equivalent system described below. It is arrived at by reduction on the basis of a four-wheel vehicle, with the share of the body mass apportioned to the wheel considered substituting the body mass. The influence of mass coupling, among other things, is neglected.

Fig. 1.4-5 shows the structure of a dual-mass equivalent system. The system consists of the proportional body mass, a wheel or axle mass, the body springs and dampers as well as the tire (wheel) suspension and damping.

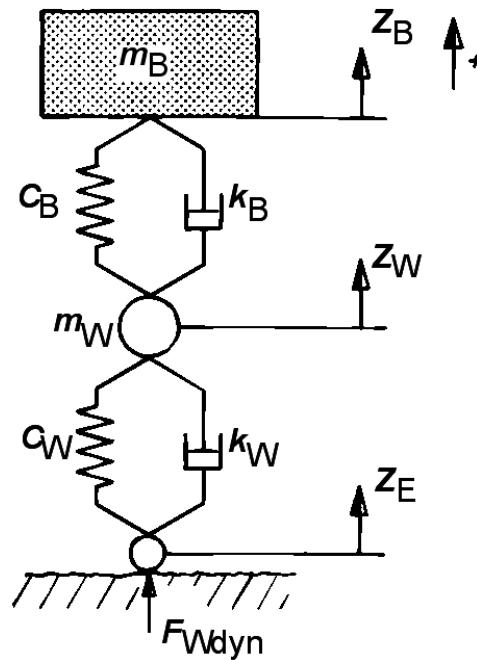


Fig. 1.4-5: Dual-mass suspension model

The differential equations describing the system result from the formulation of the force balance on body mass (equation 1.4-7) and wheel mass (equation 1.4-8):

$$m_B \cdot \ddot{z}_B = -k_B \cdot (\dot{z}_B - \dot{z}_W) - c_B \cdot (z_B - z_W) \quad (1.4-7)$$

$$m_W \cdot \ddot{z}_W = -k_B \cdot (\dot{z}_W - \dot{z}_B) - c_B \cdot (z_W - z_B) - k_W \cdot (\dot{z}_W - \dot{z}_E) - c_W \cdot (z_W - z_E) \quad (1.4-8)$$

These differential equations are coupled via body suspension or body damping. For *approximate* determination of the two natural radian frequencies  $\omega_e$  and the damping values  $D$ , coupling of the two differential equations is to be neglected, so that only the homogenous parts of the differential equations are considered.

Thus, for the body mass  $m_A$  follows:

$$m_B \cdot \ddot{z}_B + k_B \cdot \dot{z}_B + c_B \cdot z_B = 0 \quad (1.4-9)$$

from which follow:

$$\omega_{eB} = \sqrt{\frac{c_B}{m_B}} \quad (1.4-10)$$

$$D_B = \frac{k_B}{2m_B \omega_{eB}} \quad (1.4-11)$$

for natural radian frequency  $\omega_{eA}$  and damping  $D_A$ .

For the wheel mass  $m_R$  from :

$$m_W \cdot \ddot{z}_W + (k_W + k_B) \cdot \dot{z}_W + (c_W + c_B) \cdot z_W = 0 \quad (1.4-12)$$

follow natural radian frequency  $\omega_{eR}$  and damping  $D$  at:

$$\omega_{eW} = \sqrt{\frac{c_W + c_B}{m_W}} \quad (1.4-13)$$

$$D_W = \frac{k_B + k_W}{2 m_W \omega_{eW}} = \frac{k_B + k_W}{2 \sqrt{m_W (c_W + c_B)}}$$

Furthermore, through formulation of the force balance at the tire contact center and with the aid of the equations 1.4-6 and 1.4-7, an expression can be determined for the tire forces acting on the roadway, i.e. an equation for the dynamic wheel load  $F_{W_{dyn}}$  :

$$F_{W_{dyn}} = -k_W \cdot (\dot{z}_W - \dot{z}_E) - c_W \cdot (z_W - z_E) = m_B \cdot \ddot{z}_B + m_W \cdot \ddot{z}_W \quad (1.4-14)$$

With the aid of this equation, a method of indirect measurement of dynamic wheel load can be derived through the measurement of body and wheel mass acceleration and knowledge of the masses.

In the single-mass equivalent system, the magnification function was determined by means of a sliding sinusoid acting on the system as excitation signal  $z_E$  and calculation of the peak values of the body amplitude  $z_A$ . It is also possible to excite the system with the aid of a synthetically generated roadway, and from this to infer the magnification function. This method is demonstrated for the dual-mass equivalent system.

This method uses simulation to determine the spectral power density of body acceleration  $\phi_{\ddot{z}_A}(\omega)$ . The spectral density of the excitation amplitude  $\phi_{z_E}(\omega)$  is determined by the roadway. It must be converted to the spectral density of the excitation acceleration  $\phi_{\ddot{z}_E}(\omega)$ . From the combination between power density and the quadratic mean value of the amplitude in the time domain

$$\bar{z}_E^2(t) = \int_0^{\infty} \Phi_{z_E}(\omega) d\omega \quad (1.4-15)$$

and the analogous relation for the exciter acceleration

$$\overline{\ddot{z}_E}^2(t) = \int_0^{\infty} \Phi_{\ddot{z}_E}(\omega) d\omega \quad (1.4-16)$$

as well as from the interrelationship between exciter acceleration and exciter amplitude

$$\ddot{z}_E(t) = -\omega^2 \cdot z_E(t) \quad (1.4-17)$$

follows the relation between the power density spectrum of the exciter amplitude and the exciter acceleration:

$$\Phi_{\ddot{z}_E}(\omega) = \omega^4 \cdot \Phi_{z_E}(\omega) \quad (1.4-18)$$

The magnification function  $V$  can then be determined on the basis of the following relationship:

$$V^2 = \left( \frac{\ddot{z}_B}{\ddot{z}_E} \right)^2 = \frac{\phi_{\ddot{z}_B}(\omega)}{\phi_{\ddot{z}_E}(\omega)} \quad (1.4-19)$$

Fig. 1.4-6 illustrates above relationships.



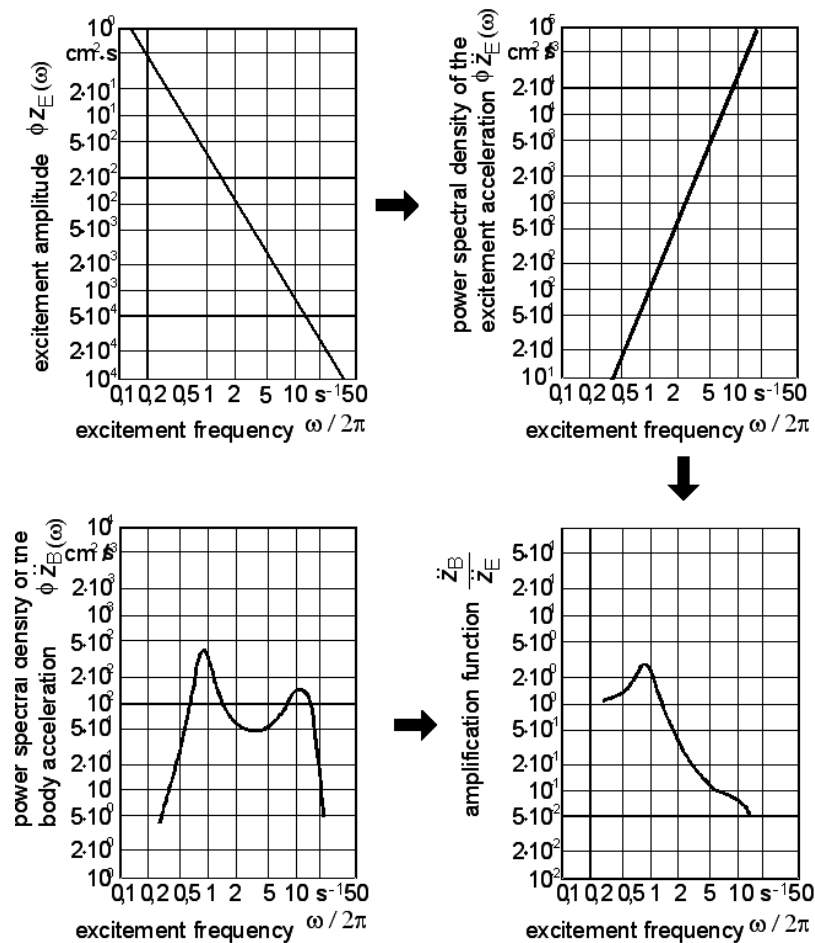


Fig. 1.4-6: Determination of the magnification function  $\ddot{z}_A / \ddot{z}_E$  on the basis of the spectral density of the body acceleration  $\phi_{\ddot{z}_A}(\omega)$  and the spectral density of the excitation amplitude  $\phi_{z_E}(\omega)$

With the aid of the relationships explained above, the influence of various roadways (degree of irregularity  $\phi_h(\Omega_0)$  and waviness  $w$ ) on the spectral density of body acceleration  $\phi_{\ddot{z}_A}(\omega)$  can be discussed.

For example, a roadway with a very high share of short-wave excitations (low waviness  $w$ ) would on the basis of equation 1.4-17 result in a high density of the excitation acceleration in the range of high frequencies. This again would on the one hand overrate the resonance peak in the range of the wheel natural frequency ( $f_{nW} \approx 12 \text{ Hz}$ ) and on the other hand underrate the range of the body natural frequency ( $f_{nB} \approx 1 \text{ Hz}$ ).

Analogous to the magnification function for the body amplitudes, a magnification function for the dynamic wheel load variations relating to the exciter amplitudes  $F_{W,dyn} / z_E$  can be

determined. This magnification function is given here as a standard value for the static wheel load  $F_{W,stat}$  (Fig. 1.4-7). It follows direct from the spectral density of the exciter amplitude  $\phi_{Z_E}(\omega)$  :

$$V^2 = \left( \frac{F_{W,dyn}}{F_{W,stat} \cdot Z_E} \right)^2 = \frac{\phi_{F_{R,dyn}/F_{R,stat}}(\omega)}{\phi_{Z_E}(\omega)} \tag{1.4-20}$$

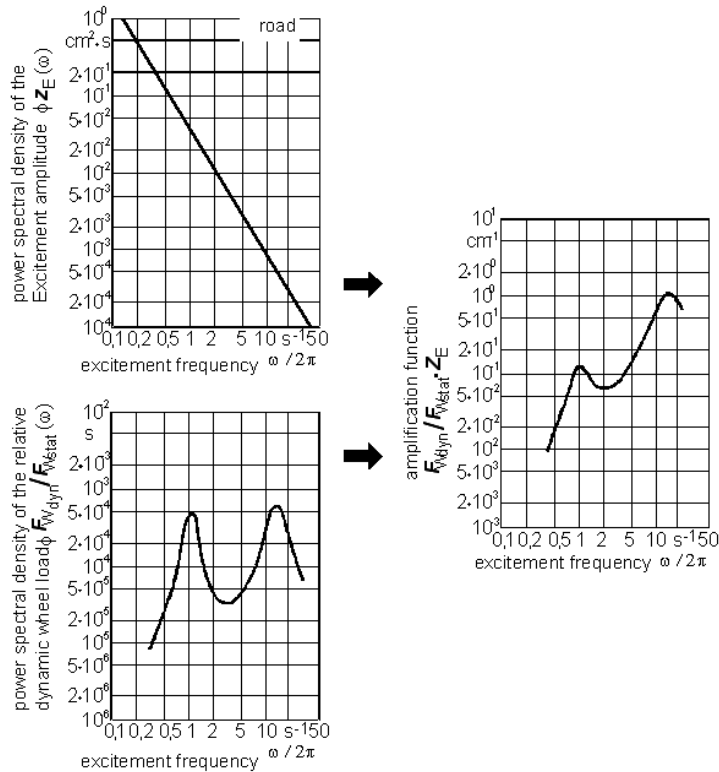


Fig. 1.4-7: Determination of the magnification function  $F_{R,dyn} / (F_{R,stat} \cdot Z_E)$  from the spectral density of excitation amplitude  $\phi_{Z_E}(\omega)$  and dynamic wheel load  $\phi_{F_{R,dyn}/F_{R,stat}}(\omega)$

### 1.4.2.1 Parametric Study - Automobile Suspension

In the following we are investigating how modification of essential parameters of the dual-mass model affects body acceleration, which even without seat suspension and vibration measurement is considered by rough human assessment a criterion of suspension comfort, and relative (specific) dynamic wheel load, i. e. road grip of the wheels (driving safety).

The oscillation equations of the dual-mass model, equation 1.4-7 and equation 1.4-8, are mapped by means of the MATLAB program and excited by a synthetically generated road signal. On the basis of the simulation results, the spectral power densities of body

acceleration and dynamic wheel load are determined. The road signal used for simulation is shown in Fig. 1.4-8 as path-time function as well as time-frequency-dependent power density.

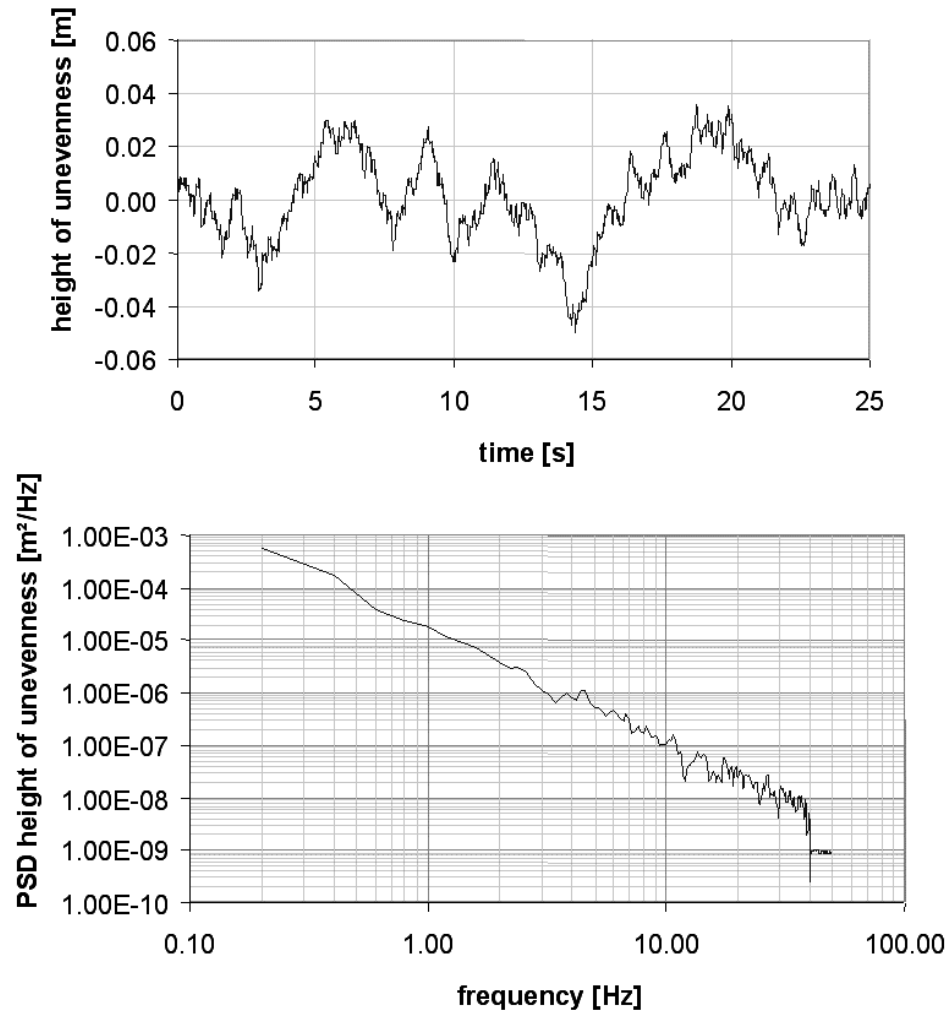


Fig. 1.4-8: Synthetically generated road signal with  $w = 2.14$  and  $\phi_h(\Omega_0) = 3.7 \cdot 10^{-6} \text{ m}^3$

Original variant is a quarter vehicle with the following parameters:

$R = 150,000 \text{ N/m}$ ;  $A = 21,000 \text{ N/m}$ ;  $k_W = 100 \text{ Ns/m}$ ;  $k_B = 1500 \text{ Ns/m}$ ;  $m_W = 40 \text{ kg}$ ;  $m_B = 400 \text{ kg}$

Fig. 1.4-9 shows how in this vehicle the road signal from Fig. 1.4-8 affects the vertical quantities of motion of wheel and body. Damping and reduction of the motion parameters between road and body can be clearly seen. For better perception, the curves of body and wheel have been vertically displaced.

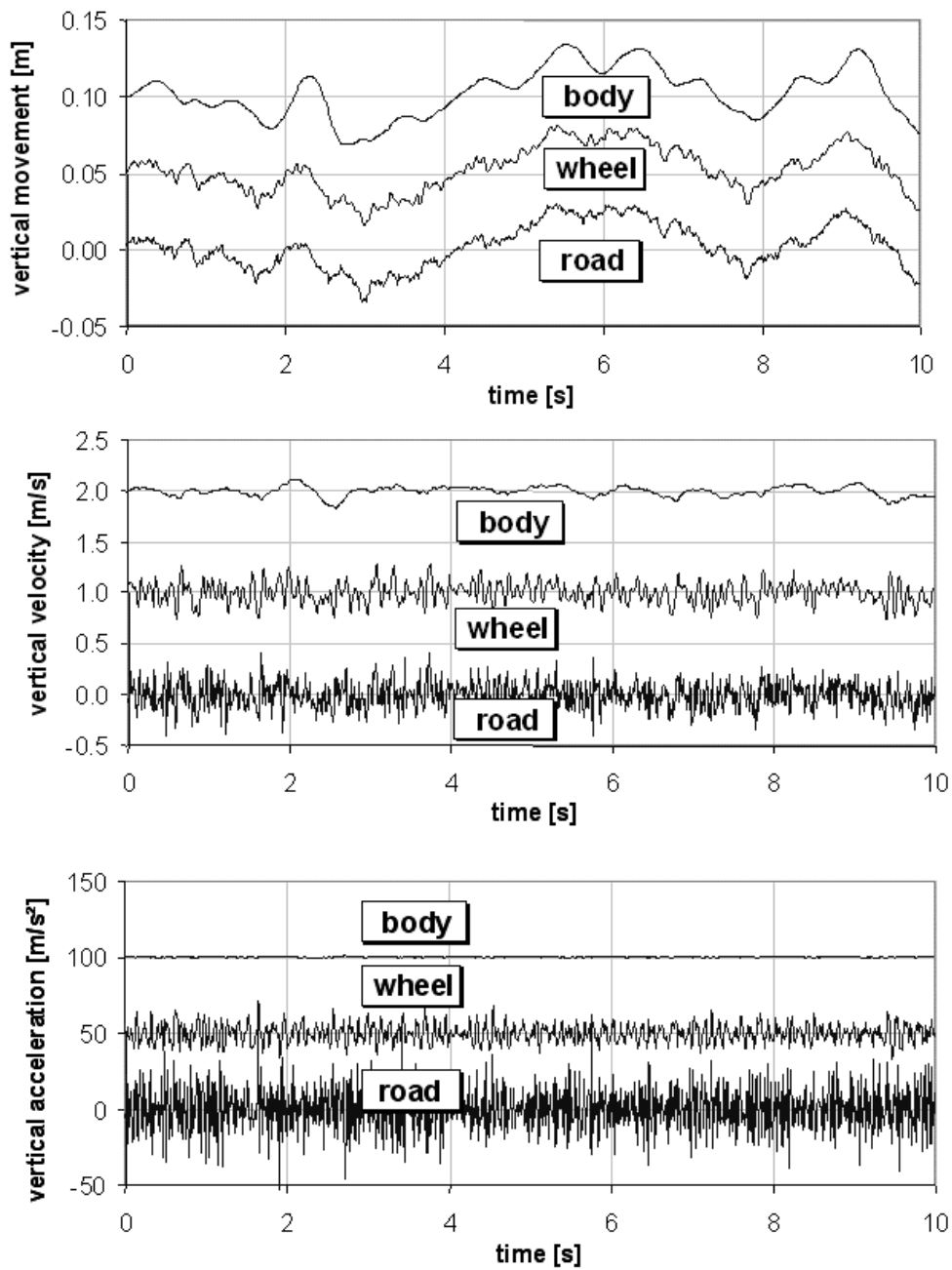


Fig. 1.4-9: Vertical motion, speed and acceleration of road, wheel and body

- Variation of the wheel mass  $m_w$

In Fig. 1.4-10 the wheel mass is varied first. With regard to body resonance, this has neither an effect on the position of the body natural frequency nor on the intensity of the body resonance.

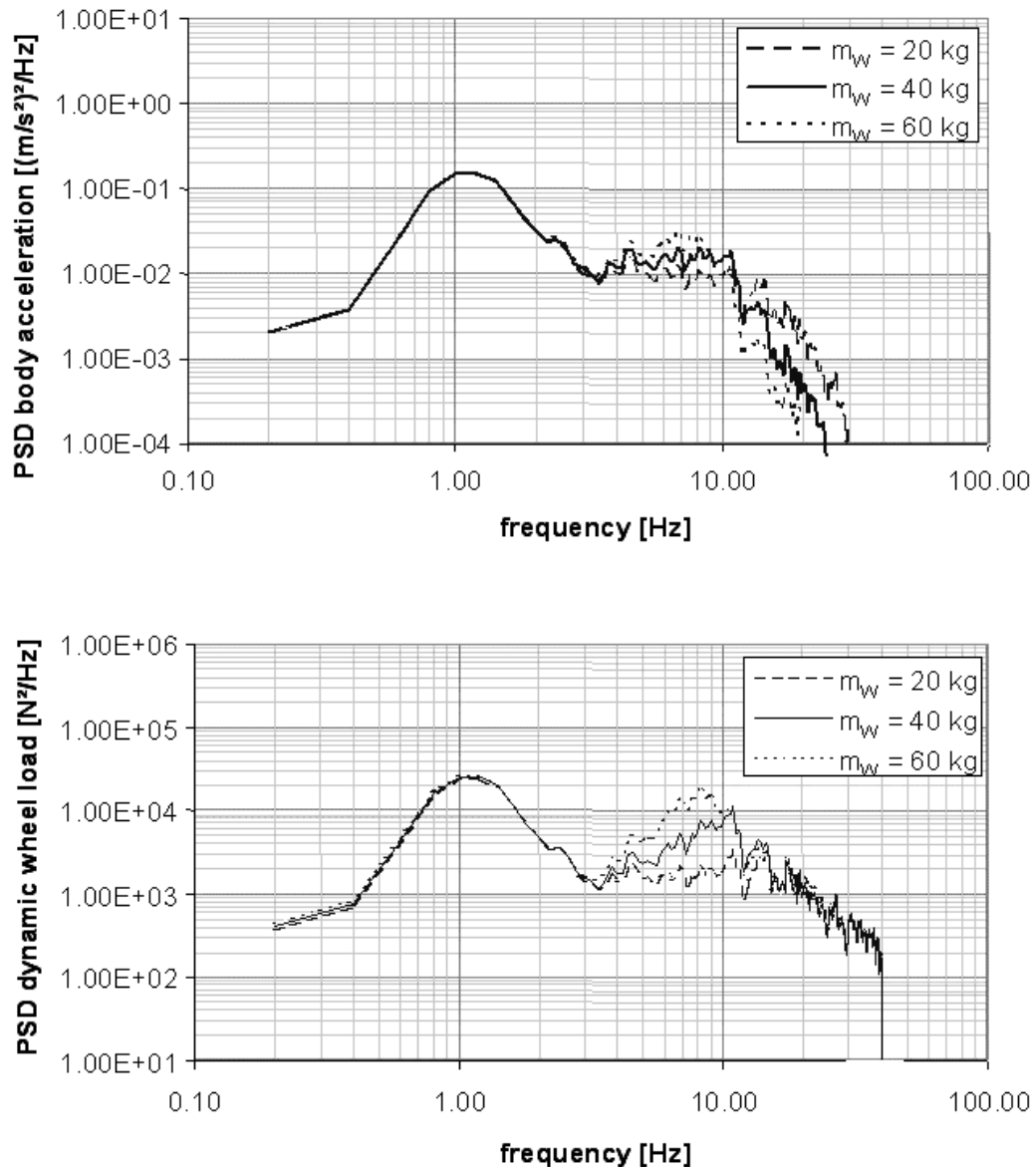


Fig. 1.4-10: Parameter variation with varying wheel mass

With regard to wheel resonance, however, the elevated relative (specific) dynamic wheel loads resulting from a greater wheel mass are conspicuous. This is due to the fact that a larger mass has to be stabilized by unchanged dampers. Consequently, a wheel mass as small as possible is to be aimed at with regard to the dynamic wheel load variations, and therefore also with regard to driving safety.

- Variation of the stiffness/spring rate of the tire (tire rate)  $c_w$

In Fig. 1.4-11 the spring rate of the tire (tire rate) is varied. A softer tire rate tends to reduce wheel natural frequency and the dynamic wheel loads, i.e. road grip is improved. Softer tires

would thus clearly improve driving safety. Realization of such tires is, however, only possible within narrow limits due to the associated increase in rolling resistance and flexing energy.

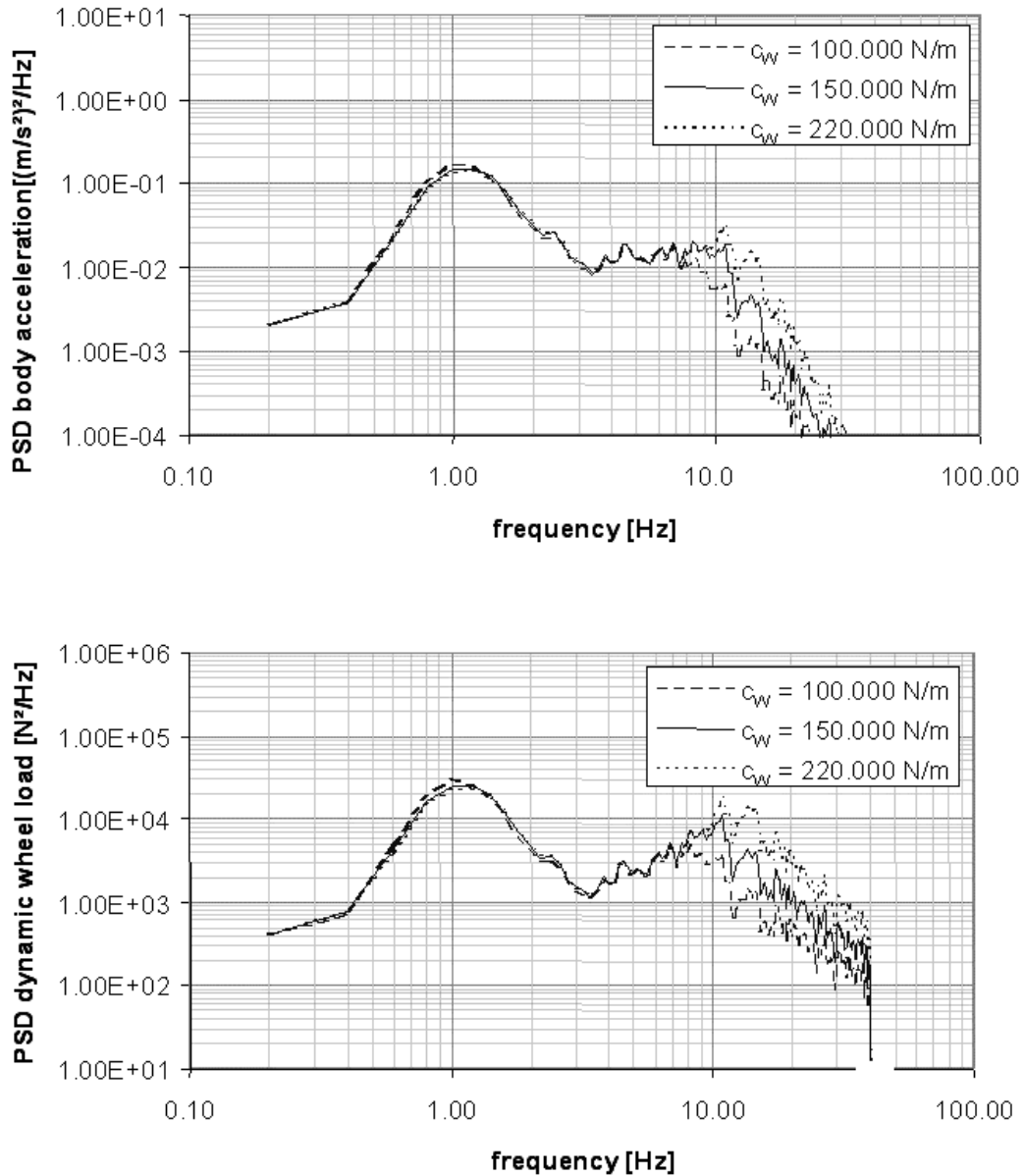


Fig. 1.4-11: Parameter variation with varying stiffness/spring rate of the tire

- Variation of the stiffness/spring rate of body suspension  $c_B$

In Fig. 1.4-12 the spring rate of the body suspension is varied. A softer body suspension rate reduces body natural frequency, and relative damping is increased as a result. Body acceleration and relative (specific) dynamic wheel load are reduced.

A softer body suspension rate would thus have a positive effect with regard to the criteria driving safety and ride comfort. Realization, however, is only possible to a limited degree because of effects such as body inclination due to cornering, brake dive, major ride height changes due to loading, and especially because of the considerable spring travels then needed.

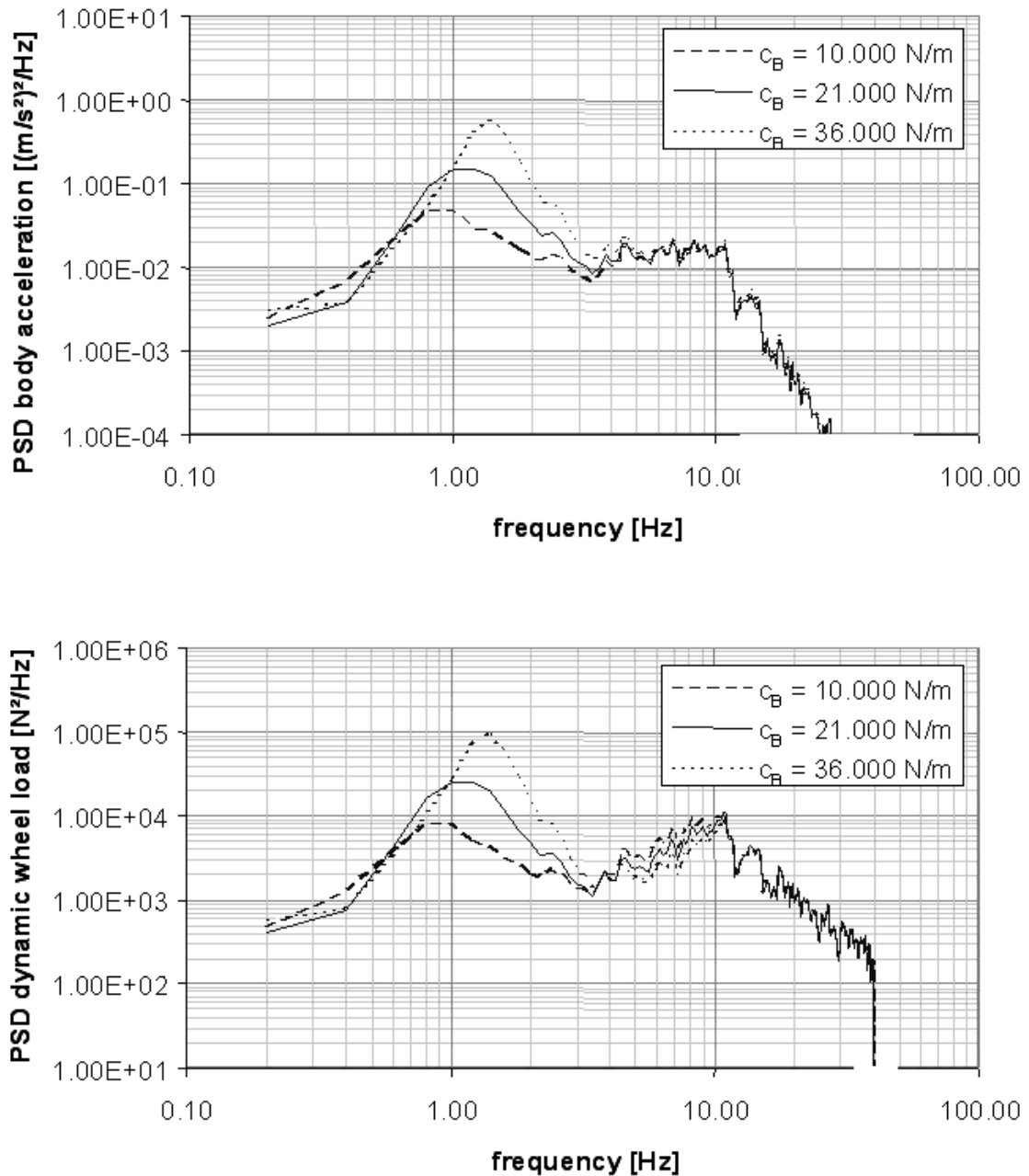


Fig. 1.4-12: Parameter variation with varying stiffness/spring rate of body suspension

• Variation of body damping  $k_B$

In Fig. 1.4-13 body damping is varied. Stiffer body damping has a positive effect in the range of the natural frequencies of both body acceleration (suspension comfort) and the dynamic wheel loads (road grip of the wheels, active safety). In the range outside the points of resonance, however, it is especially the body acceleration which is positively influenced by a soft damper.

Tuning of body damping consequently always requires a compromise to be made between the requirements of the various frequency ranges.

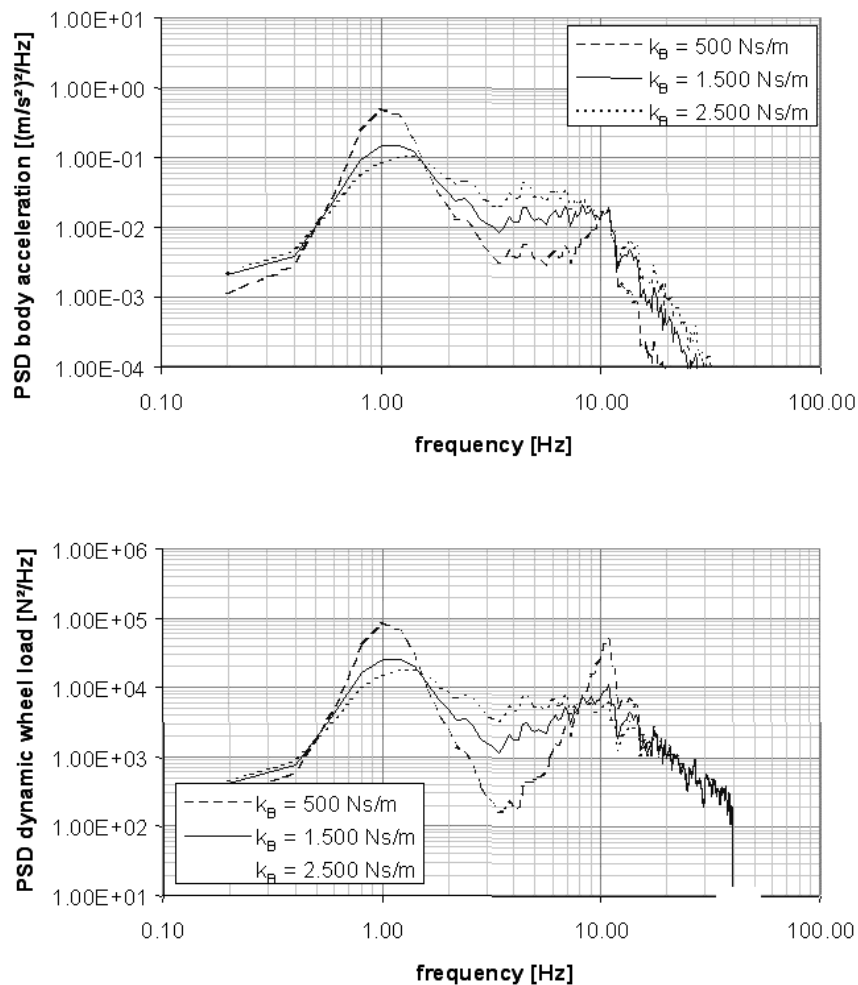


Fig. 1.4-13: Parameter variation with varying body damping

In Fig. 1.4-14 the results gained on the basis of Figs. 1.4-10 - 1.4-13 with regard to driving safety and riding comfort are summarized in a table. Analogous to body and wheel natural frequencies, a difference is made between long-wave and short-wave effects.



|                       | driving safety |            | ride comfort |            |
|-----------------------|----------------|------------|--------------|------------|
| excitement:           | long wave      | short wave | long wave    | short wave |
| <b>action:</b>        |                |            |              |            |
| soft support spring : | ↑              | ↑          | ↑            | ↑          |
| soft shock absorber:  | ↓              |            | ↓            | ↑          |
| softer tires:         |                | ↑          | ↑            | ↑          |
| lighter axle:         |                | ↑          |              | ↑          |
| <b>advice:</b>        |                |            |              |            |
| support spring:       | soft           |            | soft         |            |
| shock absorber:       | strong         | strong     | strong       | weak       |
| tires:                | soft           |            | soft         |            |
| axle:                 | light          |            | light        |            |

Fig. 1.4-14: Effects of design changes effected on the suspension system on driving safety (dynamic wheel loads) and riding comfort (body acceleration);  
 ↑ = positive, ↓ = negative

In addition to the "conventional" ways of influencing suspension behavior dealt with so far, "unconventional" solutions are being presented below. In contrast to passive systems, the force  $F$  acting here on the body does not depend via a single characteristic on the compression travel  $z$  and the compression rate  $\dot{z}$  of the components. Fig. 1.4-15 presents a summary of controlled suspension systems.

*Adaptive* systems, unlike the passive system, can switch between various component characteristics. Here too, however, the force direction remains determined by the signs of compression travel and compression rate.

In the *semiactive* state, the switching frequencies exceed the characteristic vibration periods of wheel and body. Switching from one characteristic to the other can thus take place at a speed permitting each point located in between to be reached dynamically.

Adaptive and semiactive systems only need energy for the control of actuators and the electronics.

Only with *active* suspension does the force  $F$  between body and wheel become independent of the compression movement of the wheel. Positioning force, however, requires external energy supply.

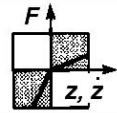

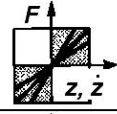

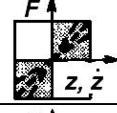
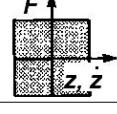
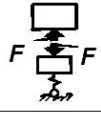
|            | forces  | switching frequency                                 | power demand |   |
|------------|---|---|--------------|---|
| passive    |  | -   | -            |  |
| adaptive   |  | smaller than characteristic oscillating frequencies | little       |  |
| semiactive |  | larger than characteristic oscillating frequencies  | little       |   |
| active     |  | larger than characteristic oscillating frequencies  | large        |  |

Fig. 1.4-15: Classification of controlled suspension systems

• Adaptive damper control

The results of parameter variation regarding damper stiffness (Fig. 1.4-13) suggested that body acceleration as well as wheel load variations can be minimized for a wide frequency range if a relatively high level of damping is available in the body and wheel resonance ranges and if the level of damping is low in the range outside these points of resonance.

A clear improvement of conventional suspension systems can thus theoretically also be achieved by means of a damping system that depends on the excitation frequency of the system, Fig. 1.4-16.

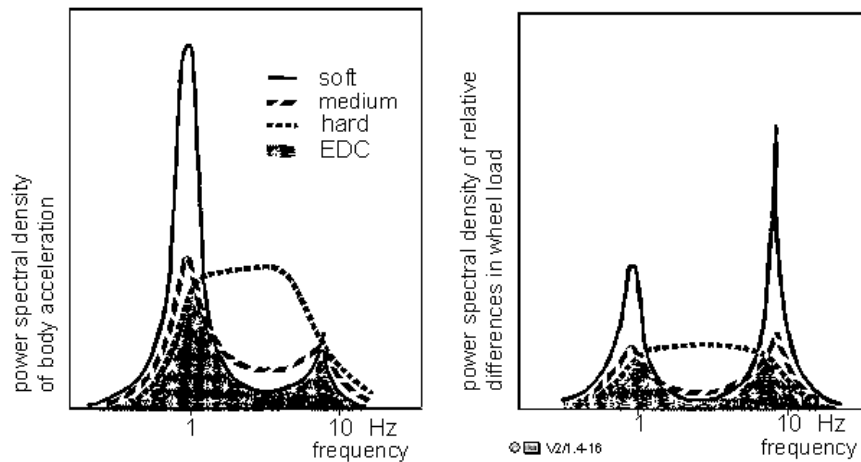


Fig. 1.4-16: Simulation results with a single-wheel suspension model for ideal frequency-dependent damper force adjustment /21/

The improvement potential attainable by means of such damper control is limited by the fact that a definite frequency selection is not possible due to the randomness of road irregularity. Apart from that, the improvement potential also depends on the realizable range of variation of damper characteristics and on the potential extent of reduction of system life.

The EDC system (Electronic Damper Control) of BMW was developed in cooperation with Boge and VDO. Here, the damper characteristics are adapted in three steps by means of control electronics. The EDC system identifies road excitation by means of an acceleration sensor mounted to the body.

The sensor signals are processed by the ECU in a manner allowing determination of separate characteristic values of excitation with regard to body and axle natural frequencies. Depending on vehicle load and the intensity of instantaneous vibration excitation, different threshold values will result in graded damper adjustment.

System efficiency is illustrated by the conflict diagram between comfort and driving safety, Fig. 1.4-17.

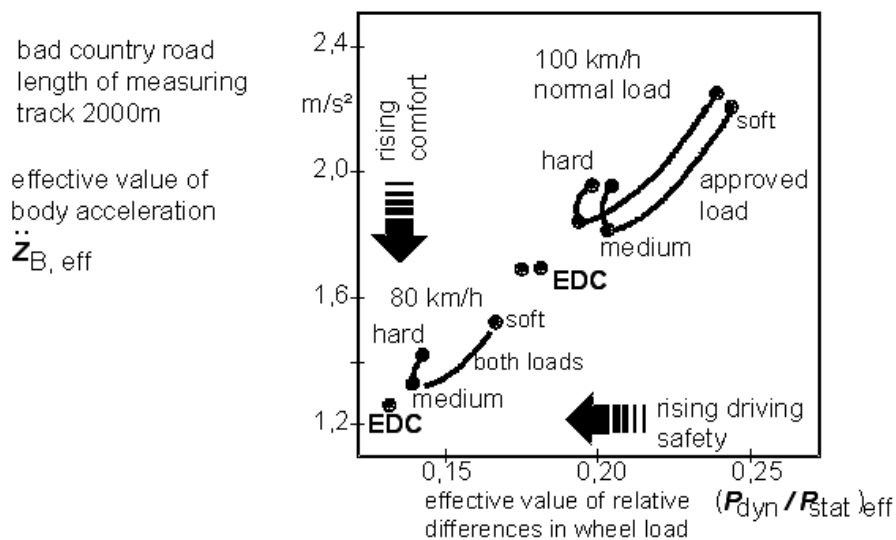


Fig. 1.4-17: Comparison of suspension behavior of a test vehicle with different damper settings of the EDC system illustrated by the conflict diagram comfort/driving safety /21/

The adaptive damping system (ADS) of Mercedes-Benz, whose system functions are comparable to those of the EDC system, effects irregularity-dependent damper setting in 4 steps according to a characteristic map considering a comparative value for the spectral power density of the irregularities  $\Phi(\Omega_0)$  and a comparative value for the waviness  $w$  of the road being traveled on, Fig. 1.4-18.

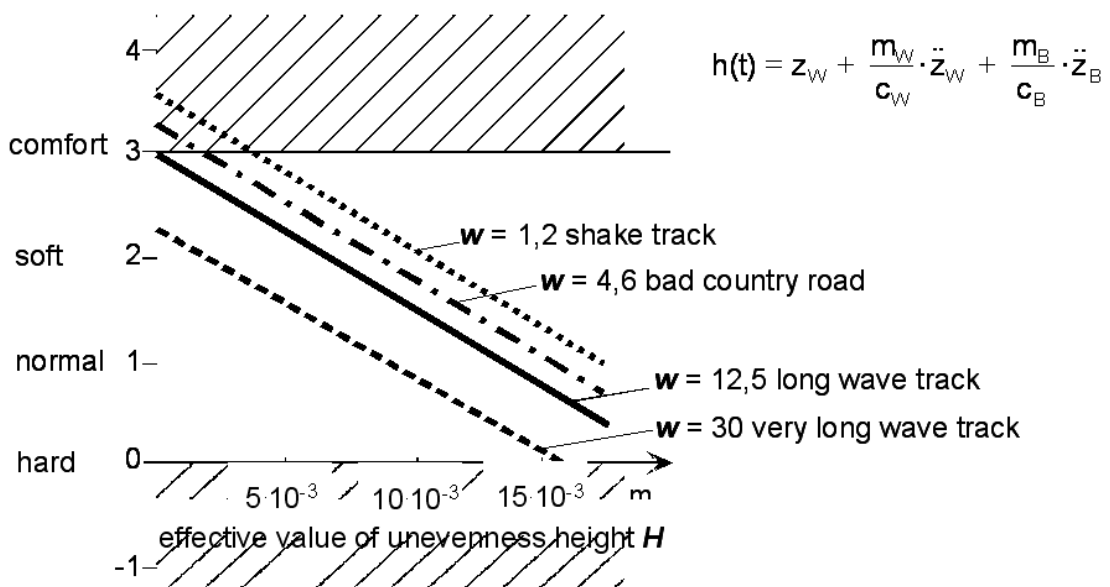


Fig. 1.4-18: Map for damper force adjustment of the adaptive damping system ADS of Mercedes-Benz /25/

An effective value  $H$  of the course of irregularity  $h(t)$  in the frequency range 0.5 - 20 Hz. ( $\Phi' = H(0.5 - 20 \text{ Hz})$ ) determined by exponential floating calculation is used as a comparative value for the spectral power density  $\Phi(\Omega_0)$ .

The comparative value for waviness is formed as a quotient resulting from the respective effective values for the body and axle resonance ranges.

$$(w' = H(0,5 - 2 \text{ Hz}) / H(8 - 20 \text{ Hz}))$$

The course of irregularity  $h(t)$  is indirectly determined by approximation through the measurement of wheel acceleration  $\ddot{z}_W$  and body acceleration  $\ddot{z}_B$ . The algorithm used can be derived from equations 1.4-7 and 1.4-8.

$$z_E = h(t):$$

$$h(t) = z_W + \frac{m_W}{c_W} \cdot \ddot{z}_W + \frac{m_B}{c_B} \cdot \ddot{z}_B \quad (1.4-21)$$

- Active suspension

Due to its low power/weight ratio and its high power density, a hydraulic cylinder is suited as a variable-length element for active ride-height control (Fig. 1.4-19).

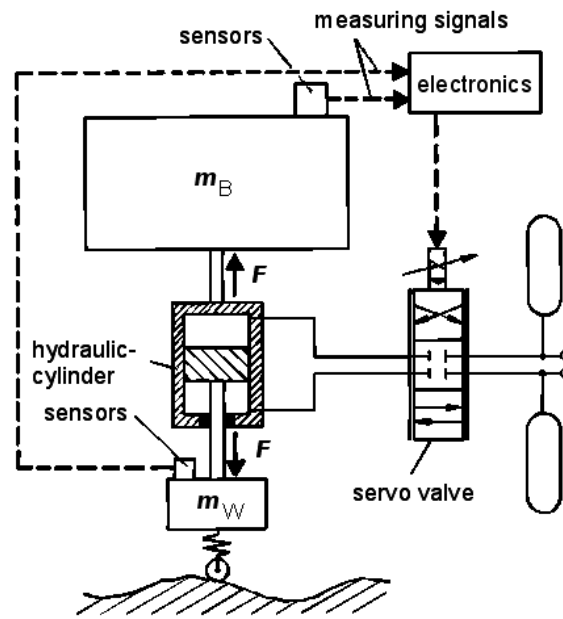


Fig. 1.4-19: Single-wheel suspension model with active suspension

Cylinder pressure is controlled by means of a quick-acting servo valve, which receives the control signals from an overriding electronic control unit. Control logic can be fed with various information about the driving condition, picked up by sensors on the vehicle. Active setting force can be controlled in relation to wheel or body acceleration or via a pre-scan of the road irregularities.

Unlike a fully active suspension, the active version of the hydropneumatic suspension provides a spring action also without inflow and outflow of hydraulic oil. The control valves supply or remove oil only if the system recognizes that it can improve vehicle handling through active intervention. The advantage is that even under extreme driving conditions, the energy input required will be significantly lower.

In Fig. 1.4-20 the spectral power densities of active hydropneumatic and fully active suspension are compared with those of passive systems. Suspension comfort as well as road grip of the wheels are clearly improved in a wide range of frequencies.

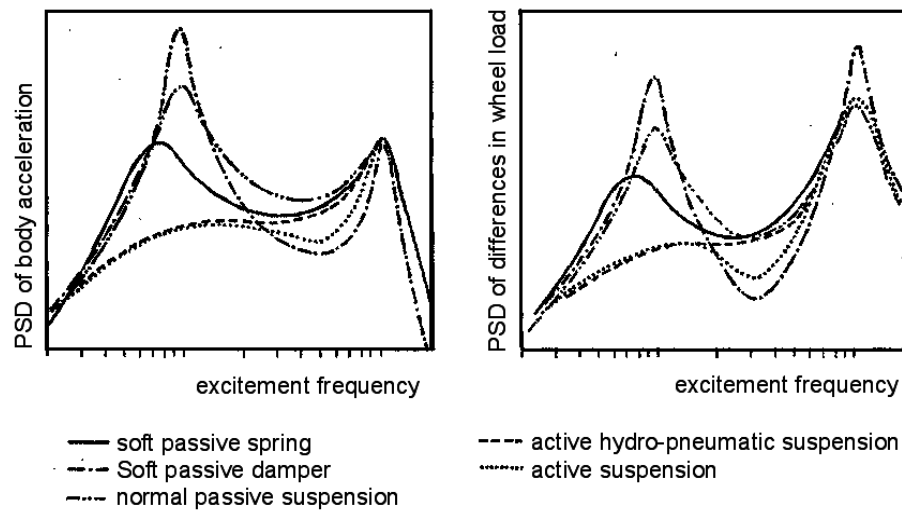


Fig. 1.4-20: Theoretical riding comfort and safety potential of various suspension systems

Realization of motor vehicles with significantly improved suspension comfort is technically possible. Drawbacks are seen in the higher design expenditure and the energy requirements, which for a standard-size car amounts to between 7 kW (active hydropneumatic suspension) and 20 kW (fully active suspension).

### 1.4.2.2 Parametric Study of a Truck Suspension

The suspension characteristics of trucks differ substantially from those of a passenger car.

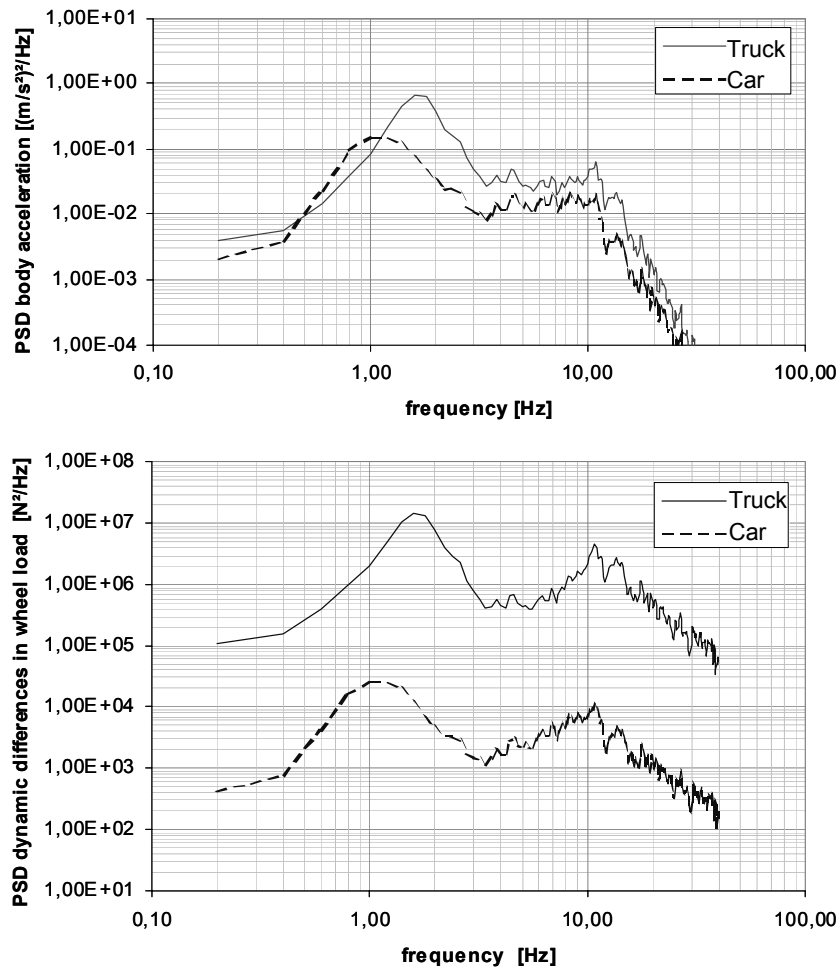


Fig.1.4-21: Comparison of body acceleration and dynamic wheel load between trucks and passenger cars

Fig. 1.4-21 shows the spectral power densities of body acceleration and dynamic wheel load of a truck in comparison to a passenger car.

The simulation of the truck is based on the following data:

$R = 3,000,000 \text{ N/m}$ ;  $A = 570,000 \text{ N/m}$ ;  $k_W = 100 \text{ Ns/m}$ ;  $k_B = 21,000 \text{ Ns/m}$ ;  $m_W = 650 \text{ kg}$ ;  
 $m_B = 4500 \text{ kg}$

The body's natural frequency of 1.4 Hz is significantly higher than that of the example passenger car. Also, the magnitudes of body acceleration and the dynamic wheel load are

larger. The suspension behavior of trucks is therefore less favourable than that of passenger cars.

- Influence of frictional forces within springs

As body springs of trucks usually stacked leaf springs are used. The characteristic curves show a hysteresis (see paragraph 1.2.1.1), resulting from the friction between the spring leaves. This leads to a temporary blockade of the body spring during the course of an oscillation, thereby turning the two-mass system into a single mass system according to Fig.1.4-3 during these periods. Body and wheel mass then oscillate in conjunction on the stiff and little damped tire spring. Fig.1.4.-22 shows the velocity difference between body and wheel with and without friction. With the friction-affected model, the phases where the leaf springs blockade and the velocity difference becomes zero are clearly visible.

Fig.1.4-23 shows, how the friction force affects the body acceleration of the example LKW. In particular within the range of the highest oscillation sensitivity of humans between 4-8 Hz, the friction causes a significant degradation of the suspension behavior.

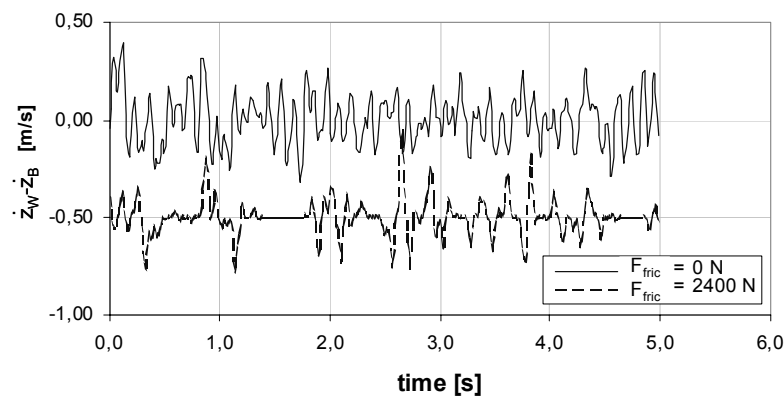


Fig.1.4-22: Velocity difference between body and wheel

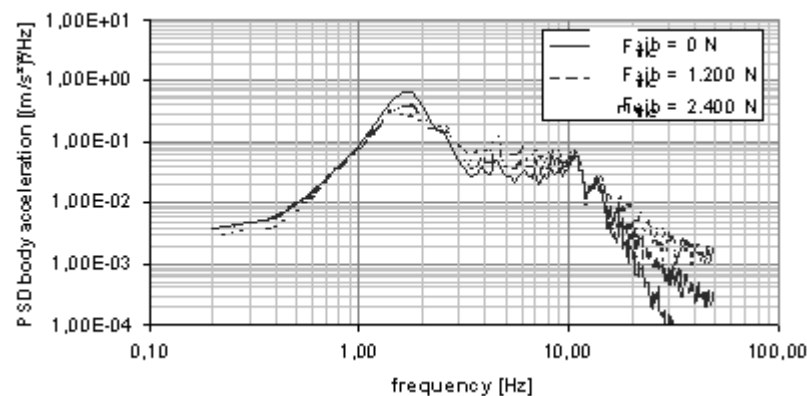


Fig.1.4-23: Parametric variation with different amounts of friction within the leaf spring



### 1.4.3 Enhancement of the Model by Seat Suspension

Enhancing the two-mass suspension model, which has been discussed so far, by the seat suspension, leads to a three-mass suspension model (Fig.1.4-24).

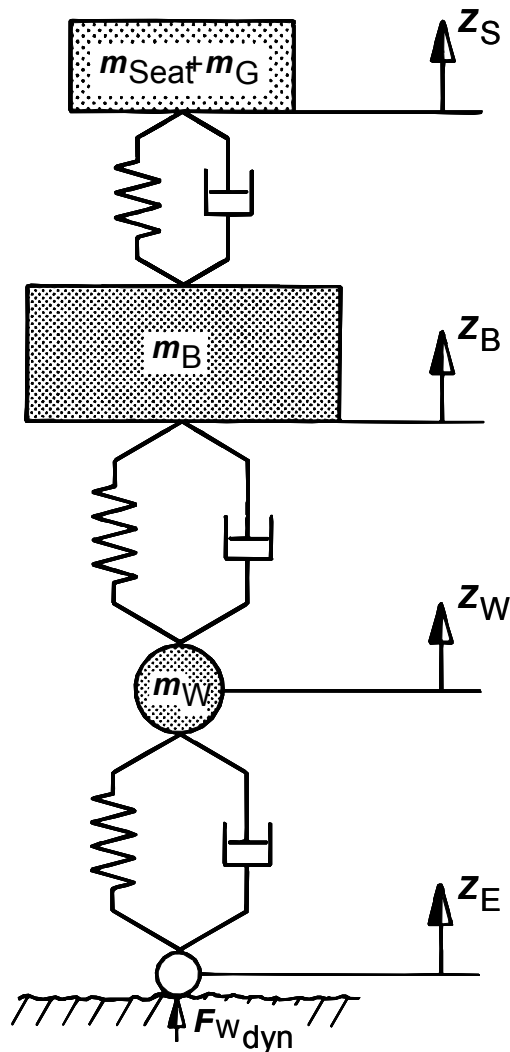


Fig.1.4-24: Structure of a three-mass suspension model

The added mass represents the mass of the sprung parts of the seat and the person sitting on it. Due to the small amount of mass added with respect to the mass of the body, the feedback on the body can generally be neglected. One can therefore begin with a two-mass system and add a simple oscillator.

In the following figures, this enhancement is done by superposing on the example car from paragraph 1.4.2.1 for two different seat masses. Fig.1.4-5 shows the amplification function, and Fig.1.4-6 shows the spectral power density of seat acceleration resulting from the seat's filter effect.

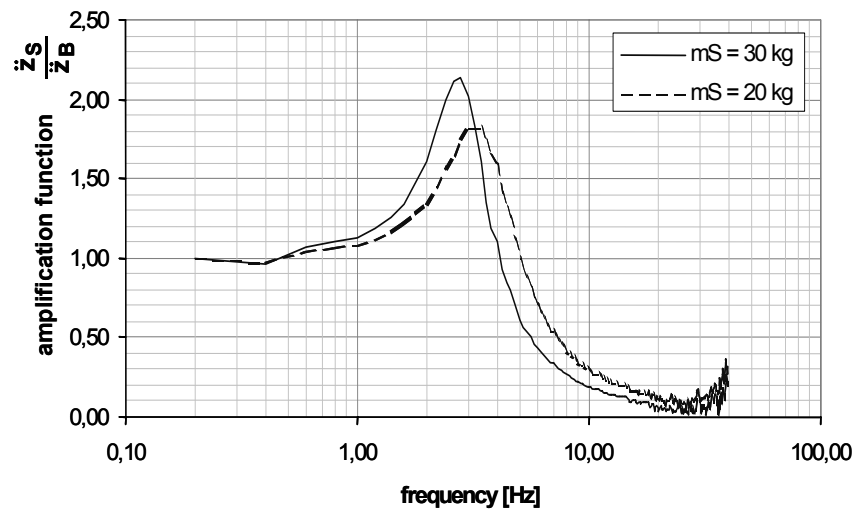


Fig.1.4-5: Amplification function of a three-mass suspension model

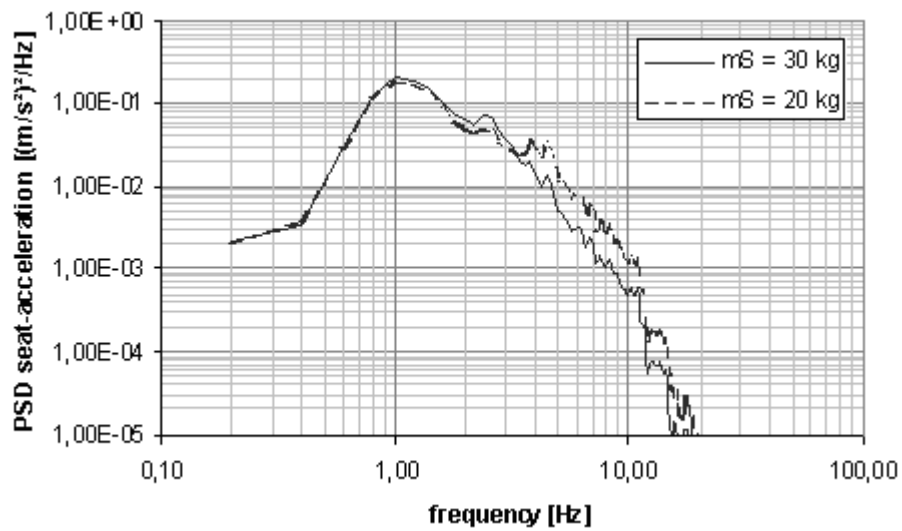


Fig.1.4-6: Seat acceleration of a three-mass suspension model

## 1.5 Single-Track Suspension Model

### 1.5.1 Double-axle Vehicle with bending resistant Structure

In single-track suspension models, the body is not seen as a mass point (lumped mass) but as a massive beam. In the simplest case, we are dealing with a model of a two-axle vehicle with a stiff body, i.e. a flexurally stiff beam (Fig. 1.5-1).

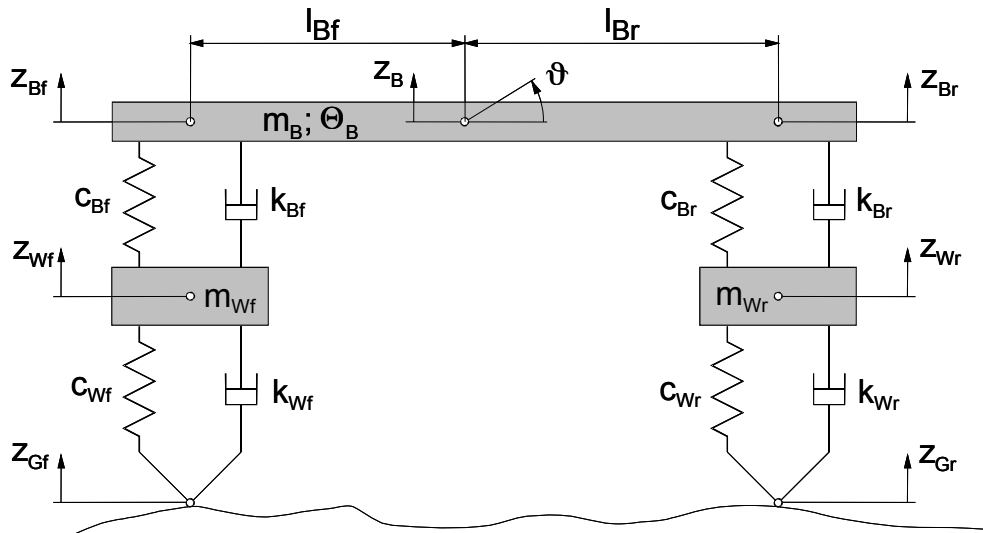


Fig.1.5-1: Single track suspension model

First we need to formulate the differential equations. The single-track suspension model for a two-axle vehicle according to Fig. 1.5-1 has four degrees of freedom:

- lifting and pitching of the body,
- lifting of front and rear axles.

The equations applicable for the center of gravity of the body are:

$$m_B \ddot{z}_B = -k_{Bf} (\dot{z}_{Bf} - \dot{z}_{Wf}) - c_{Bf} (z_{Bf} - z_{Wf}) - k_{Br} (\dot{z}_{Br} - \dot{z}_{Wr}) - c_{Br} (z_{Br} - z_{Wr}) \quad (1.5-1)$$

$$\Theta_B \ddot{\Theta}_B = l_f k_{Bf} (\dot{z}_{Bf} - \dot{z}_{Wf}) + l_f c_{Bf} (z_{Bf} - z_{Wf}) - l_r k_{Br} (\dot{z}_{Br} - \dot{z}_{Wr}) - l_r c_{Br} (z_{Br} - z_{Wr}) \quad (1.5-2)$$

Front and rear axles follow the equations:

$$m_{Wf} \ddot{z}_{Wf} = k_{Bf} (\dot{z}_{Bf} - \dot{z}_{Wf}) + c_{Bf} (z_{Bf} - z_{Wf}) - k_{Wf} (\dot{z}_{Wf} - \dot{z}_{Gr}) - c_{Wf} (z_{Wf} - z_{Gr}) \quad (1.5-3)$$

$$\begin{aligned}
 m_{W_r} \ddot{z}_{W_r} &= k_{B_r} (\dot{z}_{B_r} - \dot{z}_{W_r}) - c_{B_r} (z_{B_r} - z_{W_r}) \\
 &- k_{W_r} (\dot{z}_{W_r} - \dot{z}_{G_r}) - c_{W_r} (z_{W_r} - z_{G_r})
 \end{aligned} \tag{1.5-4}$$

Between the body movements above the axles  $z_{A_v}$  and  $z_{A_h}$ , the movement of the body center of gravity  $z_A$  and the pitch angle  $\vartheta$  there are the following relationships:

$$z_{B_f} = z_B - l_f \vartheta \tag{1.5-5}$$

$$z_{B_r} = z_B + l_r \vartheta \tag{1.5-6}$$

As for the single-wheel suspension model, natural radian frequencies and damping values can be derived from the differential equations for the single-track suspension model as well if coupling of the differential equations is neglected. Starting from the notion that all degrees of freedom – except for the one concerned – are blocked, we get:

|            | natural circular frequency                                      | damping factor  |         |
|------------|---|---|---------|
| travel     | $\sqrt{\frac{c_{B_f} + c_{B_r}}{m_B}}$                          | $\frac{k_{B_f} + k_{B_r}}{2\sqrt{m_B(c_{B_f} + c_{B_r})}}$  |         |
| body front | $\sqrt{\frac{c_{B_f}}{m_{B_f}}}$                                | $\frac{k_{B_f}}{2\sqrt{m_{B_f}c_{B_f}}}$  |         |
| body rear  | $\sqrt{\frac{c_{B_r}}{m_{B_r}}}$                                | $\frac{k_{B_r}}{2\sqrt{m_{B_r}c_{B_r}}}$  |         |
| pitch      | $\sqrt{\frac{l_{B_f}^2 c_{B_f} + l_{B_r}^2 c_{B_r}}{\Theta_B}}$ | $\frac{l_{B_f}^2 k_{B_f} + l_{B_r}^2 k_{B_r}}{2\sqrt{\Theta_B(l_{B_f}^2 c_{B_f} + l_{B_r}^2 c_{B_r})}}$ |         |
| front axle | $\sqrt{\frac{c_{B_f} + c_{W_f}}{m_{W_f}}}$                      | $\frac{k_{B_f} + k_{W_f}}{2\sqrt{m_{W_f}(c_{B_f} + c_{W_f})}}$  |         |
| rear axle  | $\sqrt{\frac{c_{B_r} + c_{W_r}}{m_{W_r}}}$                      | $\frac{k_{B_r} + k_{W_r}}{2\sqrt{m_{W_r}(c_{B_r} + c_{W_r})}}$  | (1.5-7) |

The axle-proportionate body masses result from the position of the centre of gravity:

$$m_{Bf} = m_B \frac{l_{Br}}{l_{Bf} + l_{Br}} \quad (1.5-8)$$

$$m_{Br} = m_B \frac{l_{Bf}}{l_{Bf} + l_{Br}} \quad (1.5-9)$$

With regard to suspension comfort, pitch natural frequency should be low. With specified suspension stiffness for lifting suspension, however, target-specific influencing is difficult, because the other influencing parameters are usually determined by different aspects (center-of-gravity location, wheelbase) or more or less result from the vehicle concept (moment of inertia).

### 1.5.1.1 Excitation by real unevenness Routing

Unlike the single-wheel suspension model, the single-track suspension model is excited by a single road irregularity twice: that is, first on the front axle and then once more on the rear axle. As a result, body acceleration of the two-axle model does not only depend on the excitation frequency but also on parameters like driving speed, the body natural frequency and the position of the measuring point in the vehicle.

In the following, excitation of the vibration system vehicle by the irregularity profile of the road is performed on front and rear axles deferred by the time differential  $\Delta t = l / v$  ( $l$  wheelbase,  $v$  driving speed). The motion equations are solved with the aid of the MATLAB simulation tool.

- Influence of driving speed

While the power density spectra of body acceleration and relative (specific) dynamic wheel load variation permit a differentiated assessment of a vehicle suspension, it is possible to assess a trend also on the basis of the respective effective values.

This approach makes sense, for example, if for trend assessment those parameters are varied that affect the entire power density spectrum, since then a value for suspension comfort or road grip can be stated as a function of the varied parameter.

The effective value of body acceleration can be determined on the basis of the time curve of acceleration:

$$\ddot{z}_{Beff} = \sqrt{\frac{1}{T} \cdot \int_0^T \ddot{z}_B^2 dt}$$

The effective value of body acceleration above the rear axle with average load was determined in this way in relation to the driving speed of a model vehicle, Fig. 1.5-2.

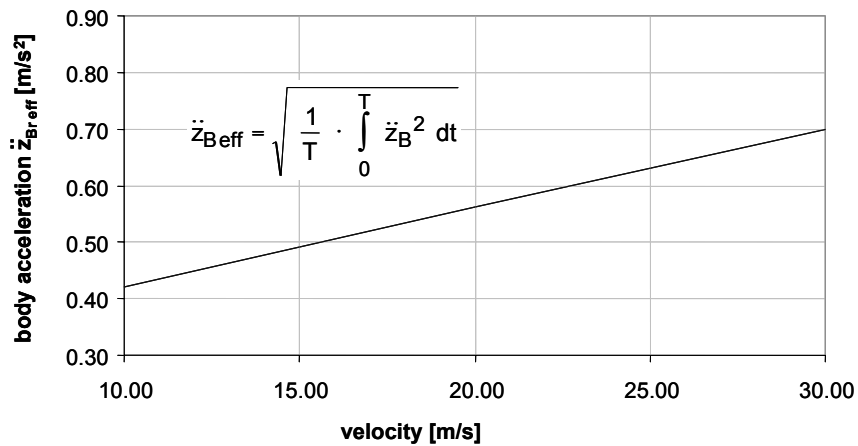


Fig.1.5-2: Body acceleration  $\ddot{z}_{Ah}$  in relation to the driving speed

- Influence of body natural frequency

For determining the influence of the spring rates of the body springs – and thus of the body natural frequency – on body acceleration, these spring rates are gradually reduced. For the model vehicle with average load and a driving speed of 22 m/s we thus obtain a curve as shown in Fig. 1.5-3.

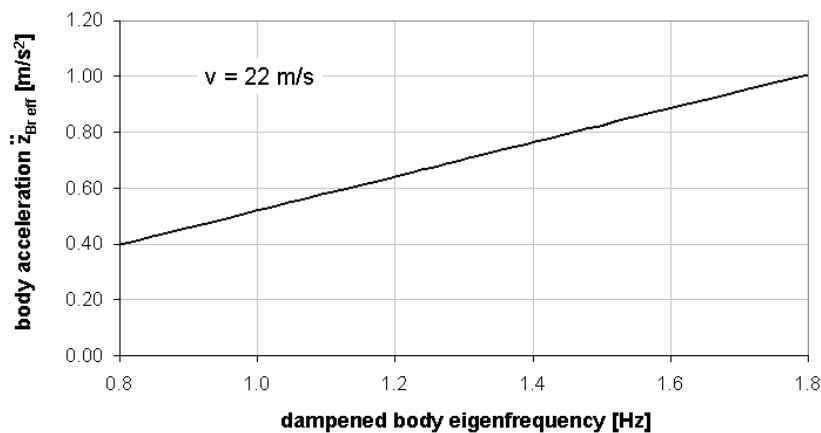


Fig.1.5-3: Body acceleration  $\ddot{z}_{Ah}$  in relation to the body natural frequency

For low body acceleration and good suspension comfort to be attained, it is of crucial importance to realize soft body springs, i.e. a low body natural frequency. This, however, requires a suitable vehicle concept, such as a low center of gravity, wide spring tracks. These boundary conditions were neglected in the considerations according to Fig. 1.5-3.

- Measuring point location

In Fig. 1.5-2 and Fig. 1.5-3, the body directly above the rear axle was defined as the "measuring point" of body acceleration. With otherwise identical conditions, the value of body acceleration also depends on the location of the measuring point on the body in vehicle longitudinal direction. This influence is shown in Fig. 1.5-4 for the original state.

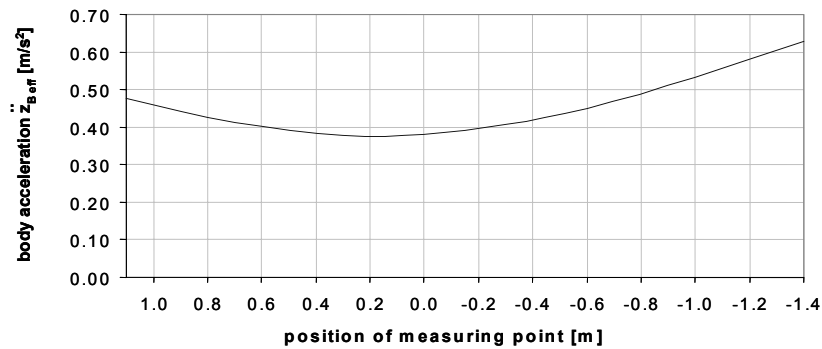


Fig.1.5-4: Body acceleration in relation to the location of the measuring point in the vehicle (The 0-value marks the center of gravity)

A minimum amount of body acceleration is found in the area of the center of gravity of the vehicle. With increasing distance from the center of gravity, the effect of the overlap of lift and pitch oscillations of the body on the resulting acceleration increases.

### 1.5.1.2 Mass and Spring Coupling

For further considerations, it seems practical to split the mass of the beam-shaped body into three single point (lumped) masses (Fig. 1.5-5).

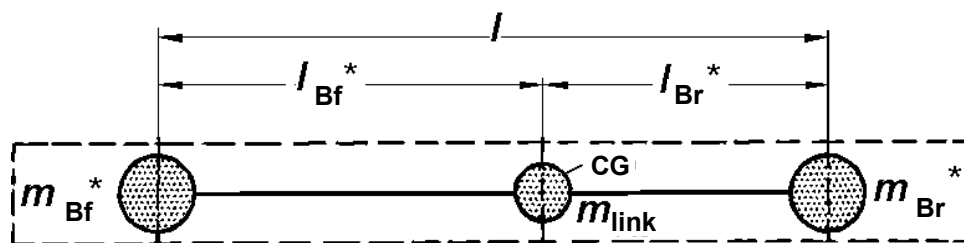


Fig.1.5-5: Configuration of the single-track suspension model with coupled mass  $m_{Link}$

Since total mass  $m_B$  center-of-gravity location  $l_{AV}^*$ ,  $l_{Ah}^*$  and moment of inertia  $\Theta_B$  must remain the same, the following three conditional equations follow:

$$m_{Bf}^* + m_{Br}^* + m_{link} = m_B \quad (1.5-10)$$

$$m_{Bf}^* \cdot l_{Bf}^* = m_{Br}^* \cdot l_{Br}^* \quad (1.5-11)$$

$$m_{Bf}^* \cdot l_{Bf}^{*2} + m_{Br}^* \cdot l_{Br}^{*2} = \Theta_B \quad (1.5-12)$$

Out of this the so-called coupling mass  $m_{link}$  results too:

$$m_{link} = m_B - \frac{\Theta_B}{l_{Bf}^* \cdot l_{Br}^*} \quad (1.5-13)$$

- Mass coupling

When a vehicle's front axle passes a bump, the shock/impact force acting on the body will result in body movement composed of the lifting motion of the body center of gravity  $S_A$  and a rotary motion around the vehicle transversal axis (pitching motion) through the center of gravity.

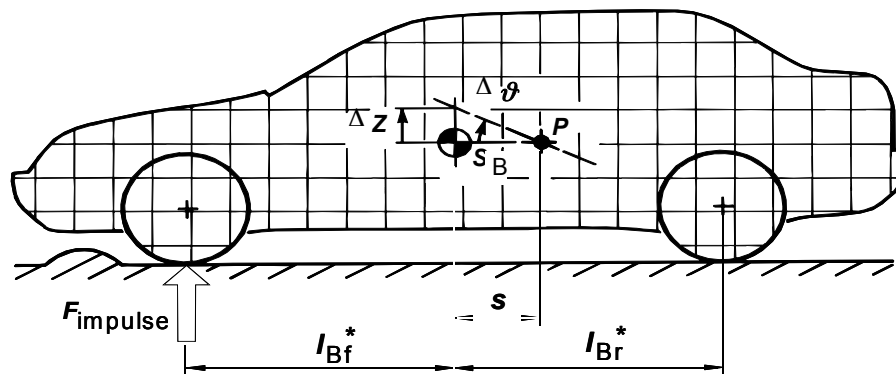


Fig.1.5-6: Shock excitation in the single-track suspension model

Associated with this body movement, there is a point of rest in the longitudinal center plane of the vehicle, which is referred to as center of impact /1/. The location of this point can be determined with the aid of the principles of linear and angular momentum:

$$\int_{t_1}^{t_2} F_{impulse} dt = m_B \cdot \dot{z}_2 - m_B \cdot \dot{z}_1 \quad (1.5-14)$$

$$\int_{t_1}^{t_2} F_{impulse} \cdot l_{Bf}^* dt = \Theta_B \cdot \dot{\vartheta}_2 - \Theta_B \cdot \dot{\vartheta}_1 \quad (1.5-15)$$



In consideration of the geometric relationship

$$s \cdot \Delta \vartheta \approx \Delta z$$

$$s (\dot{\vartheta}_2 - \dot{\vartheta}_1) = \dot{z}_2 - \dot{z}_1 \quad (1.5-16)$$

follows:

$$s = \frac{\Theta_B}{I_{Bf}^* \cdot m_B} \quad (1.5-17)$$

With the aid of this relation, the three potential cases regarding the value of the coupled mass, which as a purely theoretical operand can also turn out to be negative, can be illustrated:

1. Couple mass equals zero ( $m_{link} = 0$ ):

For the special case that the coupled mass equals zero,

$$\Theta_B = m_B \cdot I_{Bf}^* \cdot I_{Br}^*$$

applies and thus for the impact (shock) on the front axle

$$s = I_{Br}^*$$

In this case, the body above the rear axle remains at rest (unexcited). We have shock decoupling.

2. Couple mass greater than zero ( $m_{link} > 0$ ):

If the coupled mass is greater than zero, the following equation applies for the impact on the front axle:

$$s < I_{Br}^*$$

The center of impact in this case is located between body center of gravity and rear axle. This means that with identical total mass and identical wheelbase, the pitching motion of the body is more intense, which is to be considered a drawback with regard to riding comfort.

3. Couple mass less than zero ( $m_{link} < 0$ ):

If the relation between body mass, mass moment of inertia and center-of-gravity distances is such that the coupled mass is less than zero, then the following equation applies for the impact on the front axle:

$$s > I_{Br}^*$$

The center of impact in this case is no longer found between the axles. In the body movement resulting from the shock force on the front axle, we then usually find the share of lifting motion to be higher than that of pitching motion, which is to be considered favorable with regard to riding comfort.

These considerations can be made in a similar way for a rear axle passing a bump.

- Spring coupling :

Spring coupling as realized, for example, by the BLMC hydrolastic springing system, acts in the same way as mass coupling,  $m_{k0} < 0$ . By means of a hydraulic connection, compression of the front axle (due to a bump) causes rebounding of the rear axle, a response which counteracts the pitching motion of the body.

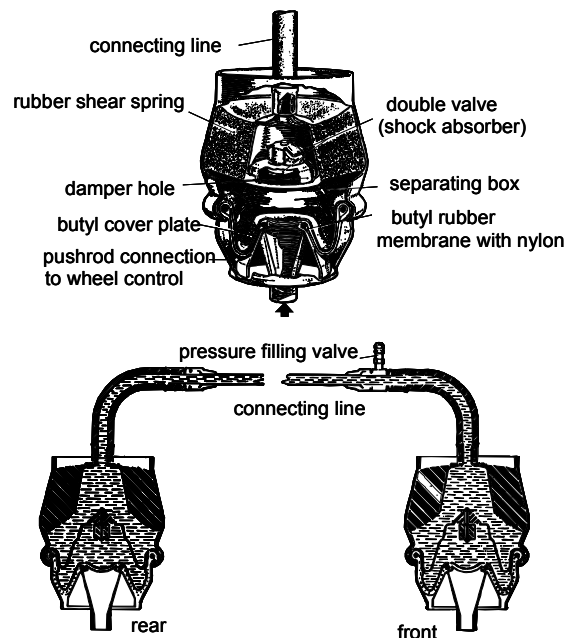


Fig.1.5-7: "Hydrolastic" compound suspension system in the Morris 1100, 1962

Spring coupling acc. to Fig. 1.5-8 is an alternative way of reducing pitching natural frequency with unchanged lifting natural frequency. While all springs are involved in the lifting motion, only the exterior springs are involved in the pitching motion.

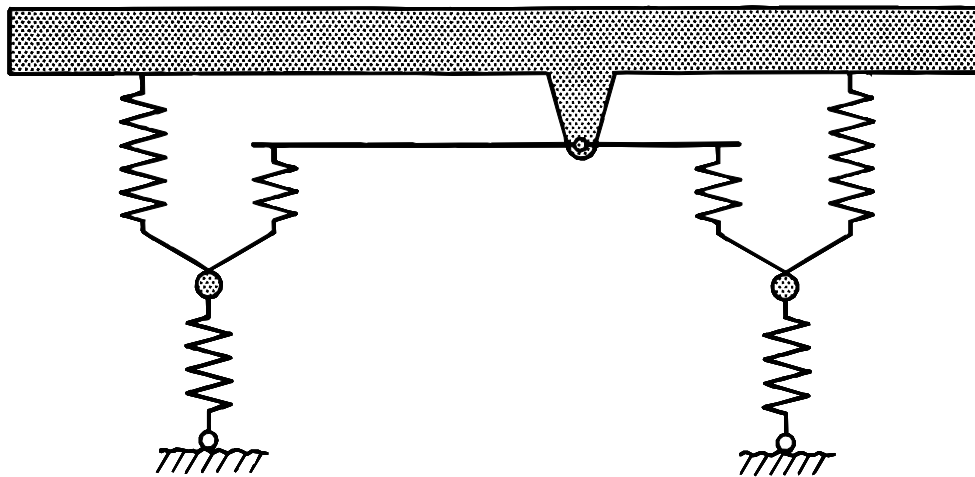


Fig.1.5-8: Two-axle vehicle with spring coupling

The potential of improvement of suspension behavior by means of coupled masses or springs is very limited, because the measures required are mostly hardly realizable or there is no latitude of design with regard to the influencing parameters.

### 1.5.2 Two axle Vehicle with additional Degrees of Freedom

In the two-axle vehicle according to Fig. 1.5-1, the body was assumed to be rigid. As opposed to cars and vans, the bending elasticity of the chassis frame as well as the elasticity of engine and cab suspension (heavy commercial vehicles usually feature elastic cab suspension for better isolation against vibration and torsion of the frame) in trucks cannot be neglected, because these factors significantly influence suspension behavior in these vehicle types. Fig. 1.5-9 shows a truck equivalent system with 15 degrees of freedom.

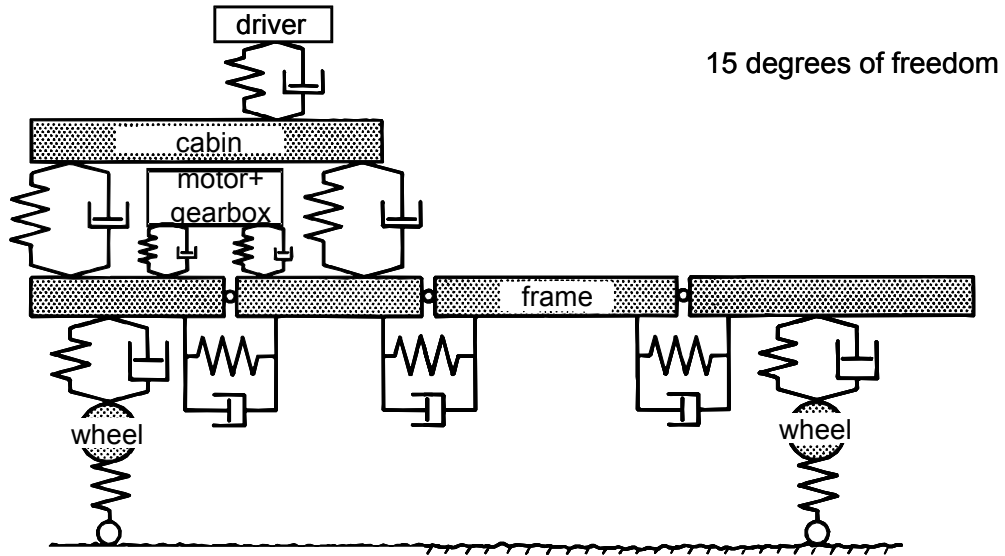


Fig.1.5-9: Structural model of a platform truck

### Semi trailer truck

The articulated vehicle is a vehicle type that presents particular problems with regard to suspension and driving stability. With this vehicle type, semitrailer and road tractor are linked via a joint in the vertical and transverse axes, Fig. 1.5-10.

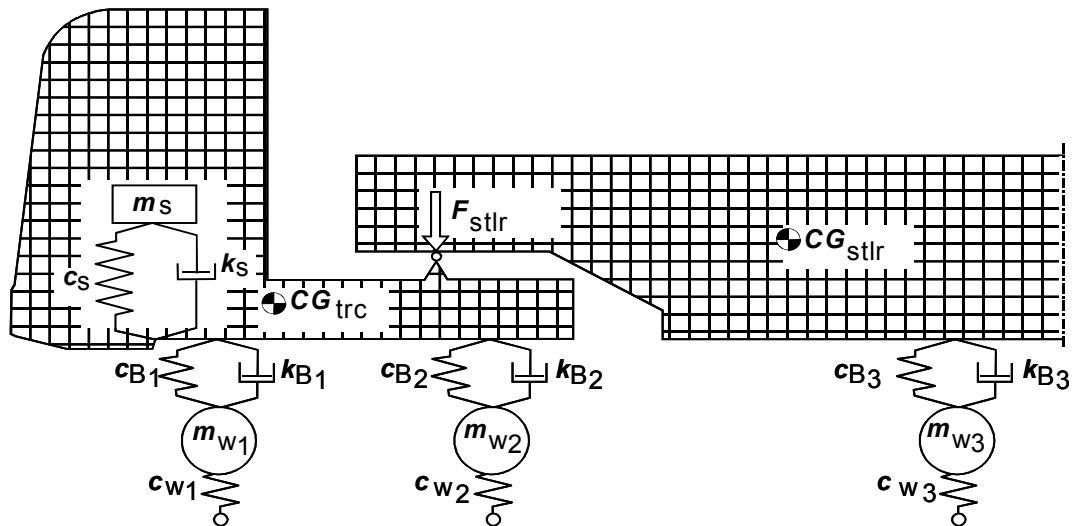


Fig.1.5-10: Structural model of a semitrailer unit

Since the semitrailer transfers the vertical load (fifthwheel load)  $F_{Sattel}$  to the road tractor, adequately loadable, i.e. stiff suspension is required. The moment of inertia acting during the pitching motion of the road tractor is, however, relatively small. The high moment of inertia of the semitrailer has no effect due to the fifthwheel coupling. The consequence of this is a

correspondingly high pitch natural frequency resulting in high K-values. Some improvement can be achieved by means of soft front springs of the road tractor.

It is a drawback of this measure that getaway jacking-up and brake dive are aided and in extreme cases even dynamic pitch angle and center-of-gravity acceleration are increased.

By means of a number of additional measures and determined tuning development, the suspension behavior of articulated vehicles has been significantly improved and adapted to that of other commercial vehicles in the meantime.

- Tandem axles of commercial motor vehicles

In HD trucks, tandem axles are used as:

- powered rear axles of trucks and articulated vehicles,
- nonpowered rear axles of trailers and semitrailers

The following example shows the powered tandem axle of a 22-t semitrailer truck, Fig. 1.5-11, the design of which is described by the equivalent system according to Fig. 1.5-12.

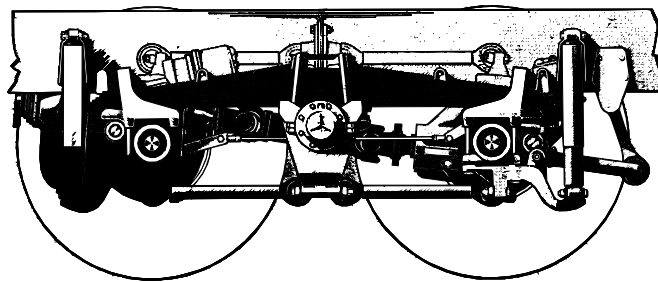


Fig.1.5-11: Swinging tandem axle with hydraulic damping (MB)

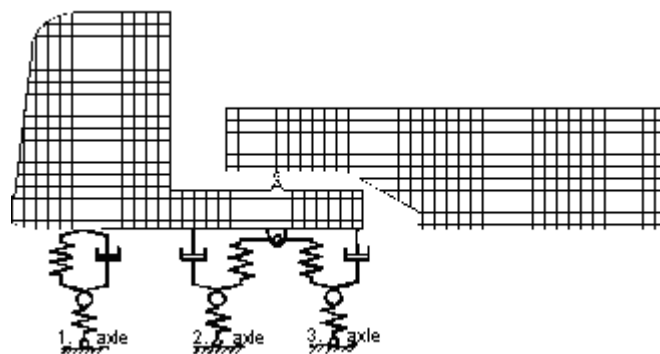


Fig.1.5-12: Equivalent system of a semitrailer truck with hydraulically damped tandem axle

Such tandem axles possess two degrees of freedom: homodirectional and heterodirectional vertical motion of the two axles. Natural vibration is characterized in particular by high dynamic axle loads, i.e. roadway load.

## 1.6 Two-Track Suspension Model

Using a two-track suspension model as shown in Fig. 1.6-1, the degrees of freedom

- Roll springing
- Distortion of the body
- Trampling of rigid axles

shall be dealt with in this chapter.

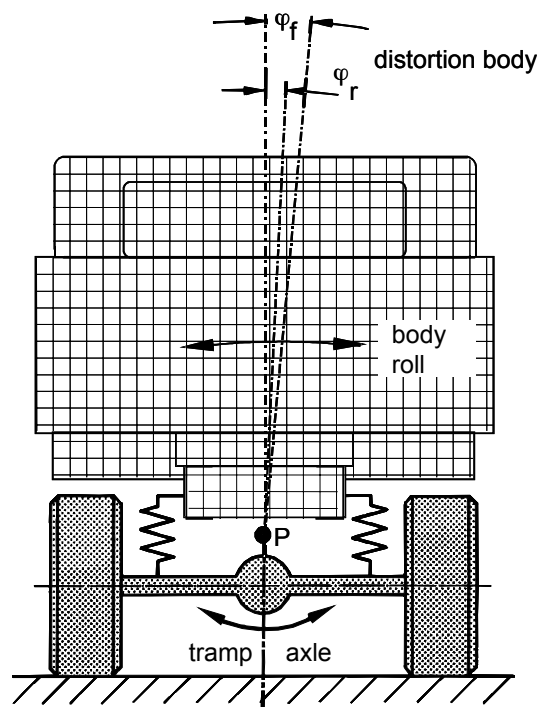


Fig.1.6-1: Two-track suspension model (truck)

### 1.6.1 Roll Springing

Roll springing is to be regarded first for a vehicle with rigid front and rear axles (e.g. truck, jeep), since this case is kinematically simple.

While cornering, the body is laterally displaced due to the centrifugal force. This deflection takes place around an axis of rotation, which passes through the roll poles at the front and rear axles and is called the Roll axis.

The positions of the roll poles, which depend on the kinematics of the wheel control or the axle coupling to the body, will be dealt with in the chapter "wheel suspensions".

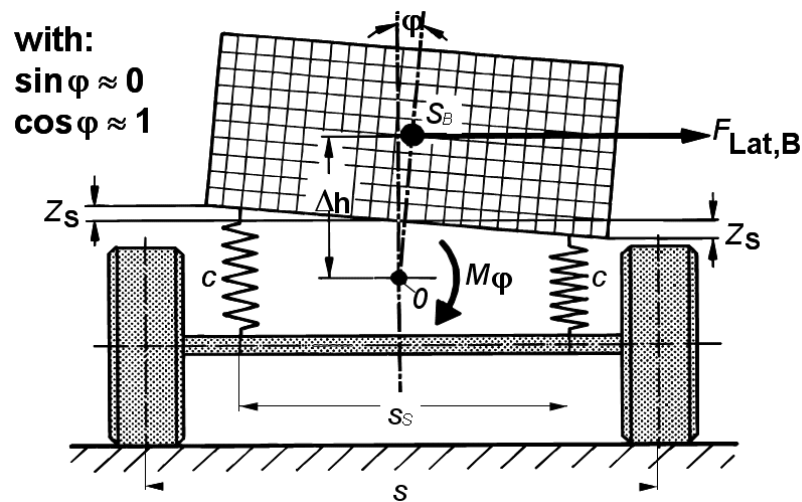


Fig.1.6-2: Equivalent system model for the suspension

The centrifugal force  $F_{Lat,B}$ , acting at the centre of gravity of the body, gives rise to a torque  $M_\varphi$  around the roll axis according to fig. 1.6-2:

$$M_\varphi = F_{Lat,B} \cdot \Delta h \cdot \cos \varphi + m_B \cdot g \cdot \Delta h \cdot \sin \varphi \quad (1.6-1)$$

with  $\Delta h$ : vertical distance between the centre of gravity of the body  $S_B$  and the roll axis

The inclination of the roll axis in the vehicle longitudinal plane is thus neglected. The torque created by the body weight is also usually neglected with passenger cars, i.e. applies here:  $\sin \varphi \ll \cos \varphi$ .

With these simplifications, the aligning torques applied by the body springs around the roll axis are given by:

$$F_{Lat,B} \cdot \Delta h = 2 \cdot \frac{s_{Sf}}{2} \cdot c_{Bf} \cdot f_{Sf} + 2 \cdot \frac{s_{Sr}}{2} \cdot c_{Br} \cdot f_{Sr} \quad (1.6-2)$$

with:  $s_{Sf,r}$ : Spring track width in front, rear

$f_{Sf,r}$ : Spring compression in front, rear

$c_{Bf,r}$ : Body spring rigidity in front, rear

With  $f_F \approx \varphi \cdot \frac{s_S}{2}$  one finally receives for the roll angle  $\varphi$ :

$$\varphi = \frac{2 \cdot \Delta h}{c_{B,f} \cdot s_{S,f}^2 + c_{B,r} \cdot s_{S,r}^2} \cdot F_{Lat,B} \quad (1.6-3)$$



The roll angle ' $\varphi$ ' is thus inversely proportional to the square of the spring track width. For a small body inclination, the spring track width should therefore be as high as possible while driving along curves.

### 1.6.1.1 Stabilizer and Compensating Spring

Anti-roll suspension (roll damping) can be stiffened without changing vertical suspension through installation of a stabilizer spring, Fig. 1.6-3.

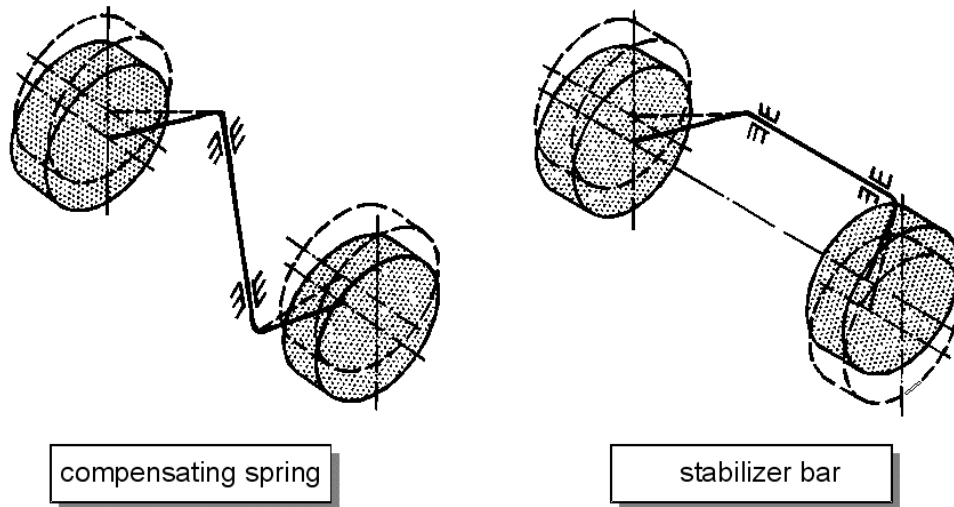


Fig. 1.6-3: Functional principle of stabilizer and compensating spring

During the rolling motion of the body, i.e. a heterodirectional compression motion of the wheels, the stabilizer is torqued and thus provides a self-aligning torque around the roll axis, which reduces body inclination. In case of a pure lifting motion of the body suspension on the axle considered, the stabilizer will have no effect. A stabilizer track width  $s_{\text{Stab}}$ , to which the stabilizer stiffness  $c_{\text{Stab}}$  relates, is defined analogous to the spring track width  $s_F$ .

Stabilizer stiffness  $c_{\text{Stab}}$  then corresponds to the stabilizer force at the ends of the stabilizer spring referred to half the differential compression of these ends.

For the roll angle  $\varphi$  thus applies:

$$\varphi = \frac{2 \cdot \Delta h \cdot F_{\text{Lat,B}}}{c_{B,f} \cdot s_{F,f}^2 + c_{\text{Stab},f} \cdot s_{\text{Stab},f}^2 + c_{B,r} \cdot s_{F,r}^2 + c_{\text{Stab},r} \cdot s_{\text{Stab},r}^2} \quad (1.6-4)$$

Should the ratio of the shares of the rolling moment  $M_\varphi$  supported by the stabilizers on front and rear axles differ from the ratio of the shares supported by the body suspension, or if only one axle has a stabilizer spring installed, then not only the roll angle will be reduced, but the

distribution of the wheel load differentials, which occur during cornering between the wheels of the right and left vehicle sides, among front and rear axle will be influenced.

The influences on vehicle handling caused by this are dealt with in the chapter "Transverse Dynamics".

The compensation spring is an antagonistic spring that has an effect counteracting that of the stabilizer spring. As a purely vertical suspension element it has not effect on the rolling motion of the body.

In the past, the compensating spring was used for axle designs whose wheel suspension kinematics required wheel load differentials to be as low as possible for the so-called bump effect (bottoming-out effect) to be suppressed (cf. chapter on wheel suspensions). The stiffness of body suspension and thus the share of the rolling moment supported on the axle considered could then be reduced accordingly. The compensating spring is no longer found in modern wheel suspension systems.

Fig. 1.6-4 shows an automobile front axle (Opel Senator) as an example for the installation of a stabilizer

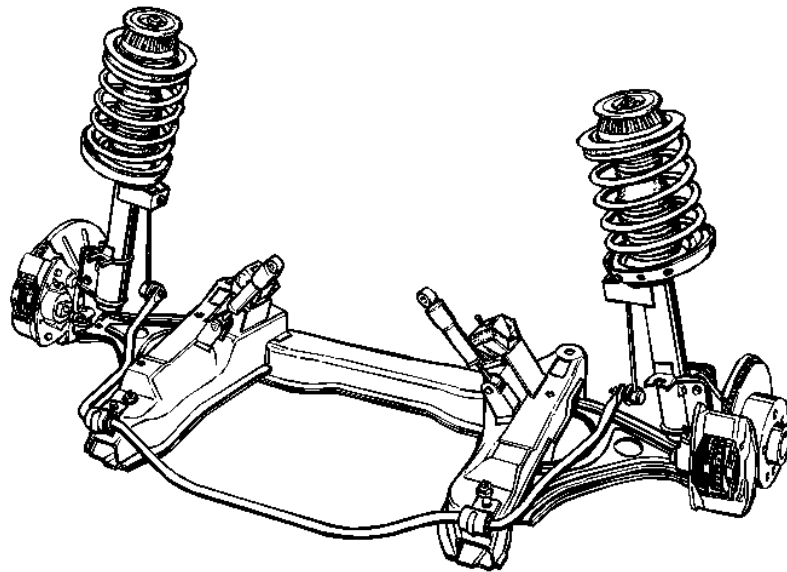


Fig. 1.6-4: Stabilizer spring on an automobile front axle

### 1.6.1.2 Vehicle Conception and Suspension Characteristics

The parameter studies in the paragraph 1.4.2.1 (passenger car) and 1.4.2.2 (truck) show that a necessary prerequisite for the achievement of good suspension characteristics is a low body- eigenfrequency or sufficiently soft body springs.

On the other hand, the lower limit of body eigenfrequency or spring rates is determined in particular by static and quasi-static effects such as level modification by load and body inclination while driving along curves. While static level modifications could be eliminated by load-sensitive regulating springs, curve inclination can be only be reduced in small limits by means of stabilizers. The relationship between body inclination, body natural frequency and body acceleration is therefore considered in the following.

According to paragraph 1.6.1.1, while driving along curves (steady-state circular-course driving) a roll angle is generated:

$$\varphi = \frac{2 \cdot \Delta h \cdot F_{\text{Lat,B}}}{(c_B + c_{\text{Stab}}) \cdot s_S^2} \quad (1.6-5)$$

By using centrifugal force

$$F_{\text{Lat,B}} = \frac{m_B \cdot v^2}{r} \quad (1.6-6)$$

arises

$$\varphi = \frac{2 \cdot \Delta h \cdot m_B \cdot v^2}{(c_B + c_{\text{Stab}}) \cdot s_S^2 \cdot r} \quad (1.6-7)$$

With the equation

$$f_{eB} = \frac{1}{2\pi} \cdot \sqrt{\frac{2 \cdot c_B}{m_B}} \quad (1.6-8)$$

For the body eigenfrequency of the stroke oscillation, resolved to  $m_B$

$$m_B = \frac{2 \cdot c_B}{4\pi^2 \cdot f_{eB}^2} \quad (1.6-9)$$

The roll angle is given by

$$\varphi = \frac{2 \cdot \Delta h \cdot v^2 \cdot 2 \cdot c_B}{(c_B + c_{\text{Stab}}) \cdot s_S^2 \cdot r \cdot 4 \cdot \pi^2 \cdot f_{eB}} \quad (1.6-10)$$

and by solution  $f_{eB}$  is given by

$$f_{eB} = \frac{v}{\pi} \cdot \sqrt{\frac{1}{r}} \cdot \sqrt{\frac{1}{\varphi}} \cdot \sqrt{\frac{\Delta h}{s_S^2}} \cdot \sqrt{\frac{1}{1 + \frac{c_{\text{Stab}}}{c_B}}} \quad (1.6-11)$$

Note  $c_B = c_{Bf} + c_{Br}$ , where  $c_{Bf}$  or  $c_{Br}$  is the spring rate of one spring on the front or rear axle.

The first three factors of this product depend on the respective driving condition. If a standard case is assumed, which is characterized by a curve radius  $r = r_0 = 50$  m and a driving speed  $v = v_0 = 16$  m/s, then the recalculation shows - in agreement with subjective feeling - that for this case, a roll angle of  $\varphi = \varphi_0 = 3^\circ$  is acceptable. With this standardisation the body eigenfrequency of a vehicle still depends on the various factors related to the design of the vehicle, i.e. on the dimensions  $\Delta h$  and  $s_S$  as well as the relation of the spring constants  $c_{Stab}$  and  $c_B$ .

This relationship is represented in the lower section of Fig.1.6-5.

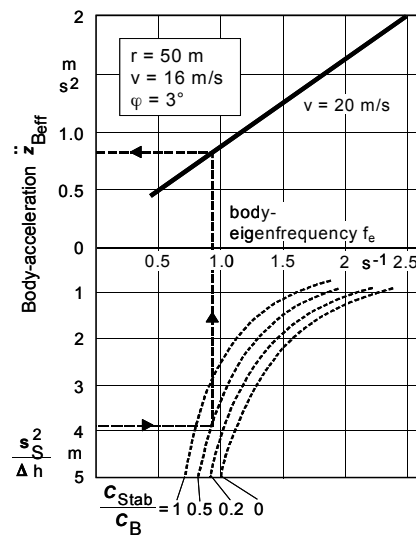


Fig.1.6-5: Influence of the height of the centre of gravity and spring track width on body natural frequency and effective value of body acceleration

In the upper part of Fig.1.6-5, the relationship between body eigenfrequency and body acceleration is represented for a vehicle with two axles at  $v=20$  m/s. The characteristic curve is well-known from fig. 1.5-3 for the single track model of the exemplary passenger car.

### 1.6.2 Distortion of the structure (twisting)

The closed bodies of vehicles such as sedans, transporters and buses can be assumed to be rigid in terms of the handling of the vehicle suspension system, since the bending or torsional rigidity of the body is much higher here than the rigidity in the suspension system.

In contrast, the torsional rigidity of the chassis in commercial vehicles with ladder-type frames, Fig.1.6-6, can not be neglected. The frame is designed to be torsionally elastic here, in order to reduce the stress of the material in the interconnecting points between transverse

and longitudinal members, i.e. riveting is used instead of welding at the joints and open profiles are used instead of closed profiles for longitudinal and transverse beams.

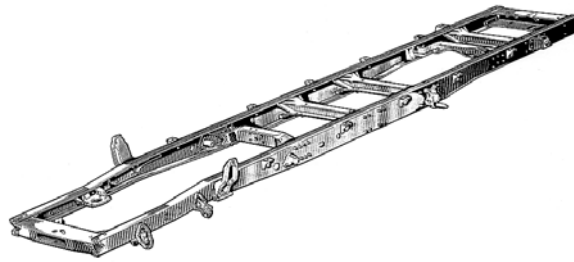


Fig.1.6-6: Torsionally elastic framework of a light truck

For commercial vehicles used on construction-sites or off-road torsionally elastic framework offers the advantage that larger surface irregularities can be absorbed without loss of traction (wheels lifting off the surface of the road) than with sole use of the spring travel offered by the body springs.

A computational handling of the twisting of the framework is relatively simple, if one divides the body into two subsystems with individual centres of gravity, Fig.1.6-7.

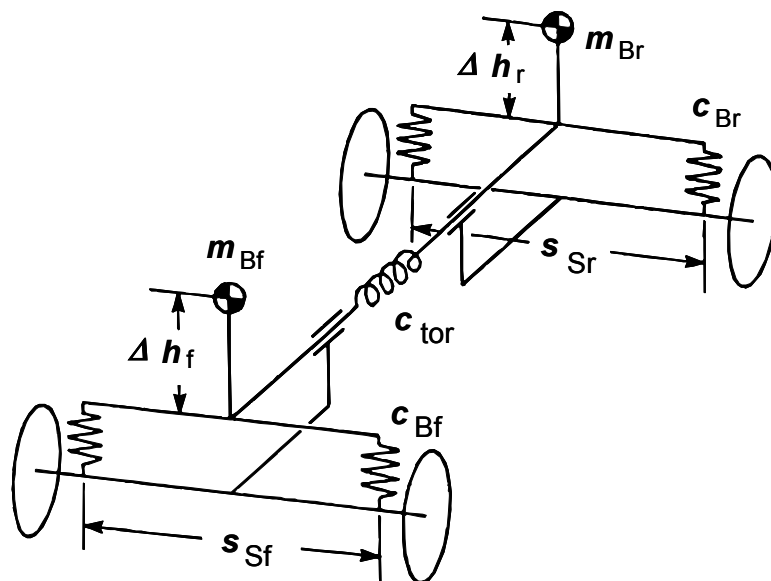


Fig.1.6-7: Replacement system of a vehicle with a torsionally elastic framework

For steady-state cornering, the equilibriums of torques set up around the roll axis for front and rear ends separately result in two equations for the two unknown roll angles  $\varphi_f$  and  $\varphi_r$ :

$$m_{Bf} \cdot a_y \cdot \Delta h_f = \varphi_f \cdot \frac{s_{Sf}^2}{2} \cdot c_{Bf} + (\varphi_f - \varphi_r) \cdot c_{tor} \quad (1.6-12)$$

$$m_{Br} \cdot a_y \cdot \Delta h_r = \varphi_r \cdot \frac{s_{Sr}^2}{2} \cdot c_{Br} + (\varphi_r - \varphi_f) \cdot c_{tor} \quad (1.6-13)$$

Since the difference between spring forces on one axle depends on the roll angle of the appropriate body sub-system, the proportion of the total roll torque supported at the regarded axle in vehicles with torsionally elastic chassis is influenced not only by distribution of the body spring stiffness and stabilizer stiffness on the front and rear axles, but also by the torsional rigidity of the framework. Accordingly, the wheel load differences during cornering at the front and the rear axle depend additionally on the torsional rigidity of the framework.

The influence of these wheel load differences on the steering behavior during cornering is treated in the section 'Lateral Dynamics' in connection with the effects of stabilizer springs.

### 1.6.3 Rigid axle Tramp

Fig. 1.6-8 shows an equivalent model for the investigation of the vibrational behavior of rigid axles.

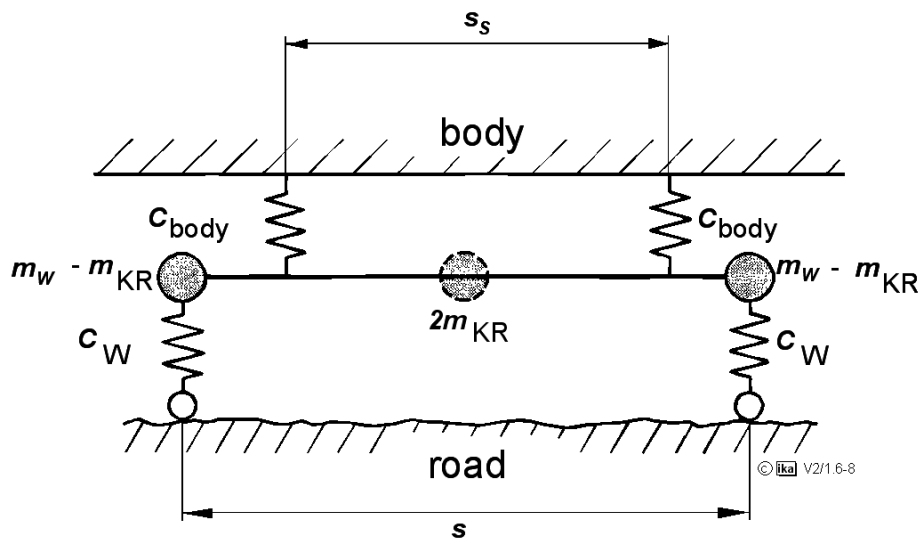


Fig. 1.6-8: Axle equivalent system

Rigid axle excitation not only results in the vertical motion (bounce) discussed so far but also in tramp motion due to irregular road roughness. The two forms of motion are usually (with left/right axle symmetry) decoupled. Approximate vertical motion natural frequencies are obtained from:

$$\omega_{e\text{rec}} = \sqrt{\frac{c_{\text{Body}} + c_{\text{W}}}{m_{\text{W}}}} \approx \sqrt{\frac{c_{\text{W}}}{m_{\text{W}}}} \quad (1.6-14)$$

Only if the theoretical case is assumed that  $2 m_{\text{KR}} = 0$ , i.e. the mass of the entire axle is concentrated on the two wheels, will also apply to tramp motion (axle tramp).

$$\omega_{e\text{Tr}} \approx \sqrt{\frac{2(s/2)^2 \cdot c_{\text{W}}}{\Theta}} \approx \sqrt{\frac{2(s/2)^2 \cdot c_{\text{W}}}{2(s/2)^2 \cdot m_{\text{W}}}}$$

$$\omega_{e\text{Tr}} \approx \sqrt{\frac{c_{\text{W}}}{m_{\text{W}}}} \quad (1.6-15)$$

In reality, tramp natural frequency exceeds vertical motion natural frequency, with the latter being in the range of  $f_e = 9 - 14 \text{ s}^{-1}$  (with tandem axles and powered truck front axles also lower).

Analogous investigation of damping  $D$  reveals that with tramp motion it is lower than with vertical motion. Rigid axle tramp would therefore result in higher dynamic wheel loads than vertical motion, provided the excitation of both forms of motion by the roadway is of about the same magnitude. Usually, however, we find the (symmetric) vertical motion excitation to be dominant with normal roadways.

The resulting dynamic wheel loads of the rigid axle are higher than for independent wheel suspension. Moreover, the rigid axle is heavier.

## 1.7 Suspension Investigation Methods

The term riding comfort usually characterizes the vibrational comfort of a motor vehicle. The low-frequent comfort impression in an automobile is not only the result of vibration excitation of the automotive body due to road roughness but also of irregularities (wheel, tire) and the gas and inertia forces of the engine, Fig. 1.7-1.

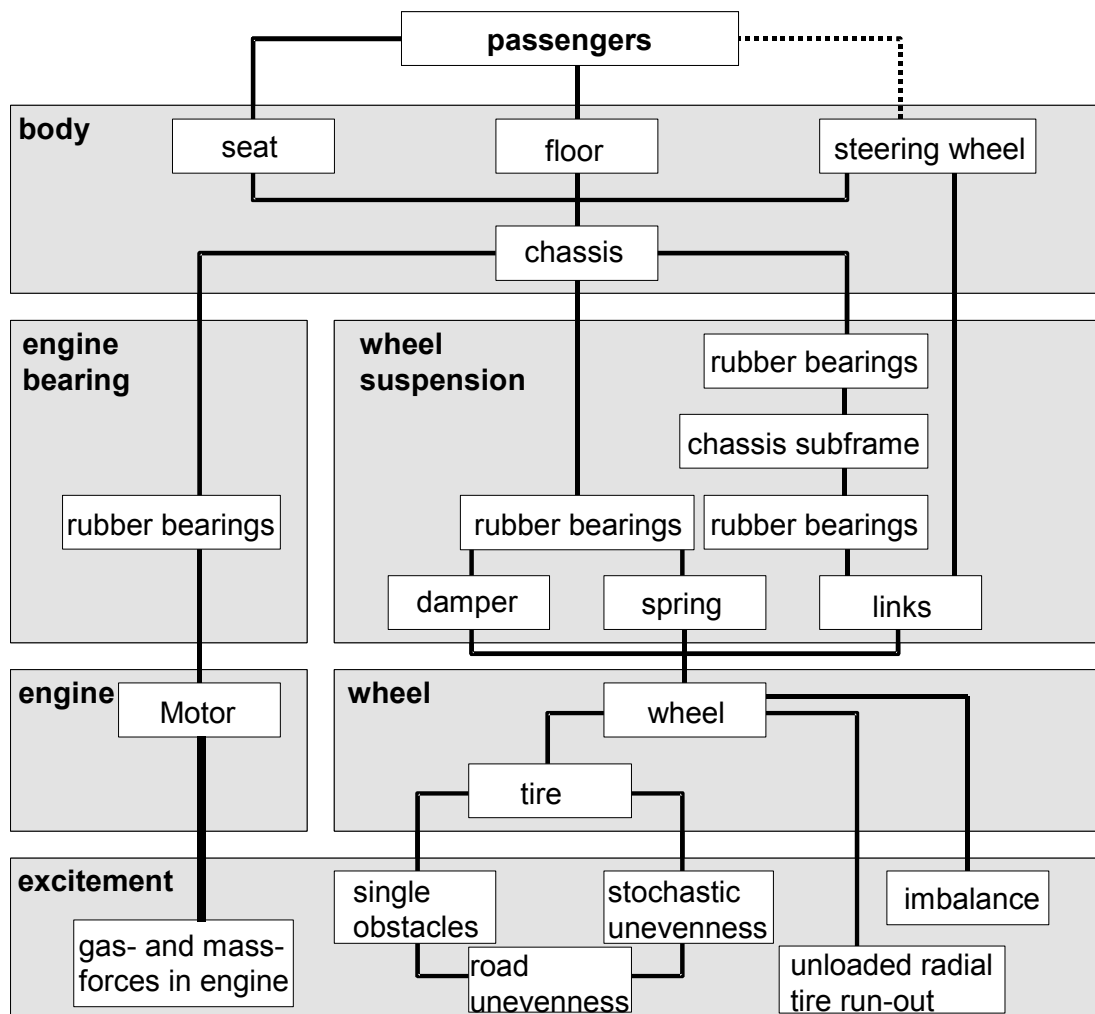


Fig.1.7-1: Paths of transmission of vibration excitation to the vehicle occupant

The forms of excitation listed cause a multitude of vibration phenomena perceived by the vehicle occupant via floor, seat and steering wheel (driver) as body, chassis and engine suspension vibration, shaking, jerking, or in the form of shocks (bumps).

Fig. 1.7-2 provides a more detailed overview of vibration phenomena determining riding comfort. In addition to information about the frequency ranges involved, the excitations are shown as well as the influences of individual assemblies of the vehicle on the vibration



phenomena.

| <ul style="list-style-type: none"> <li>● great influence</li> <li>○ small influence</li> </ul> |                    | <u>excitement</u><br>road unevennesses<br>unloaded radial tire<br>run-out (wheel, brake)<br>gas- and mass-forces<br>within engine | influence of parameters |       |            |           |                     |                   |        |             |                 |         |
|--|--------------------|---|-------------------------|-------|------------|-----------|---------------------|-------------------|--------|-------------|-----------------|---------|
|  |                    |   | body                    | cabin | front axle | rear axle | suspension/ damping | steering assembly | engine | drive train | engine bearings | exhaust |
| vibration/<br>noise phenomenon   | frequency<br>range |   |                         |       |            |           |                     |                   |        |             |                 |         |
| body vibrations  | 1 - 2              | ●   |                         |       |            | ○         |                     |                   | ○      |             |                 |         |
| lateraljerking   | 4 - 10             |   |                         |       |            | ○         |                     |                   | ○      |             | ●               | ○       |
| abrupt load alteration   | 8 - 20             |   |                         |       |            |           |                     |                   |        |             | ●               | ○       |
| engine shake   | 10 - 13            |   |                         |       |            |           |                     |                   |        |             | ●               | ○       |
| axle vibrations  | 10 - 15            | ●   | ○                       |       |            |           |                     |                   |        |             | ○               | ○       |
| wheelight  | 10 - 20            |   |                         |       |            |           |                     |                   |        |             | ○               | ○       |
| brake judder   | 15 - 25            |   |                         |       |            |           |                     |                   |        |             | ○               | ○       |
| idle shake/ drone  | 20 - 30            |   |                         |       |            |           |                     |                   |        |             | ○               | ○       |
| steering wheel shake   | 20 - 35            | ○   | ●                       |       |            |           |                     |                   | ●      |             | ○               | ○       |
| body shake   | 20 - 35            | ○   | ○                       |       |            |           |                     |                   |        |             |                 |         |
| body drone   | 25 - 75            | ●   | ○                       |       |            |           |                     |                   |        |             | ○               |         |
| axle roughness   | 30 - 80            | ●   |                         |       |            |           |                     |                   |        |             |                 |         |
| drive roughness  | 50 - 100           |   |                         |       |            |           |                     |                   |        |             | ●               | ○       |
| exhaust vibrations   | 50 - 200           |   |                         |       |            |           |                     |                   |        |             |                 | ●       |
| driving noise  | 50 - 250           | ●   |                         |       |            |           |                     |                   |        |             |                 |         |
| engine resonances  | 100 - 250          |   |                         |       |            |           |                     |                   |        |             | ●               | ○       |

Fig.1.7-2: Vibrational phenomena / 27 /

A high level of riding comfort requires a low level of disturbing vibrations, shaking, jerking or bumping (shocks).

Various methods of measuring and analysis are employed for the design and tuning of vehicle suspensions. On the following pages, the most important methods will be described and their advantages and disadvantages will be discussed.

- Calculating model

Simple calculating models, such as the single-wheel suspension model or the single-track suspension model, were comprehensively dealt with in the preceding chapters. With modern computer aid, significantly more complex models can be generated, which produce results of much greater precision. Fig. 1.7-3 , for example, shows the FE simulation model of a complete vehicle. This model not only considers the dynamic properties of chassis and drive train but also the deformation behavior of the body.

FE-simulation model of a complete vehicle  
(Audi A8)

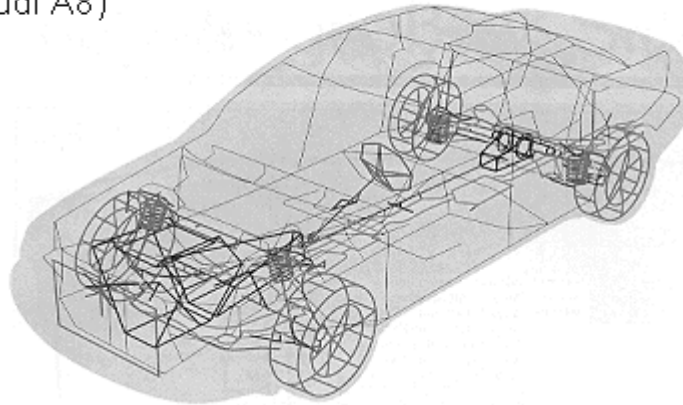


Fig.1.7-3: FE complete-vehicle simulation model of the Audi A8

In addition to complete vehicles, also individual vehicle assemblies are subjected to simulation studies. Fig. 1.7-4 shows an example of FE modeling of a front end with steering, wheel suspension, axle bracket and wheels.

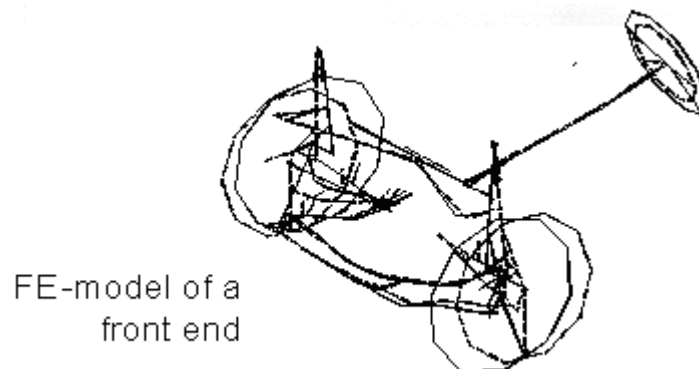


Fig.1.7-4: FE modeling of an automobile front end

Such a model can be used to define remedial measures against the vibration from wheel/flight (niggle) (cf. Fig. 1.7-2), which can be excited by unloaded radial tire run-out or wheel imbalance.

Nevertheless, even very complex models involve a multitude of simplifications which significantly affect the precision of calculating models and under certain circumstances may even result in incorrect statements as to trends. The major benefits of calculating models are represented by the fact that they can be employed at a very early stage of development and that their transparency facilitates analysis and the implementation of target-specific improvement measures.

- Excitation on the hydraulic pulse test rig

While computer models are applicable any time during vehicle development, vibrational analysis based on a measurement on the hydraulic pulse usually requires a complete vehicle. Thereby, the excitation can be done in form of a 'real' or simulated road unevenness profile, or a sinusoidal signal. Fig.1.7-5 shows the testing of an ambulance on the hydraulic 4-post test rig at the ika.

**advantages:**

- good insight into complete suspension system (analysis and diagnosis)
- reproducibility of measuring results
- shortening of measuring time by enlarging amplitudes for endurance testing possible
- short conversion time
- vehicle does not have to be in running condition

**disadvantages:**

- components must already exist
- considerable effort with equipment



© Ika KFZ II 1-7 eno.nl

Fig.1.7-5: Hydraulic 4-post test rig

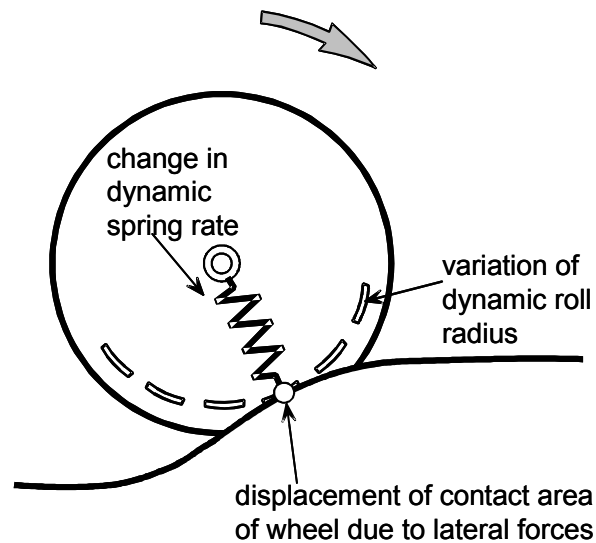
While calculation methods can be employed at any stage of vehicle development, vibration analysis by means of hydropulse testing as a rule requires a finished vehicle. Excitation can be effected by means of a "real" as well as by means of a

simulated road spectrum, or by means of a sinusoidal signal. **Fig. 1.7-5** shows the testing of a motorized ambulance unit by means of the 4-ram hydropulser of the ika.

The lab environment of hydropulse measurement offers a number of advantages:

- good insight into the overall suspension system (analysis and diagnosis),
- reproducibility of measuring results,
- accelerated endurance testing through amplitude magnification,
- fast conversion,
- vehicle does not have to be ready for driving.

Problems are regularly encountered in hydropulse testing if the influence of the rolling wheel and the longitudinal dynamics in the chassis play a role, Fig. 1.7-6.



- Spring rate and damping factor of rolling wheel are distinctively different from those of a resting wheel.
- Variation of the dynamic roll radius due to vertical impression of the tire causes rotational accelerations of the wheel and therefore lateral forces in the contact area.
- Unevennesses lead to local incline and therefore to a displacement of the wheel-contact area. This also causes lateral forces within the suspension.

Fig.1.7-6: Effects of the rolling wheel that cannot be simulated on the hydropulser

- Stiffness and damping of the rolling wheel differ greatly from the stiffness and damping of the stationary wheel.
- Variation of the dynamic rolling radius as a result of vertical deformation of the wheel causes rotational acceleration of the wheels and thus longitudinal forces in the tire-contact center (footprint center).
- Unevenness results in local grades and thus in displacements of the tire-contact center (footprint center). This effect also causes additional longitudinal forces in the chassis.

The considerable amount of equipment required and the fact that at least one prototype has to be available are also disadvantages of hydropulse testing.

- Driving tests

Subjective assessment of the suspension behavior of a vehicle by means of an on-road test is the most obvious and still also the most important method, because the driver can obtain an immediate impression of the behavior of the vehicle.

The drawback of this method is the fact that assessment is only possible after design and construction of at least one prototype, i.e. at an advanced stage of development that usually allows only details to be changed. Moreover, analysis of a suspension evaluation composed of many individual effects is very difficult and constitutes a poor basis for specific improvement measures. On-highway testing is nowadays usually only used for fine-tuning at a late stage of development.

Fig. 1.7-7 summarizes the methods discussed

| technique                           | mathematical model                  | hydropulser   | driving test   |
|-------------------------------------|-------------------------------------|---|--|
| statement of subjective assessments |                                     | certain effects are neglected, problems can be clearly approached | identical with reality, use of appropriate roads necessary |
| relevance of measuring results      | only as good as the models used     | can be complicated under certain circumstances                    | good   |
| reproducibility                     |                                     | good  | medium   |
| representative for analysis         | good within the limits of the model | good  | can be complicated due to superposition of both axles      |

Fig.1.7-7: Summary of methods discussed

ika - Institut für Kraftfahrwesen der RWTH Aachen - Opera

Datei Bearbeiten Ansicht Lesezeichen Extras Hilfe

Google: **Studium Wirtschaft** • www.fhm-mittelstand.de **Mut zum Leben - Beratung** • www.mutzumleben.info  
**Betriebswirtschaft studieren an der Fachhochschule des Mittelstands FHM** **Professionelle, schnelle Hilfe per Email - Krise als Chance nutzen!**

Neue Seite UMFRAGE Leere Seite Bedienungsanleitungen ika - Institut für Kraftfahr...

http://www.ika.rwth-aachen.de/

**ika** INSTITUT FÜR KRAFTFAHRWESEN AACHEN  
 Univ.-Prof. Dr.-Ing. Henning Wallentowitz

Aktuell  
 Über uns  
 Forschung  
 Lehre  
 Veranstaltungen  
 Stellenangebote  
 Kontakt  
 Anfahrt  
 Links

English Site

Suche:

Disclaimer

Ministerium für Wissenschaft und Forschung des Landes Nordrhein-Westfalen  
 Stärkung der Zukunftsmobilität in NRW (.pdf)

**EUR motor**  
 Vehicle Dynamics in Simulation and Testing  
 21.-23.09.2005

**14**  
**AACHENER KOLLOQUIUM AACHEN COLLOQUIUM**  
 Fahrzeug- und Motorentechnik  
 Automobile and Engine Technology  
 04.-06. Oktober 2005  
 EUROGRESS Aachen

Aachener Kolloquium: Fahrzeug- und Motorentechnik  
 4.-6.10.2005, Aachen

Automobilindustrie im globalen Verdrängungswettbewerb - Standort Deutschland im

www.ika.rwth-aachen.de

ika - Forschungsgesellschaft Kraftfahrwesen Aachen - Opera

Datei Bearbeiten Ansicht Lesezeichen Extras Hilfe

Google: **Firmenwerbung im Internet** • www.adword-agentur.de **schnell, erfolgreich, effektiv, 1.000 Interessenten für 110 €**

Neue Seite UMFRAGE Leere Seite Bedienungsanleitungen ika - Forschungsgesellsch...

http://www.fka.de/

**fka** ANGEWANDTE FORSCHUNG, ENTWICKLUNG UND CONSULT  
 FORSCHUNGSGESellschaft KRAFTFAHRWESEN mbH AACHEN

Über uns  
 Dienstleistungen  
 Veranstaltungen  
 Produkte  
 Schriftenreihe

Stellenangebote  
 Kontakt  
 Anfahrt  
 Links  
 English Site

Suche:

Impressum

Ministerium für Wissenschaft und Forschung des Landes Nordrhein-Westfalen  
 Stärkung der Zukunftsmobilität in NRW (.pdf)

**EUR motor**  
 Vehicle Dynamics in Simulation and Testing  
 21.-23.09.2005

**14**  
**AACHENER KOLLOQUIUM AACHEN COLLOQUIUM**  
 Fahrzeug- und Motorentechnik  
 Automobile and Engine Technology  
 04.-06. Oktober 2005  
 EUROGRESS Aachen

Aachener Kolloquium: Fahrzeug- und Motorentechnik  
 4.-6.10.2005, Aachen

Automobilindustrie im globalen Verdrängungswettbewerb - Standort Deutschland im

www.fka.de